TÉCNICO LISBOA

Automatic Arrhythmia Classification:

A Pattern Recognition Approach

Diana Paiva Moreira Batista

Thesis to obtain the Master of Science Degree in

Biomedical Engineering

Supervisors: Prof. Ana Luísa Nobre Fred, Dr. Rui Cruz Ferreira

Examination Committee

Chairperson: Prof. Paulo Rui Alves Fernandes

Supervisor: Prof. Ana Luísa Nobre Fred

Members of the Committee: Prof. Maria Margarida Campos da Silveira

Dr. Eduardo Antunes

November 2014

Acknowledgments

A few people were fundamental to the successful elaboration of this work and I use this section to acknowledge their contribution.

First, I thank Dr. Eduardo Antunes for the enthusiasm towards this project. I thank him for his availability and willingness to share his medical expertise, as well as the efforts made to organize ECG acquisition sessions at the Hospital de Santa Marta.

Thanks to the medical and technical staff at the Hospital de Santa Marta, for providing me all the help necessary during the acquisitions. A special mention to Sofia Silva, whose unparalleled patience and availability even during the busier days were much appreciated.

I thank Dr. Rui Cruz Ferreira for his guidance.

Last but not least, I thank my supervisor, Ana Fred, for the knowledge transmitted, the ideas shared, and the advice given during the elaboration of this thesis.

Resumo

Nas últimas décadas tem-se assistido ao contínuo desenvolvimento de aparelhos de monitorização cardíaca. A quantidade de dados recolhida é portanto cada vez maior e torna-se necessário desenvolver algoritmos que auxiliem a sua análise, automatizando-a sempre que possível. A identificação de ritmos a partir de registos electrocardiográficos (ECGs) é parte importante deste problema e pode ser abordada utilizando técnicas de reconhecimento de padrões.

Este estudo focou-se no processamento de ECGs, dando particular ênfase à classificação automática de arritmias. Utilizaram-se características espectrais, extraídas recorrendo à transformação de wavelet, e características temporais. Comparou-se o desempenho de três classificadores: k-vizinhos mais próximos, perceptrão multi-camada e máquina de vectores de suporte (SVM, do inglês Support Vector Machine). O método proposto foi validado recorrendo a uma reconhecida base de dados. Foi ainda possível efectuar testes iniciais com ECGs adquiridos nos dedos com o sistema BITalino.

Na distinção entre ritmo sinusal e fibrilação auricular o melhor classificador foi o SVM, que atingiu uma taxa global de exactidão de 99.08%. Este resultado foi obtido com uma combinação de características espectrais e temporais pelo que nas experiências com múltiplas classes se utilizaram estas mesmas características. Considerando oito ritmos, divididos em cinco classes, foi possível atingir uma exactidão próxima de 94%. Os testes iniciais realizados com aquisições do BITalino provaram que também é possível classificar automaticamente, com sucesso, ECGs adquiridos com este sistema.

Palavras-chave: Arritmia, Reconhecimento de Padrões, Redes Neuronais, k-Vizinhos Mais Próximos, Máquina de Vectores de Suporte

Abstract

With the continuous development of tools for cardiac monitoring, an enormous amount of data can be collected and has to be analyzed. It is therefore crucial to develop new algorithms that will aid in the analysis of electrocardiograms (ECGs), automatizing, to a certain extent, the process. The recognition of arrhythmias is one important part of the problem and pattern recognition methods have been successfully employed.

In this work, a methodology for ECG analysis was presented. The main focus was on automatic arrhythmia classification. Both spectral features, extracted using the wavelet transform, and time domain parameters were considered for classification. The performance of three supervised learning classifiers was compared: k-nearest neighbor, multilayer perceptron and support vector machine (SVM). Validation of the proposed method was performed resorting to benchmarked data from a widely used arrhythmia database. Additionally, initial experiments were carried out to assess the feasibility of classifying ECG records acquired with the BITalino system at the fingers.

An overall accuracy of 99.08% was achieved with the SVM classifier when distinguishing between normal sinus rhythm and the most common arrhythmia, atrial fibrillation. A feature set containing a combination of spectral and time domain parameters proved to be the most suitable choice and was then used in multiclass experiments. Classification of eight types of rhythms, divided in five classes, was achieved with a correct classification rate close to 94%. The initial experiments carried out with records from the BITalino attested the possibility of automatically classifying ECGs acquired with this device.

Keywords: Arrhythmia, ECG, Pattern Analysis, Artificial Neural Network, k-Nearest Neighbors, Support Vector Machine

Table of Contents

List of Figures

List of Tables

List of Acronyms

AF	Atrial Fibrillation
ANN	Artificial Neural Network
AV	Atrioventricular
bpm	Beats per minute
ECG	Electrocardiogram
kNN	k-Nearest Neighbor
LAFB	Left Anterior Fascicular Block
LBBB	Left Bundle Branch Block
LGL	Lown–Ganong–Levine
LPFB	Left Posterior Fascicular Block
MLP	Multilayer Perceptron
PAC	Premature Atrial Contraction
PJC	Premature Junctional Contraction
PSD	Power Spectral Density
PVC	Premature Ventricular Contraction
RBBB	Right Bundle Branch Block
RDWT	Redundant Discrete Wavelet Transform
SA	Sinoatrial
SVM	Support Vector Machine

1. Introduction

1.1 Motivation

An electrocardiogram (ECG) is a recording of the heart's electrical activity. This recording can be obtained in a non-invasive manner, typically by placing electrodes on the surface of the chest. Besides the standard 12-lead ECG, widely used in clinical practice, a number of other cardiac monitoring tools have been developed in the last few decades. Portable ECG devices include Holter monitors, mobile cardiac outpatient telemetry systems, event recorders and patch monitors. An enormous amount of data can be collected by such devices and it is therefore essential to develop algorithms that aid in the analysis of these records.

An arrhythmia is any disturbances in rate, rhythm, or conduction of the electrical impulse through the heart. While some arrhythmias are harmless others can really compromise the cardiac output and be potentially life threatening. Hence, the diagnosis of cardiac arrhythmias, which can be achieved by analyzing ECG records, is an important medical topic.

Automatic analysis of ECG strips for the diagnosis of arrhythmias is an ongoing research. Numerous algorithms have been proposed to classify beat or rhythm types. Some of these studies show promising results but there is certainly room for improvement. Furthermore, the proposed algorithms are sometimes tested on small and/or private databases, which hinder an objective validation.

1.2 Goals and Proposed Approach

The objective of this work is the automatic classification of cardiac rhythms from one-lead ECG records. Ultimately, pervasive ECG acquisition, processing, and classification, is sought. Therefore, all these steps are approached but main attention is given to the classification phase. Pattern recognition techniques are employed to carry out this classification task. The focus is put on the features to extract from the records and the classifiers used.

Two types of features are assessed, first individually and then in combination: spectral features, extracted using the wavelet transform, and time domain parameters, representing heart rate characteristics. This analysis is carried out while trying to distinguish between normal sinus rhythm and the most common arrhythmia, atrial fibrillation. The performance of three supervised learning classifiers is compared: k-nearest neighbor, multilayer perceptron and support vector machine.

The feature set offering the best results is then used to perform multiple tests including more rhythms in the classification task. This is a more realistic approach to the rhythm classification problem.

Validation of the proposed method is performed recurring to benchmark data from a widely used arrhythmia database. Additionally, a few tests are performed with data acquired with the BITalino system.

1.3 Contributions

The contributions of this thesis are:

- Analyzes the performance of spectral and time domain features, considered individually and in combination, on the classification of normal sinus rhythm and atrial fibrillation ECG records.

- Evaluates the performance of the best set of features on multiclass classification tasks, including up to eight different rhythms.

- Compares the performance of three supervised learning classifiers, k-nearest neighbor, multilayer perceptron and support vector machine, on the classification of ECG records according to the type of rhythm.

- Validates the proposed methodology by acquiring, processing and classifying ECG records acquired with the BITalino system at the fingers.

Part of the work developed in this thesis has been submitted to *8th International Conference on Bio-inspired Systems and Signal Processing* (Batista and Fred, 2014).

1.4 Structure

This thesis is organized in six chapters.

In this first chapter the problem at hand was detailed and the proposed approach was outlined. The contributions of this thesis were then stated. The remaining of this work is organized as follows.

In Chapter 2, important concepts concerning the electrophysiology of the heart and the available solutions for monitoring its electrical activity are revised.

Chapter 3 contains a review of the algorithms developed for classification of beat and rhythm types. It further details the theory necessary for the implementation of the proposed algorithm.

The methodology proposed is explained in Chapter 4: details about data acquisition and processing, the feature extraction process, the classifiers used and the validation setup are specified.

The experimental setup and the results obtained are presented and discussed in Chapter 5.

Chapter 6 contains the main conclusions of this work and presents some ideas for future development.

2. Electrophysiology and Cardiac Monitors

2.1 Electrical Conduction System of the Heart

The heart is the muscle responsible for pumping blood, making it circulate through the body and thus assuring appropriate quantities of oxygen and nutrients are delivered. Four chambers constitute the heart, two atria and two ventricles, and four valves control the blood flow through it. The oxygenated blood leaves the heart through the left ventricle and flows throughout the body. Deoxygenated blood returns to the heart via the right atrium. This part of the circulatory system is known as systemic circuit. The other part, pulmonary circuit, is much smaller and is responsible for oxygenating the blood. Deoxygenated blood leaves the heart through the right ventricle and travels through the lungs before returning, rich in oxygen, through the left atrium.

The correct blood flow depends on a suitable cardiac muscle contraction which is the result of the generation and transmission of electrical impulses. It is this biological electrical activity that can be recorded in an electrocardiogram (ECG) and is very useful in the diagnosis of an important number of conduction abnormalities. In the next paragraphs the different phases of this conduction system are briefly reviewed and the corresponding events in the ECG are pointed out.

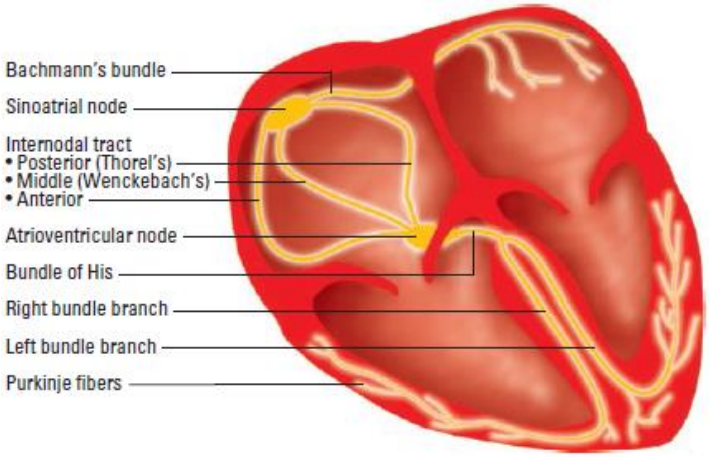

Figure 1: Elements of the cardiac electrical conduction system (Williams, 2010).

The sinoatrial (SA) node is referred to as pacemaker of the heart since in a normal situation it is the specialized cells in this location that set the pace of the heart by generating impulses 60 to 100 times per minute. Electrical stimulation (depolarization) of the left and right atria is the result of the conduction of the impulse respectively along Bachmann's bundle and internodal tracts. Contraction of the two atria is almost simultaneous due to the fast impulse transmission.

The atrioventricular (AV) node is the conduction pathway between atria and ventricles. It is important to assure that the ventricles do not contract too quickly otherwise the atria will not be able to empty its

content into the lower chambers. This is one of the main functions of the AV node (impulses are delayed by approximately 0.04 seconds) and some impulses may even be blocked if the atrial rate is dangerously high. Additionally, cells in the vicinity of the AV node are capable of acting as backup pacemaker, generating impulses at a rate of 40 to 60 beats per minute. After the delay at the AV node, the electrical impulse moves through the bundle of His. A division between right and left bundle branches occurs at this point which will assure the conduction respectively to the right and left ventricles. Purkinje fibers form an elaborate web that extends from the bundle branches deep into the myocardial tissue allowing fast impulse conduction. The ventricles are also able to act as backup pacemaker with rates of 20 to 40 times per minute, sometimes less.

2.2 Electrocardiogram

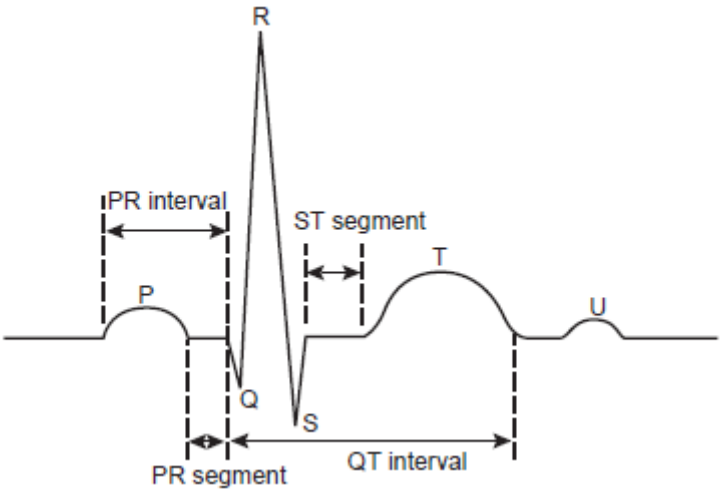

Figure 2: Basic components of the ECG complex (Huff, 2006).

The basic components of the ECG complex are represented in Figure 2. The first deflection, named P wave, corresponds to the depolarization of both atria: the electrical impulse spreads from the SA node trough the atria. In normal adults the duration of this wave can vary between 0.08 and 0.11 seconds.

The PR (or PQ) interval is the time period between the onsets of atrial and ventricular depolarization. Normal PR intervals range from 0.12 to 0.20 seconds. A short isoelectric line is present within the PR interval. This is referred to as PR segment and extends from the end of the P wave until the beginning of the QRS complex.

Ventricular depolarization translates into the QRS complex. Although many morphologic variations exist, the QRS complex is often composed of three waves. The Q wave is the first negative deflection following the P wave. The R wave is the first positive deflection after the P wave. The negative deflection following the R wave is the S wave. The QRS complex should be measured from the beginning of the first wave to the end of the last wave of the complex. In normal situations its duration is 0.06 to 0.10 seconds. It should be noted that atrial repolarization occurs during ventricular depolarization and is hidden in the QRS complex.

Following ventricular depolarization an isoelectric line is visible in the record. This is called ST segment and extends from the end of the QRS complex to the beginning of the T wave. It corresponds to an electrically neutral time for the heart, between ventricular depolarization and repolarization. Elevation or depression of the ST segment may be indicative of myocardial damage.

The T wave always follows the QRS complex because it represents ventricular repolarization. The normal T wave should be in the same direction of the QRS complex and is slightly asymmetrical (first part slowly sloping to the peak and returning more abruptly to the baseline).

The time between the onset of ventricular depolarization and the end of ventricular repolarization is denominated QT interval. It is therefore measured from the beginning of the Q wave to the end of the T wave. The duration of this interval varies according to age, sex, and mostly heart rate. For regular rhythms QT duration shouldn't exceed half of the RR interval (time between two consecutive R waves).

The U wave, small deflection that follows the T wave, represents late ventricular repolarization. This wave is not always visible in the record and its absence is not a sign of abnormality. U waves are more easily discernable with slower heart rates.

2.3 Arrhythmias and Conduction Abnormalities

The four arrhythmogenic zones shown in Figure 3 are often used to classify arrhythmias according to their source of origin (Garcia and Miller, 2004; Huff, 2006; Williams, 2010). Rhythms originating in the sinus node, atria or atrioventricular (AV) junction can be more generally referred to as supraventricular rhythms. The main arrhythmic events are summarized in Table 1 below using this classification and their characteristics are reviewed in the following sections.

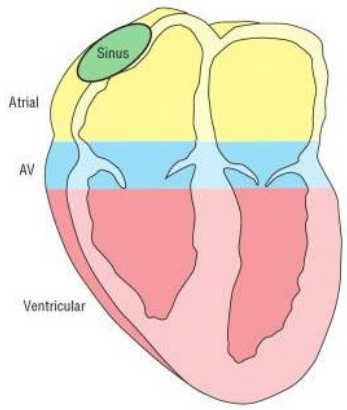

Figure 3: Four arrhythmogenic zones (Garcia and Miller, 2004).

2.3.1 Sinus Node Rhythms

Sinus node rhythms all originate in the SA node. The normal cardiac rhythm is referred to as normal sinus rhythm; the impulse generated at the SA node follows the pathway described in section 2.1, with

atrial and ventricular rates ranging from 60 to 100 beats per minute (bpm). A recording of such rhythm is presented in Figure 4.

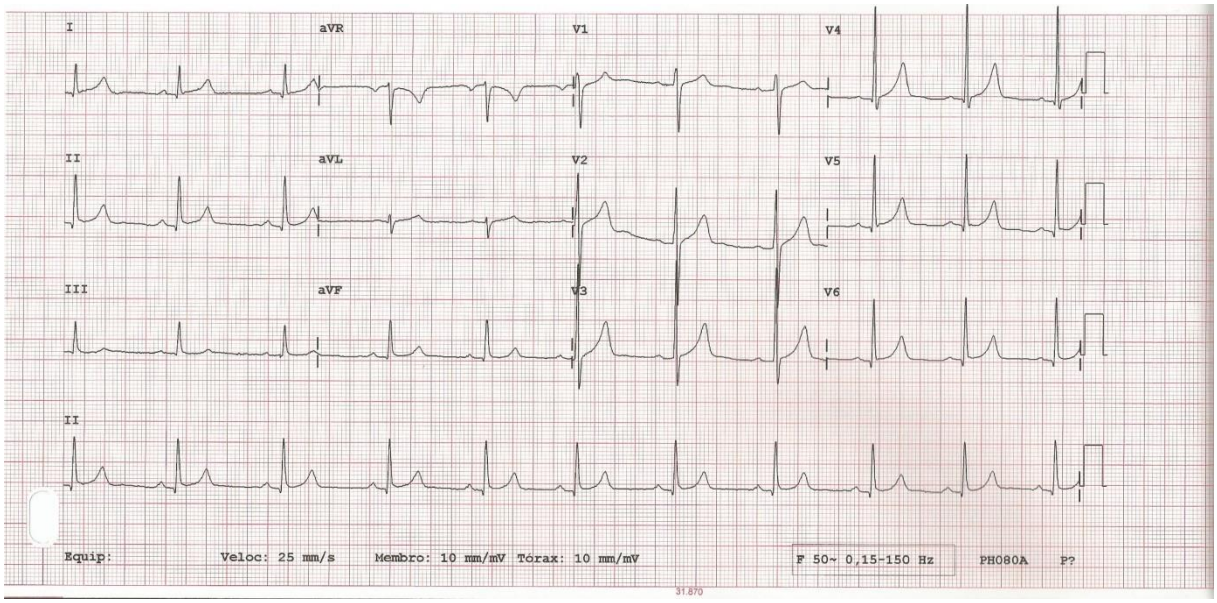

Figure 4: Recording of a normal sinus rhythm ECG.

Sinus tachycardia and sinus bradycardia are regular rhythms characterized respectively by a fast and slow heart rate. The only distinguishing feature of both these rhythms is the heart rate and all other ECG features are within the normal range. In sinus bradycardia the SA node regularly discharges impulses at a rate between 40 and 60 bpm. This may be the normal response of the heart when metabolic demands are reduced, e.g. during sleep, and trained athletes commonly develop this condition. Although non-symptomatic sinus bradycardia is not a cause of alarm, when symptoms appear treatment must be initiated. In sinus tachycardia impulses are discharged at a rate between 100 and 160 bpm. No clinical significance should usually be attributed to this arrhythmia when it is caused by exercise or high emotional states (e.g. stress or anxiety). However, persistent sinus tachycardia should be dealt with.

Sinus arrhythmia is characterized by an irregular discharge of impulses by the pacemaker cells of the SA node. The heart rate may be normal or slow. Sinus arrhythmia is frequently associated with respiration: during inspiration the heart rate increases and during expiration it slows down. Unless associated with symptomatic bradycardia, no intervention is necessary to revert this rhythm.

SA exit block, sinus pause and sinus arrest all result in missing beat(s) in an otherwise normal sinus rhythm. The terminology used among authors slightly differs. Huff (2006) encompasses sinus arrest and SA exit block in the general term sinus pause. Garcia and Miller (2004) and Williams (2010) separate SA exit block from sinus pause and sinus arrest, differentiating these two by their duration. In a SA exit block the sinus node is still firing impulses but these are blocked at the exit of the node and thus are not conducted through the atria. Because the pacemaker is still intact, a SA block is a multiple of the P-P interval. When the SA node fails to generate an impulse the time period between consecutive P waves will be longer than normal. The P-P interval of the pause will not be a multiple of

the baseline P-P interval. Garcia and Miller (2004) define a sinus pause as being three times shorter than the normal P-P interval and sinus arrest as being greater three times greater than this normal P-P interval.

2.3.2 Atrial Arrhythmias

A beat or rhythm is said to be ectopic if it originates from a source other than the SA node. Atrial arrhythmias have their origin in ectopic sites in the atria.

When the underlying regular rhythm is interrupted by an early beat originating from the atria this is referred to as premature atrial contraction (PAC). Figure 5 shows an ECG with a recording of this arrhythmic beat. Both the P wave and the QRS complex associated with a PAC appear prematurely after the last beat. The morphology of the P wave is abnormal and a pause follows the beat. PACs can be caused by substances such as nicotine and alcohol or due to emotional stress and are usually asymptomatic. A PAC is said to be nonconducted if the impulse arrives to the AV junction too early, when it is still in its refractory period, and thus no impulse is conducted through the ventricles. In this case the abnormally shaped and premature P wave will not be followed by a QRS complex.

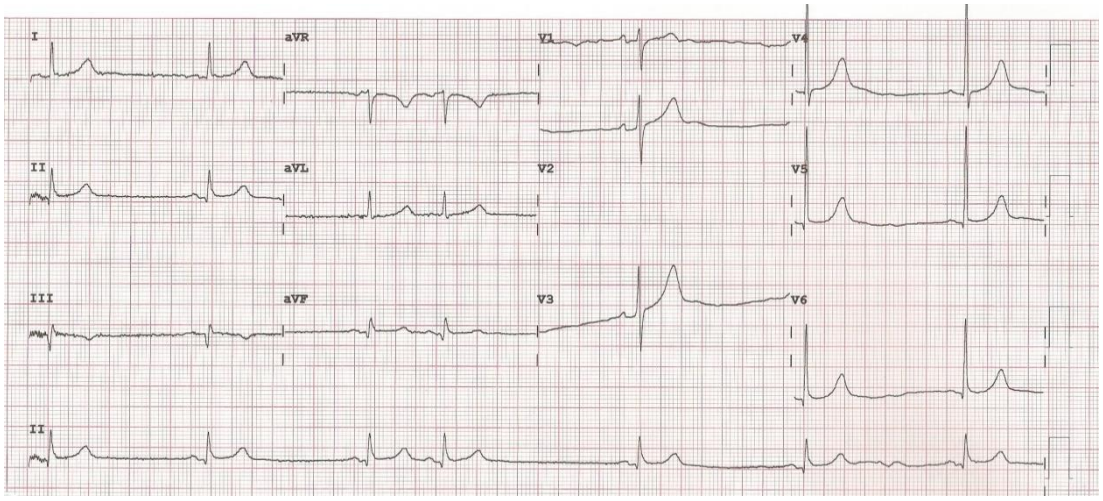

Figure 5: ECG showing a premature atrial contraction with an underlying sinus bradycardia rhythm.

Wandering atrial pacemaker refers to the irregular rhythm caused by shifts in the pacemaker site from the SA node to ectopic sites within the atria. P waves will present different morphologies according to the origin of the impulse. The rate is usually within normal limits but may also be slower. Wandering atrial pacemaker is commonly asymptomatic and not clinically significant; it is more frequent among young patients and athletes.

Atrial tachycardias are ectopic atrial rhythms with fast atrial rates (greater than 100 bpm and going up to 250 bpm). P waves differ from normal sinus rhythm P waves by their morphology and may be hidden in the preceding T wave. Atrial rhythm is usually regular whereas ventricular rhythm may either be regular or irregular depending on whether the AV node is obstructing the passage of some of the impulses. Atrial tachycardia with block is characterized by an impaired AV conduction. The block may or may not be variable. Paroxysmal atrial tachycardia starts and stops abruptly and corresponds to at

least three consecutive PACs. The rhythm is regular and the heart rate is usually between 140 and 250 bpm. Multifocal atrial tachycardia is an infrequent arrhythmia commonly associated with chronic pulmonary disease. Impulses are fired by numerous loci which translate into varying P waves. Both atrial and ventricular rhythms are irregular in this type of atrial tachycardia.

Atrial flutter originates from a single ectopic site that generates impulses usually at a rate around 300 bpm (varying from 250 to 400 bpm). The P waves appear with a saw-toothed shape and are referred to as flutter waves; they affect the entire baseline. Due to the work of the AV node, the ventricular rate will not be as high as the atrial rate. This is essential since the lower chambers are not able to tolerate such high heart rates. The AV conduction ratio will determine the ventricular rate and define the regularity of the rhythm. Atrial flutter is seldom present in healthy hearts. Control of ventricular rate, assessing anticoagulation needs and convert the rhythm are the intervention steps to follow.

Atrial fibrillation is the most common type of arrhythmia. The electrical activity on the atria is chaotic, asynchronous, with rates higher than 400 bpm. Instead of regular contractions, the atria quiver. The P waves are replaced by irregular wavy deflections, fibrillatory waves, which affect the entire baseline, as shown in Figure 6. As with atrial flutter, the AV node will block the conduction of the majority of the impulses thus protecting the ventricles. The irregular conduction of impulses through the AV node results in a characteristic irregularly irregular ventricular response. Atrial fibrillation can occur temporarily in healthy individuals, in which case it may revert spontaneously to normal sinus rhythm, or be associated with heart disease. The same guidelines followed to deal with atrial flutter should be applied to atrial fibrillation. Controlling the ventricular rate and restoring the sinus rhythm are the priorities. Some patients may present a chronic atrial fibrillation that will not revert: ventricular rate control is the only solution in these cases.

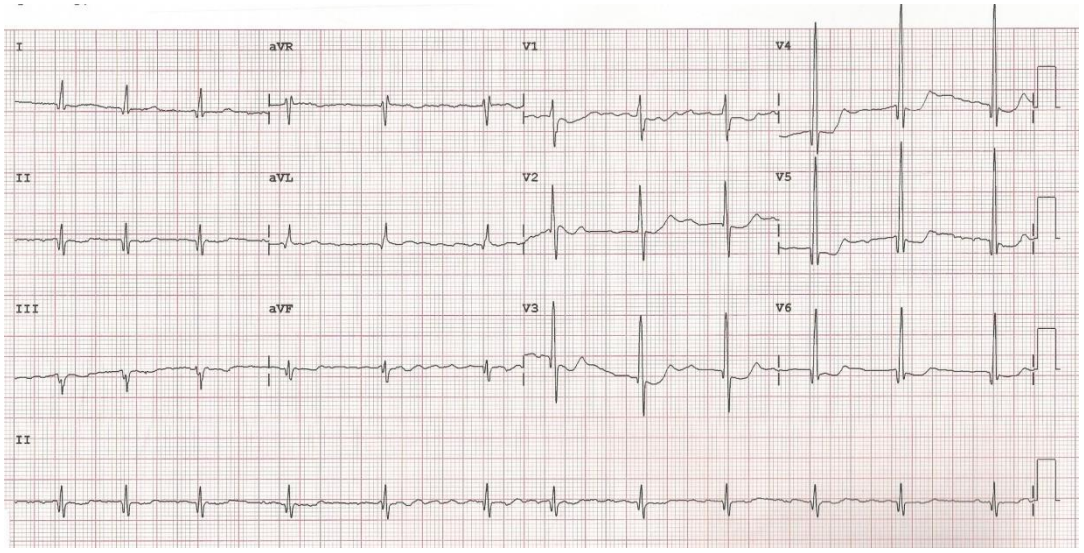

Figure 6: Recording of atrial fibrillation.

2.3.3 Junctional Arrhythmias and Atrioventricular Blocks

The area around the AV node and the bundle of His is denominated AV junction. Arrhythmias that originate in this area are referred to as junctional arrhythmias. When pacemaker cells in the AV junction fire, the impulse spreads backward into the atria (resulting in an inverted P wave) and forward into the ventricles. Depending on the speed of retrograde and antegrade conductions, the P wave will either follow or precede the QRS complex. If simultaneous depolarization takes place, the P wave will be hidden in the QRS complex.

A premature junctional contraction (PJC) is an early beat originating in the AV junction. An abnormally shaped, premature P wave and a premature QRS complex interrupt an otherwise regular rhythm. The most common cause of PJCs is digitalis toxicity and if symptoms are present the condition should be dealt with by correcting the underlying cause. Frequent PJCs may indicate the development of other junctional rhythms.

The junctional escape rhythm is a backup mechanism activated when the ventricles are not depolarized by impulses arising from the SA node or ectopic sites in the atria. This rhythm is regular and its rate is determined by the intrinsic firing rate of pacemaker cells in the AV junction: 40 to 60 bpm. Figure 7 shows an ECG with such a rhythm. Children during sleep, or healthy athletic adults, may present an asymptomatic, not harmful, junctional escape rhythm. However, the slow heart rate and abnormal atrial contraction can cause a decrease in cardiac output which will harm individuals with less tolerant hearts. In such cases intervention consists of increasing the heart rate and attempt to correct the underlying cause of the rhythm.

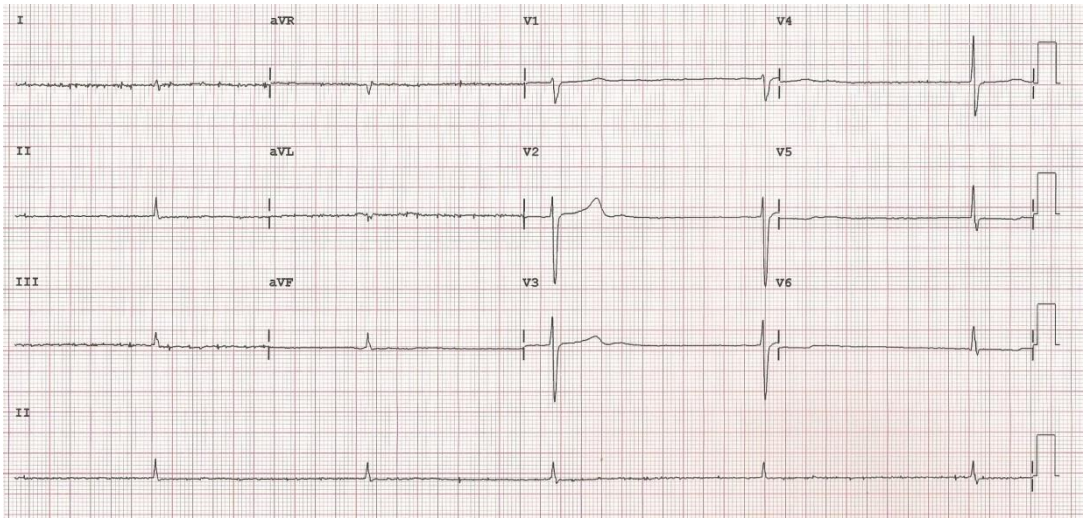

Figure 7: Recording of junctional escape rhythm.

Accelerated junctional rhythm is an infrequent arrhythmia. Like junctional escape rhythm, this rhythm is regular and retrograde atrial depolarization occurs. The difference relies on the higher rate, which ranges from 60 to 100 bpm. Although this is the same rate occurring with normal sinus rhythm, the cardiac output is decreased due to loss of atrial kick. Patients may present symptoms such as hypotension or syncope.

Junctional tachycardia is defined as the occurrence of three or more consecutive PJCs. The rate of this rhythm is high, above 100 bpm, and the remaining characteristics are the same as junctional escape rhythm and accelerated junctional escape rhythm. The most common cause of this arrhythmia is again digitalis toxicity and symptoms of decreased cardiac output may present.

AV blocks refer to the types of arrhythmia in which there is a delay or a fail in the conduction of electrical impulses through the AV node. This block may be situated in the AV node, the bundle of His or the bundle branches. AV blocks are classified according to their severity into first-degree, second-degree (type I and II) and third-degree. In first-degree AV block, the less severe, all the impulses are conducted through the AV node but this conduction is delayed. This rhythm is regular and atrial and ventricular rate are the same. The distinguishing feature in an ECG rhythm strip will be the prolonged but consistent PR interval (superior to 0.20 seconds). This block can progress to a more severe one. Type I second-degree AV block, or Mobitz type I block, is characterized by a progressive increase of PR interval until a nonconducted P wave occurs. Although atrial rhythm is regular, the ventricular rhythm will be irregular and ventricular rate will depend on the number of impulses being conducted through the AV node. Type II second-degree AV block, or Mobitz type II block, is a rarer but more serious arrhythmia. In this case the ECG shows no progressive lengthening of the PR interval but missing QRS complexes will be noted. The ratio of atrial-to-ventricular beats is used to further characterize this rhythm. Ventricular rate will be regular if this ratio is constant but irregular otherwise. In third-degree AV block, or complete heart block, all the impulses arriving from the atria are blocked by the AV node and incapable of reaching the ventricles. In the ECG record, there will be no relation between P waves and QRS complexes. The atrial rhythm is controlled by the SA node and maintains a regular rate of 60 to 100 bpm. The ventricular rate will be dictated either by the AV junction or by the ventricles. In the first case the rate ranges from 40 to 60 bpm and a normal QRS complex can be observed. In the second case the rate is slower, from 30 to 40 bpm, and the QRS complex will be wider. Depending on the type of block and the symptoms experienced by the patient, it may be necessary to insert a temporary or permanent pacemaker.

2.3.4 Ventricular Arrhythmias and Bundle-Branch Blocks

When a bundle-branch block is present ventricular depolarization is said to be sequential: one ventricle will depolarize before the other. This translates into a wider QRS complex (0.12 seconds or greater). Right bundle-branch block (RBBB) may appear in a healthy heart but is more commonly associated with coronary artery disease. RBBB can be temporary, chronic or rate-related (developing when the heart rate increases). The most common cause of left bundle-branch block (LBBB), shown in Figure 8, is hypertensive heart disease. LBBB does not occur on healthy individuals and is more commonly seen among the elderly population.

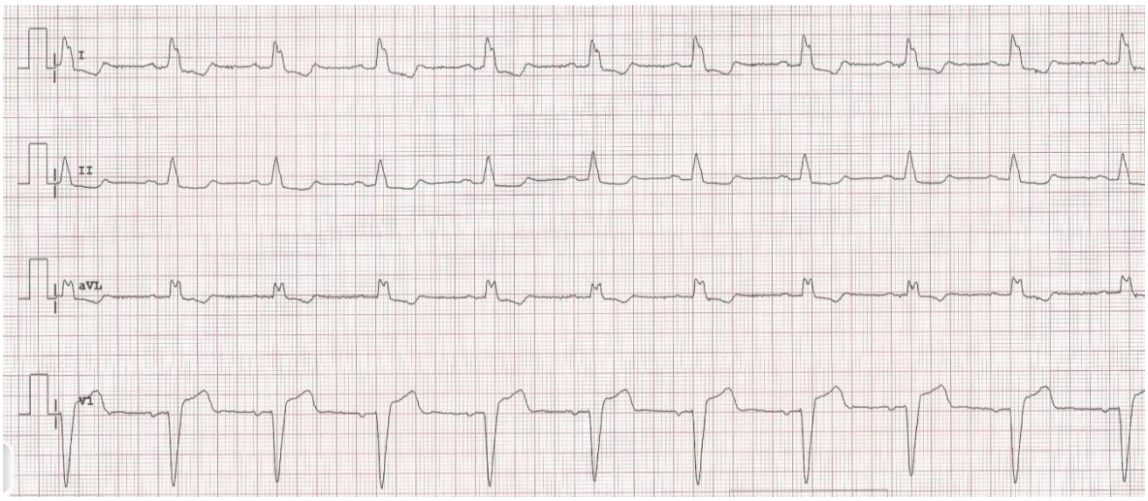

Figure 8: Rhythm strips of a LBBB.

Ventricular arrhythmias originate in the ventricles, below the bundle of His. The electrical impulse will not follow the normal conduction pathway and an asynchronous depolarization of the ventricles occurs. The aberrant conduction translates into a wide QRS complex. Ventricular repolarization will also be affected, which will cause changes in the ST segment and T wave (deflects in opposite direction to the QRS complex). Logically, since atrial depolarization does not occur, no P wave will be observable. A fast recognition and treatment of ventricular arrhythmias is necessary since they are potentially deadly.

Premature ventricular contractions (PVCs) are ectopic beats originating from the ventricles. A premature, wide, QRS complex is visible in the ECG record. No P wave is associated with the complex and a compensatory pause follows it. PVCs may occur as a single beat, in clusters of two or more, or in repeating patterns (bigeminal – see Figure 9, trigeminal or quadrigeminal patterns). PVCs are common events and can occur in healthy individuals but are more frequent in individuals with coronary heart disease. Frequent or sustained PVCs can cause a decrease of cardiac output. More serious arrhythmias can develop from PVCs.

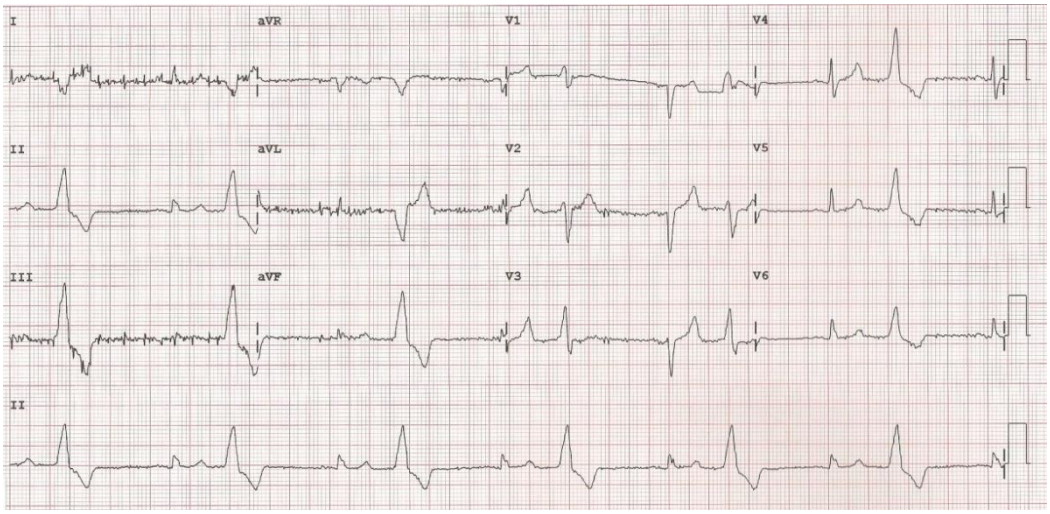

Figure 9: ECG showing a bigeminal rhythm.

Ventricular tachycardia is defined as a burst of three or more PVCs fired at a rate exceeding 100 bpm (normally ranging from 140 to 250 bpm). The ventricular rhythm is usually regular, or slightly irregular, whereas atrial rhythm and rate cannot be determined. Ventricular tachycardia can last less than 30 seconds, causing few or no symptoms, or be sustained. The latter case should be dealt with immediately since it is possibly life threatening.

During ventricular fibrillation the ventricles do not contract properly. Instead, the muscle quivers due to the chaotic electrical activity originating from multiple foci. Irregular fibrillatory waves, differing in shape and amplitude, appear in the ECG. This rhythm results in no cardiac output and the patient faces imminent death if it is not reverted (early recognition and defibrillation are key to recovery).

If electrical impulses generated above the bundle of His (either by the sinus node, the atria or the AV junction) fail to reach the ventricles, or if no impulse is being generated, the last resort pacemaker will take over. Cells in the ventricles will impose a rhythm to prevent ventricular standstill. A single beat, referred to as ventricular escape beat, will arise if the rate drops below 40 bpm. The QRS complex will be wide and the beat will appear late in the conduction cycle. Consecutive ventricular escape beats form a slow but regular rhythm, the idioventricular rhythm. The ventricular rate ranges from 20 to 40 bpm and it is not possible to determine atrial rate or rhythm. An accelerated idioventricular rhythm has the same characteristics of an idioventricular rhythm, differing only in terms of heart rate, which ranges from 50 to 100 bpm. Patients with idioventricular rhythms should be closely monitored because the progression to a more letal arrhythmia may occur. When symptomatic, the effort should be on increasing the heart rate, improving cardiac output and reestablishing a normal rhythm. Idioventricular rhythms should not be suppressed.

During asystole, or ventricular standstill, there is no electrical activity on the ventricles. As a result, there is no cardiac output and the peripheral pulse and blood pressure are not discernable. The patient is unconscious and unless the arrhythmia is immediately treated, the situation becomes irreversible. In an ECG strip, this rhythm appears either as a flat line or as P waves without a QRS complex. The latter corresponds to the situation when atrial electrical activity is still present.

Table 1: Main cardiac rhythms classified according to their origin.

Sinus node rhythms		Atrial arrhythmias		Junctional arrhythmias and atrioventricular blocks		Ventricular arrhythmias and bundle-branch blocks
Normal sinus rhythm		Wandering atrial pacemaker		Premature junctional contraction		Bundle-branch block (right or left)
Sinus tachycardia		Premature atrial contraction		Junctional escape rhythm		Premature ventricular contractions
Sinus bradycardia		Nonconducted premature atrial contraction		Accelerated junctional rhythm		Ventricular tachycardia
Sinus arrhythmia		Atrial tachycardia	Paroxysmal atrial tachycardia	Junctional tachycardia		Ventricular fibrillation
Sinus pause	Sinus arrest		Atrial tachycardia with block	AV blocks (classified according to severity)	First degree AV block	Ventricular escape beat
	Sinus exit block		Multifocal atrial tachycardia		Second degree AV block, type I (Mobitz I or Wenckebach)	Idioventricular rhythm
		Atrial flutter			Second degree AV block, type II (Mobitz II)	Accelerated idioventricular rhythm
		Atrial fibrillation			Third degree AV block (complete heart block)	Ventricular standstill (asystole)

2.4 Cardiac Monitors

2.4.1 Standard 12-Lead ECG

The primary diagnostic tool when an arrhythmia is suspected is a 12 lead surface electrocardiographic recording. This exam is safe, inexpensive and easily accessible. The electrodes are placed on the patient's extremities and chest wall, as illustrated in Figure 10. Different views of the heart's electrical activity can be obtained in this way. Limb leads include three standard, bipolar, leads (I, II and III) and three augmented leads (aV_R, aV_L e aV_F). These leads will record information in the heart's frontal plane. A transverse view of the heart's electrical activity is given by the precordial leads (V1, V2, V3, V4, V5 and V6).

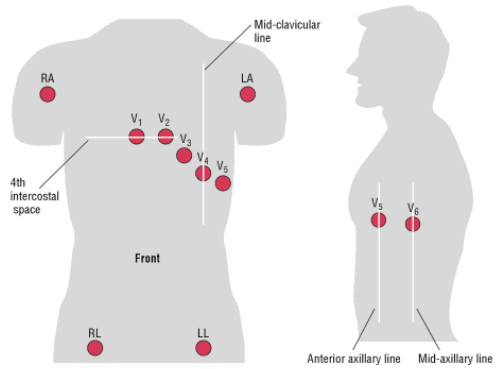

Figure 10: Lead placement for a 12-lead ECG (Garcia and Miller, 2004).

Although a 12-lead ECG can provide useful information for the diagnosis of arrhythmias, its limited observation period is an important drawback. In fact, a longer monitoring is often necessary to detect arrhythmias that occur less frequently. To deal with this limitation different devices have been developed. These are reviewed in the following sections. It is important to keep in mind that the usefulness of each device depends on the purpose of monitoring. It is therefore essential to choose the most appropriate tool for each particular situation (Zimetbaum and Goldman, 2010). Multiple studies were undertaken to compare the relative value of different devices (Barrett *et al.*, 2014; Reiffel, Schwarzberg and Murry, 2005; Rothman *et al.*, 2007; Sivakumaran *et al.*, 2003)

2.4.2 Ambulatory ECG Monitoring Systems

Holter Monitor

The first ambulatory cardiac monitoring device was introduced by Norman J. Holter during the 1940s. Since then the Holter monitor has been greatly improved in terms of portability, memory capacity, data quality and reliability of interpretation (Yan and Kowey, 2011) and today it is still the most widely used ambulatory ECG monitoring tool. One of these devices, from Philips, is shown in Figure 11. The most common monitors are meant to be worn during 24 or 48 hours but some devices already have recording capabilities of up to one week. During this period between 3 and 7 electrodes are attached to the patient's chest. Additionally, he is asked to keep a precise diary of activities and symptoms

during the monitoring period to allow for an accurate correlation between symptoms and rhythm disturbances. Holter monitors generally record the signal from 2 or 3 bipolar leads (commonly chest modified V_5, chest modified V_3 and a modified inferior lead) and some systems can derive a 12 lead ECG from this data (Crawford *et al.*, 1999). Once the recording phase is completed, the monitor is returned and software is available for the technician to analyze the ECG data. Finally the physician is provided a report that contains information about average, minimum, and maximum heart rate, presence and morphology of atrial and ventricular ectopy, nonsustained atrial and ventricular arrhythmias, AV block, QT interval, and asystole/pauses (Yan and Kowey, 2011). In the presence of atrial fibrillation (AF) episodes, relevant information such as shortest and longest duration of AF, burden of AF, heart rate during AF, and pattern of initiation and termination of AF can also be reported (Mittal, Movsowitz and Steinberg, 2011). The Holter monitor provides a continuous record of ECG but isn't prepared to automatically detect arrhythmias and doesn't have telemetry capabilities. Its short time of utilization can represent an obstacle in the detection of less frequent arrhythmic episodes.

Figure 11: Philips DigiTrak XT Holter Recorder (Philips, 2014)

Event Recorders

To address the drawbacks of Holter monitors when dealing with infrequent symptoms, the focus has been on developing other devices that allow cardiac monitoring over a more extended period, namely event recorders and more recently mobile cardiac outpatient telemetry (MCOT) systems.

Regarding event recorders, a distinction must be made between symptom event monitors and loop recorders since the latter offer the possibility of registering ECG data prior patient activation whereas the former do not. Symptom event monitor devices require no leads, they are either carried by the patient or worn on the wrist, and they can be used for up to 30 days. Small metallic discs are placed on the back of the device and work as electrodes. Once the patient experiences a symptom or an irregular beat, he should place the monitor on the chest and activate the recording (or simply press the activation button if it is a device worn on the wrist). The ECG is recorded from this point onwards but no information regarding moments preceding the activation is saved. This characteristic may represent a problem for patients who are unable to quickly activate the device when they experience symptoms, namely those with syncope (Brignole *et al.*, 2009). The memory capacity of symptom event monitors is limited and the patient is required to send the recordings to a central monitoring station via telephone.

Loop memory monitors must be worn continuously to allow new ECG data cycles to be acquired and saved as older, non-informative, cycles are deleted. The duration of the cycles is usually programmable and can last from several minutes to one hour, depending on the device (Yan and

Kowey, 2011). Both external and implantable loop recorders are available and they can usually be used for up to, respectively, 30 days and 3 years. The Reveal XT insertable cardiac monitor device from Medtronic, which is meant to be placed under the skin in the upper chest area, is shown in Figure 12. Two distinct recording functionalities can be present on loop recorders. The first one is patient-activated: as for the symptom event monitor, the user should press an activation button when he experiences a symptom. The recorded ECG will cover data relative to moments prior to the activation. The second functionality doesn't require any intervention by the patient since it automatically detects arrhythmic episodes and triggers the recording of the corresponding ECG (Brignole *et al*., 2009). This is particularly important in the case of an asymptomatic arrhythmia (e.g. asymptomatic AF episode) and profound bradycardia (including pause) and tachycardia which may incapacitate the patient (Yan and Kowey, 2011). Data is transmitted in the same manner as for the symptom event monitor. Medtronic is currently performing a usability study on the new Reveal LINQ insertable cardiac monitor, which, besides being smaller, communicates wirelessly with a monitor, allowing then an automatic transmission of data over a cellular telephone connection (Medtronic, 2013).

Figure 12: Reveal XT insertable cardiac monitor device from Medtronic (Medtronic, 2014).

Mobile Cardiac Outpatient Telemetry (MCOT) systems

MCOT systems continuously monitor ECG data acquired by 3 or 4 electrodes placed on the chest for up to 30 days. Some devices transmit the data directly from the sensor to a central monitoring station but more commonly the signal is transmitted to a closeby monitor that has arrhythmia detection capabilities (such as the MCOT system from Cardionet shown in Figure 13). Depending on the devices the ECG transmission to a central monitoring station is performed continuously or only when arrhythmic episodes are detected. The signal is analyzed in real time in the station and if a severe anomaly is present the data can be transmitted to the physician. Some systems already allow the physician to visualize the ECG in real time (Mittal, Movsowitz and Steinberg, 2011). Comparing to event recorders, MCOT systems do not require patient intervention and are therefore less subject to activation and transmission errors.

Figure 13: Mobile Cardiac Outpatient Telemetry system from CardioNet (CardioNet, 2014)

ECG Patch Monitors

Significant efforts have been made towards the development of ECG patch monitors that are directly attached to the skin and allow 1 to 3 lead long-term cardiac monitoring (up to 7 or 14 days) without the discomfort of wires. The features of these systems vary from device to device and we can distinguish two categories, recording only and recording and transmitting patch monitors (Lobodzinski and Laks, 2012). The former work as Holter monitors in the sense that recordings are analyzed after the continuous monitoring period, whilst the latter are more closely related to MCOT systems previously described (having real time transmission capability).

In the Nuvant MCT system (Figure 14, right), the Piix sensor monitors the ECG and transmits it to the zLink device via Bluetooth when a rhythm abnormality is detected or when the patient activates the recording. The Corventis monitoring center receives the data through a secure cloud-based application using cellular communication and prepares a report for the physician. The ZIO XT Patch (Figure 14, left), on the other hand, is a recording only device. It can be used for up to 14 days, and the patient can press a button on the patch to signalize a symptomatic event. After the monitoring period, the device is mailed to a monitoring center where the proprietary algorithm ZEUS is used to analyze the recordings. A certified technician reviews the data and a final report is provided to the physician (Lobodzinski *et al.*, 2013).

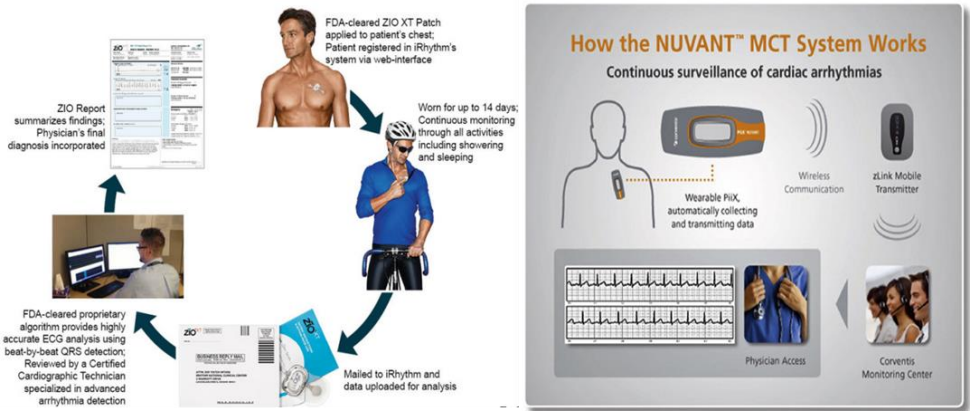

Figure 14: Left: ZIO XT Patch monitoring process (iRhythm, 2014); Right: Overview of the Corventis NUVANT/PiiX system (Lobodzinski *et al.*, 2013).

Pacing Devices

If the patient already has an implanted pacing device (pacemaker, implantable cardioverter defibrillator or cardiac resynchronization therapy device) it can also be used as an ambulatory ECG monitoring tool. Current devices have remote follow-up capabilities, diminishing the need for in-clinic visits, and allow remote monitoring. Automatic wireless transmission of data from the implant to an external transmitter is performed on a pre-scheduled basis and forward to a central station using analogue phone line or GSM network. The data is then processed and the physician is notified if critical events are detected (Burri and Senouf, 2009).

Other Ambulatory ECG monitoring systems

Other devices are also available ranging from shirts with electrodes to the Alivecor system (Figure 15). This latter enables ECG lead I acquisition by finger contact with electrodes placed on the back of a smartphone. The ECG can be visualized in real time or stored and it is immediately transmitted to a secure server. The stored file can then be interpreted by the physician. Furthermore, an algorithm that automatically detects atrial fibrillation is implemented on the device (Lau *et al.*, 2013).

Figure 15: Alivecor system (Lau *et al.*, 2013)

3. State-of-the-Art

3.1 Review of Beat / Rhythm Classification

In the last few decades a considerable effort was dedicated to develop methods for automatic analysis of ECG records. A large number of algorithms were developed both to differentiate between different types of beats and to detect and classify arrhythmias. These vary widely in terms of features extracted from the ECGs, and classification scheme. When analyzing an ECG, a cardiologist focuses on the morphology and time domain features to reach a diagnosis. He analyzes durations of waves and intervals, regularity/irregularity of the rhythm, correspondence between the P waves and the QRS complexes, amplitudes and polarities, etc. These features have naturally been explored in automatic ECG analysis but the access to computational resources makes it much easier to extract further information. Researchers have therefore been able to deal with statistical parameters, frequency domain features or even more complex information drawn from such theories as the chaos theory. Regarding the classification scheme, some authors opted for simple methods such as a set of decision rules whilst others chose to explore more recently developed classifiers such as artificial neural networks or support vector machines. In this section studies that focused on the automatic beat or rhythm classification are reviewed. Particular interest is given to the features extracted for classification and the type of classifier used.

Moody and Mark (1983) compared the performance of multiple classifiers in the detection of atrial fibrillation. Features were based on RR intervals which are known to be irregular when atrial fibrillation is present. Markov process models with different averaging techniques (e.g. filter and interpolation) were tested, as well as a RR predictor array. Improvements were noted with variations from the basic Markov process but all detectors showed room for improvement.

In an attempt to improve the performances achieved in (Moody and Mark, 1983), Artis, Mark and Moody (1991) used an artificial neural network to detect atrial fibrillation. The inputs to the network were the cells of a so-called generalized interval transition matrix. Each RR interval was classified as short, normal or long and pairs of intervals were assigned to cells of the matrix. A sliding window of intervals was adopted, allowing a beat-by-beat classification. Atrial fibrillation sensitivity and positive predictive accuracy were respectively of 92.86 and 92.34%.

More recently other studies continued to use RR-based features for ECG classification tasks. In (Tsipouras, Fotiadis and Sideris, 2005) both beat and arrhythmia classifications were attempted. First, using a set of decision rules based on three RR intervals, beats were classified as normal, premature ventricular contractions, ventricular flutter/fibrillation or 2nd heart block. The classifications were then used as input to a deterministic automaton to detect and classify arrhythmic episodes. Six arrhythmias were considered: ventricular bigeminy, ventricular trigeminy, ventricular couplet, ventricular

tachycardia, ventricular flutter/fibrillation and 2nd heart block. 98% accuracy for arrhythmic beat classification and 94% accuracy for arrhythmic episode detection and classification were achieved.

Kaiser, Kirst and Kunze (2010) attempted to classify 5-minutes ECG records unto atrial fibrillation or no atrial fibrillation (including normal sinus rhythm and different arrhythmias). Since the authors intended to use the algorithms on mobile devices they developed low processing power techniques. Features were extracted from the RR interval tachogram. More precisely, the maximum difference between any two RR intervals and the variance of the set of RR interval durations were computed. A decision tree based on threshold comparisons was then used to classify the segments. To improve the performance of the classifier a second analysis helped by morphological filters was included. Alternative tachograms were generated in this way which increased the classification specificity of arrhythmias included in the non-atrial fibrillation dataset. A sensitivity of 99.1% and a specificity of 88.3% were achieved.

Although features based on the RR interval offered promising results, not all type of beats and rhythms can be distinguished based solely on such measurements. Therefore many authors chose to explore the potential of other features. More than two decades ago, Thakor and Zhu (1991) dealt with adaptive filtering techniques applied to ECG signals. Besides noise cancellation, the authors stated that arrhythmia detection issues could also benefit from this analysis. Particularly, by adaptively cancelling the QRS-T complex one could detect the presence of ectopic beats because of their abnormal morphology or analyze a paced rhythm and monitor pacemaker performance and failure. Atrial fibrillation detection could also benefit from adaptive filtering since the atrial rhythm can be separated and autocorrelation functions may afterwards be used for classification.

A distinction between normal beats, premature atrial contractions (PAC) and premature ventricular contractions (PVC) was attempted in (Chiu, Lin and Liau, 2005). The authors used a template for each one of these beat types and computed the normalized correlation coefficient between QRS complexes of templates and beat to be classified. A beat was classified as PVC if its correlation coefficient with the PVC template was higher than the one with the normal beat template. Additional information concerning the RR interval duration was used to define whether or not a beat should be classified as PAC. Positive predictive values of 99.44, 100 and 95.35% for, respectively, normal beats, PACs and PVCs were reached. Reported values for sensitivity were 99.81, 81.82 and 95.83%, respectively for normal beats, PACs and PVCs. It should be noted that the testing set was small, namely regarding PACs and PVCs (9 and 24 beats, respectively).

Ge, Srinivasan and Krishnan (2002) used segments of 1.2 seconds around the R peak to distinguish between normal ECGs, atrial premature contractions, premature ventricular contractions, supraventricular tachycardia, ventricular tachycardia and ventricular fibrillation. ECGs were modelled using an autoregressive model and the coefficients were used to classify the arrhythmias by means of stage-by-stage generalized linear model. Different stages of the classifier were determined by the Euclidean distances between mean autoregressive coefficients from various classes. Accuracy values varied from 93.2% (for normal segments) to 100% (for ventricular tachycardia segments).

Numerous authors chose to construct a feature set containing both temporal and morphological information.

In (Iliev, Krasteva and Tabakov, 2007) a set of decision rules was established to classify beats as either normal or ventricular ectopic beats. Morphological and time-domain features were extracted. A QRS pattern matrix was constructed (holding information about amplitude-temporal distribution of QRS) and deviation of RR interval from the mean RR interval was also considered. Sensitivity and specificity values were reported to be respectively 99.81 and 98.87% in a noise-free test set.

De Chazal, O'Dwyer and Reilly (2004) compared the performance of 12 classifier configurations in distinguishing 5 different beat types. Three categories of features were used: RR interval features, heartbeat interval features and ECG morphology features. Classifier configurations were based on linear discriminants (LDs), a statistical classifier model. The best results were obtained when two leads were used for classification (two LD classifiers employed) and the results were posteriorly combined. For supraventricular ectopic beats sensitivity and positive predictive values of 75.9 and 38.5% were obtained. Regarding ventricular ectopic beats, the sensitivity was 77.7% and the positive predictivity was 81.9%.

In (Melgani and Bazi, 2008) multiple tests were performed to compare the performance of different classifiers on distinguishing between normal beats, atrial premature beats, ventricular premature beats, right bundle branch block, left bundle branch block and paced beats. Focus was given to support vector machines and a new improved method consisting on the combination of particle swarm optimization with this classifier to improve its generalization performance. The two other classifiers used as reference were the k-nearest neighbor and the neural network and some tests included a feature selection step with principal component analysis Two types of features were extracted: morphological and temporal (QRS complex duration, RR interval and average RR interval over the 10 last beats). The authors reported an overall accuracy of 89.72% with the proposed method which was higher than the values obtained with other classifiers.

The potential of neural networks was explored from early on and continues to be one of the main machine learning classifiers used in ECG beat/rhythm analysis.

In (Hu *et al.*, 1993) an artificial neural network was used to distinguish between normal and abnormal beat patterns, as well as to classify 12 different abnormal beat morphologies. Inputs to the network consisted of an amplitude-scaled QRS beat pattern. When using a composite classifier where the first network distinguished between normal and abnormal morphologies and the second one classified the abnormal beats, a classification rate of 84.5% was obtained. Accuracy varied greatly between beat types.

Clayton, Murray and Campbell (1994) attempted to use neural networks to distinguish between ventricular fibrillation (VF) and VF-like events. Inputs to the network consisted of 5 frequency domain parameters derived from the Fourier spectrum of the signal and the mean threshold crossing interval.

Testing the classifier with segments of 4.096 seconds, sensitivity and specificity reached values of 84 and 59% respectively.

In (Yang, Devine and Macfarlane, 1994) the authors focused on observations and measures from 12-lead ECGs and chose the following 9 features: PR interval variability, RR interval regularity, presence or absence of discrete P-waves in the praecordial leads, presence or absence of discrete P waves in the limb leads, presence or absence of multiple P waves, percentage regularity of RR interval, number of leads with definite P-waves, maximum PR interval, minimum PR interval. They were interested in distinguishing atrial fibrillation ECG records from normal ones which may include supraventricular extrasystoles or ventricular extrasystoles. A comparison between deterministic logic and artificial neural network classifiers was undertaken and the possibility of combining both was also explored. The best results were obtained with the artificial neural network for which sensitivity and specificity reached values of 92.0 and 92.3% respectively.

Silipo and Marchesi (1998) explored the potential of artificial neural networks in three different ECG analysis tasks: beat classification, myocardial ischemia and chronic alterations. Normal beats, ventricular ectopic beats and supraventricular ectopic beats were considered for classification. Interestingly, the authors used an artificial neural network structured as an autoassociator so as to be able to reject unknown patterns (new or ambiguous beats). The input vector to the network consisted of samples of the beat and a measure of its prematurity degree based on RR interval measurements. Tests with different beat types included in the training set were performed. When the three beat types were considered, normal and ventricular ectopic beats were more easily recognized (99 and 96% respectively) than supraventricular ectopic beats (75%).

In (Ceylan and Özbay, 2007) 10 different rhythms were distinguished using an artificial neural network classifier. Four different structures were formed combining the network with feature extraction techniques (wavelet transform or principal component analysis (PCA)) and/or a data reduction method, fuzzy c-means clustering (FCM). The authors stated that the best combination was FCM – PCA – neural network which achieved an average test error of 0.91% with a reduced training time.

Time and time-frequency features extracted from the RR interval tachogram were used in (Tsipouras and Fotiadis, 2004) with classification purposes. Segments of 32 RR intervals were classified as either normal or arrhythmic depending on the number of normal beat types within it. In this study time domain features were SDNN (standard deviation of the normal-to-normal, NN, intervals), RMSSD (square root of the mean squared differences of successive NN intervals), pNN5 (proportion derived by dividing the number of interval differences of successive NN intervals greater than 5 milliseconds by the total number of NN intervals), pNN10, pNN50 and the standard deviation of successive differences of all normal-to-normal RR intervals. For time-frequency analysis, short time Fourier transform and 18 time-frequency distributions were used to compute the power spectral density and 6 features were chosen to represent each case. Classification was carried out by feeding to a neural network the features extracted and then use the outputs to apply a set of decision rules. The proposed

algorithms reached sensitivity and specificity values of 87.5 and 89.5%, respectively, for time domain analysis and 90 and 93%, respectively, for time-frequency domain analysis.

If artificial neural networks have drawn considerable attention as classifiers, wavelet transforms have earned their place in the feature extraction process. Compared to other frequency analysis methods, e.g. Fourier transform, wavelet analysis allows a multi-scale decomposition and overcomes some drawbacks in terms of frequency resolution.

Classification of normal sinus rhythm, atrial fibrillation, ventricular fibrillation and ventricular tachycardia ECG records was addressed in (Khadra, Al-Fahoum and Al-Nashash, 1997). The wavelet transform of the signal was computed and energy parameters were retrieved from the scalogram (squared magnitude of the wavelet transform). Different time-frequency bands were defined and the energy of the signal within each region was computed. Signals were classified as one of the 4 rhythms according to a set of rules. A relatively small number of ECG records was used and sensitivity and specificity values lied between 83.3 and 92.3%.

In (Al-Fahoum and Howitt, 1999) an attempt was made to distinguish between the same four rhythms. Wavelet transforms (WTs) were used to extract features and a radial basis function neural network was adopted as classifier. A beat-by-beat classification was performed. The feature vector consisted of 3 relative energy terms used to characterize the QRS complex at different WT scales and relative energy in the signal before the QRS, in the QRS and after the QRS. An overall correct classification of 97.5% was achieved though sensitivity and specificity values varied widely between classes. Whereas 100% correct classification of ventricular fibrillation and ventricular tachycardia signals was obtained, the sensitivity and specificity of atrial fibrillation segments was respectively 95.2 and 85.7%.

Güler and Übeyli (2005) attempted to perform a beat-by-beat classification to distinguish between normal, congestive heart failure, ventricular tachyarrhythmia and atrial fibrillation beats. Statistical features were extracted from the wavelet coefficients to try to represent both the frequency distribution of the signal and changes in frequency distribution. These were: mean of the absolute values of the coefficients in each sub-band, average power of the wavelet coefficients in each sub-band, standard deviation of the coefficients in each sub-band and ratio of the absolute mean values of adjacent sub-bands. A combined neural network model, where the outputs of the first set of networks were fed to a second level network, was employed. An overall classification accuracy of 96.94% was achieved.

Kara and Okandan (2007) developed a method to distinguish between normal sinus rhythm and atrial fibrillation ECG segments. Wavelet theory was used to decompose the 60 seconds signals until the sixth level and power spectral density of each one of the 6 details and one approximation signals were computed. Average power spectral density values over 6 frequency sub-bands were then obtained which amounted to a total of 42 features per ECG segment. Of these features, 22 were used as input to an artificial neural network. The authors reported an accuracy of 100% in a test set composed by 24 normal ECGs and 28 atrial fibrillation segments.

Martis *et al.* (2012) compared the performance of a neural network (NN), a support vector machine (SVM) and a Gaussian mixture model (GMM) in the distinction between normal beats and 12 different beat types. Features were extracted from the wavelet decomposition of the signal. A feature selection method, principal component analysis, was applied to the sub-bands that covered the frequencies of interest. This reduced set of coefficients was then fed to the classifiers. Overall accuracy values of 87.36, 93.41 and 95.60% were obtained for GMM, NN and SVM classifiers respectively.

Other studies have tested the possibility of constructing a feature set not based solely on parameters extracted from the wavelet transform. In (Prasad and Sahambi, 2003), information about RR intervals was used in combination with 23 selected wavelet transform coefficients to distinguish between normal and 12 abnormal beat types. An artificial neural network was used as classifier and an overall accuracy of 96.77% was reached. More recently beat classification was achieved after an adaptive feature extraction method was applied to a large set of features (Shen *et al.*, 2012). These included wavelet coefficients, statistical properties of the coefficients and electrophysiological measures (RR interval information, amplitude of waves, ratio between different intervals,etc.). The classification scheme included the use of k-means clustering, one-against-one support vector machine and a modified majority voting mechanism. A recognition rate of 98.92% was reported by the authors but accuracy varied between beat types.

Classification of normal, premature ventricular contraction and other beat types was attempted in (Inan, Giovangrandi and Kovacs, 2006). The feature set combined a set of coefficients from the wavelet transform and timing information. A neural network classifier was employed. Timing information consisted of a RR interval ratio which translates the deviation from a constant beat rate. Multiple tests were performed regarding both the decomposition level and the feature vector length. The best results led to an accuracy of 95.2%.

In (Sambhu and Umesh, 2013) a beat classification scheme was proposed to distinguish between normal beats, left and right bundle branch block, atrial and ventricular premature contractions, paced and fusion beats. A combination of temporal, morphological and statistical features was used for classification. Some of these features were extracted after wavelet decomposition of the signal. Prior to classification, a feature selection method was employed. Multiple one-against-one support vector machines were employed and the final classification was given by a maximum voting mechanism. The authors reported an overall accuracy superior to 98%.

In (Ye, Kumar and Coimbra, 2012), 16 different beat types were considered for classification. Morphological features were extracted by two different methods: wavelet decomposition of the signal and independent component analysis. Feature reduction of this set of features was achieved resorting to principal component analysis. Four dynamic features were also considered: previous RR, post RR, local RR and average RR. The signal recorded by each one of the two leads was independently classified by a support vector machine and a final decision was taken by fusing the two results. Overall accuracies of 99.3 and 86.4% were obtained respectively for the “class-oriented” and “subject-oriented” approaches.

In the last few years some studies were published were new approaches regarding the features for classification were explored. In (Wang *et al.*, 2001) a new approach that deals with the nonlinear and non-stationary characteristics of the ECG from the viewpoint of multifractality was presented. Atrial fibrillation, ventricular tachycardia and ventricular fibrillation ECG records were considered for classification. Short-time generalized dimensions were computed and input to a new fuzzy Kohonen network. Accuracy values of 97.8, 97.2 and 99.4% were reported respectively for ventricular tachycardia, ventricular fibrillation and atrial fibrillation. Specificity values were higher for atrial fibrillation and ventricular tachycardia records.

Owis *et al.* (2002) focused on the nonlinear dynamics of ECG signals to detect and classify arrhythmias. Two features from the field of chaotic dynamical system theory were chosen to represent 3 seconds ECG signals: the correlation dimension and the largest Lyapunov exponent. An attempt was made to distinguish between normal and abnormal ECG signals and to classify the different types of arrhythmias. These included ventricular couplet, ventricular tachycardia, ventricular bigeminy and ventricular fibrillation. The performance in such tasks of the minimum distance classifier, the k-NN classifier and Bayes minimum error classifier was accessed. The statistical analysis carried out showed the potential of the two features in the detection of ECG abnormalities but the ability to distinguish between types of arrhythmias was limited. Specificity and sensitivity values varied among classifiers.

Bakhshi *et al.* (2010) developed a linear classifier based on instantaneous frequency (IF) to distinguish between normal signals and diseased ones. The IF was estimated using the discrete power spectral density calculated by means of the Fourier transform of the ECG signal. Sensitivity and specificity values were reported to be respectively of 97.82 and 100% for 5 minutes portions of ECG records.

In (Anas, Lee and Hasan, 2010) the authors focused on ventricular tachycardia (VT) and ventricular fibrillation (VF) ECG records with the purpose of identifying such arrhythmias. A sequential detection algorithm was developed and the first step consisted of separating VT/VF signals from the remaining ones. This was achieved by computing the mean absolute value of a signal and comparing it to a predefined threshold value. An accuracy of 99.07% with a specificity value of 99.39% was obtained. In a second step an attempt was made to distinguish between VT and VF. In order to do so the authors used empirical mode decomposition to extract the intrinsic mode functions from the signals. The difference between the original signal and the sum of its first two intrinsic mode functions was then computed. The mean absolute value of this difference signal was used to classify VT and VF signals. The authors further went on to distinguish between shockable and non-shockable rhythms by determining the heart rate. An overall accuracy of 99.21% was reported.

Sufi, Khalil and Mahmood (2011) adopted an original approach for ECG diagnosis: the feature extraction process was carried out directly on the compressed ECG. By circumventing the decompression phase, compressed and encrypted ECG packets sent by a mobile phone to a monitoring service could be promptly analyzed and further delays avoided. A set of 157 attributes, corresponding to the frequency of each character/numeric sub groups, was extracted and a correlation

based feature subset selection technique was then applied. A statistical clustering technique, expectation maximization algorithm, was used to distinguish between normal and abnormal ECGs. A 100% accuracy rate was reported in a small test set of 20 segments.

In this work two types of features are used: spectral features extracted using the wavelet transform and an estimation of the power spectral density; and time domain parameters translating heart rate characteristics. The performance of three classifiers is compared: k-nearest neighbor, multilayer perceptron and support vector machine. Before detailing the methodology followed, the theoretic concepts necessary are reviewed.

3.2 Wavelet Transform

Wavelet analysis is a powerful tool to obtain a time-frequency representation of a signal. Contrary to short time Fourier transform (STFT) the wavelet transform is a multi-resolution analysis and therefore overcomes the difficulty of finding an optimal resolution for analyzing the signal. It allows us to examine the low frequency content (spread over a larger amount of time) without compromising the accurate time domain localization of high frequency features. After the choice of an analyzing wavelet function, $\psi(t)$, the wavelet transform of a continuous time signal $x(t)$ is defined as:

$$W_a x(b) = \frac{1}{\sqrt{a}} \int_{-\infty}^{+\infty} x(t) \psi^* \left(\frac{t-b}{a} \right) dt \quad (1)$$

where a and b are respectively the dilation and location parameter of the wavelet and $\psi^*(t)$ is the complex conjugate of the analyzing wavelet function. For it to be considered as analyzing wavelet, the function should satisfy a number of mathematical properties. These are reviewed in (Addison, 2005); in particular, the function must have finite energy and respect the admissibility condition which implies a zero average. The analyzing wavelet function is also referred to as mother wavelet since a family of functions is defined from this prototype by applying translations and dilations. The wavelet transform can therefore be seen as the decomposition of the signal by this set of basis functions.

A discretized version of the continuous wavelet transform described above is often used and a dyadic grid, with $a = 2^m$ and $b = 2^m n$, is commonly employed. The basis functions can then be written as:

$$\psi_{m,n}(t) = 2^{-m/2} \psi(2^{-m} t - n) \quad (2)$$

A fast implementation of the decomposition algorithm can be achieved by recursively applying high-pass and low-pass filters to the wavelet coefficients from the previous scale. This filter bank algorithm, presented by Mallat (1989), is illustrated in Figure 16. The filter coefficients of the high-pass, H, and low-pass, G, decomposition filters characterize the wavelet used.

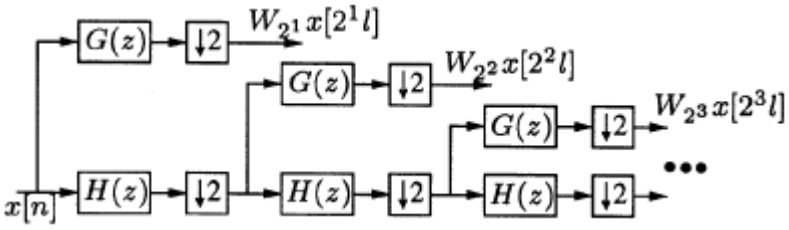

Figure 16: Mallat's algorithm for discrete wavelet decomposition (Martínez *et al.*, 2004).

The redundant discrete wavelet transform (RDWT), or *algorithme à trous*, can also be used to decompose the signal. This discretized version of the continuous wavelet transform is shift invariant, having the same spatial sampling rate in all scales. The downsampling operations represented in Figure 16 are discarded, and the filter responses are upsampled. Additional information concerning the RDWT and its implementation can be found in (Fowler, 2005).

In the last couple of decades, applications of wavelet theory to ECG analysis have been largely explored (Addison, 2005). These include signal denoising, detection and delineation of ECG characteristic points, heart rate variability analysis, ECG data compression and feature extraction for beat/rhythm classification. The choice of mother wavelet is an important step in all these applications and multiple functions have been tested including Daubechies, Morlet, spline, raised cosine and quadratic spline wavelets.

3.3 Power Spectral Density

The power spectral density (PSD) represents the distribution of the signal power over different frequencies. Welch's method is commonly employed to compute the PSD (Welch, 1967). The signal $x(j), j = 0, \dots, N-1$ is first split into K possibly overlapped segments of length L as illustrated by Figure 17. A window $w(j), j = 0, \dots, N-1$ is applied to each segment and the finite Fourier transform of these sequences are then computed as given by equation (3).

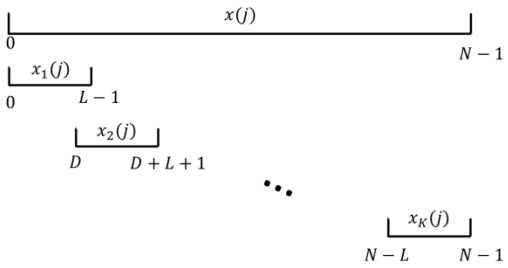

Figure 17: Schematic representation of the splitting of the signal.

$$A_k(n) = \frac{1}{L}\sum_{j=0}^{L-1} x_k(j)w(j)e^{-\frac{2kijn}{L}} \tag{3}$$

The so-called modified periodograms are obtained after squaring the magnitude of the result:

$$I_k(f_n) = \frac{L}{U}|A_k(n)|^2 \quad k = 1,2,\dots,K \tag{4}$$

where f_n and U are respectively given by:

$$f_n = \frac{n}{L} \quad n = 0,\dots,L/2 \tag{5}$$

$$U = \frac{1}{L}\sum_{j=0}^{L-1} w^2(j) \tag{6}$$

Finally, the spectral estimate $\hat{P}$ is the average of the individual periodograms:

$$\hat{P}(f_n) = \frac{1}{K}\sum_{k=1}^{K} I_k(f_n) \tag{7}$$

3.4 Classifiers

3.4.1 k-Nearest Neighbors

The concept behind the k-nearest neighbors (kNN) classifier is a very simple one. Assuming we have a dataset for which we know the true labels of the samples, new samples can be classified according to their similarity with labeled samples. A set of features is chosen to represent each sample and the similarity between samples is measured resorting to a metric. If desired, different weights can be attributed to the neighbors, assuring for instance that closest neighbors contribute in a larger extent to the fit. The 'training set' is used to construct a neighbor base and the test patterns are classified according to the class of the k most similar neighbors. An example of binary classification using two features is shown in Figure 18. A more detailed explanation of this classifier can be found in (Duda, Hart and Stork, 2001).

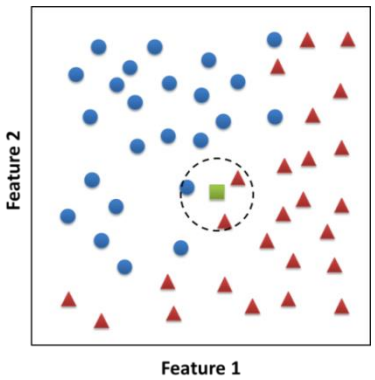

Figure 18: Example of kNN binary classification problem. Two features are used to distinguish between class 1, blue circles, and class 2, red triangles. When 3 neighbors are used for classification the test sample (green square) is assigned to class 2.

3.4.2 Multilayer Perceptrons

Multilayer perceptrons (MLP) are the most widely used type of artificial neural network (ANN). The architecture of one such network, feedforward in nature, is represented in Figure 19. Each circle represents a unit, or neuron, and a weight is associated to each connection between units. Three types of layers can be distinguished: input layer, hidden layer and output layer.

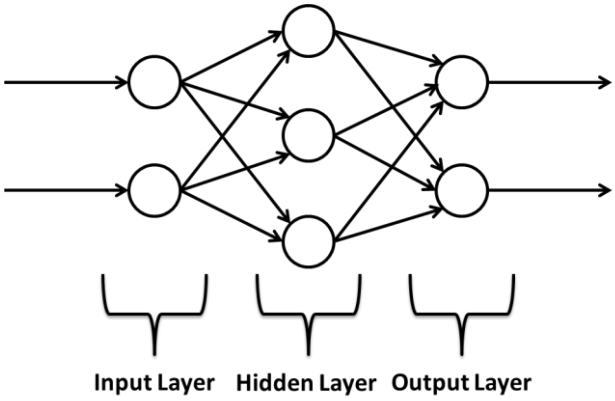

Figure 19: A multilayer perceptron with 2 neurons in the input layer, 3 in the hidden layer and 2 in the output layer.

Each neuron has the structure represented in Figure 20. The sum of the inputs to the unit i, s_i, is passed through a nonlinearity or activation function, S, as given by Equations 8 and 9. The activation function can be any differentiable function. The logistic function and the hyperbolic tangent are often used.

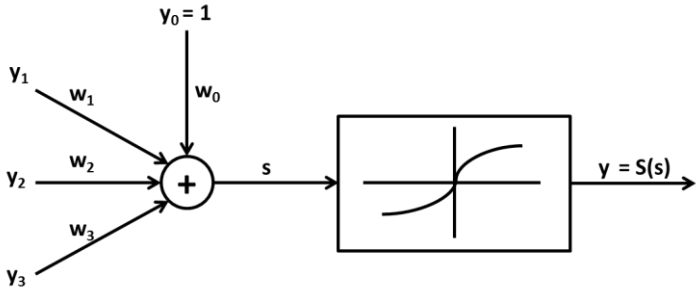

Figure 20: Basic architecture of a neuron with 4 inputs including one bias term. The sum of the inputs is then passed through a nonlinear function S.

$$s_i = \sum_{j=0}^{N} w_{ji} y_j \tag{8}$$

$$y_i = S(s_i) \tag{9}$$

Training the network consists of feeding the network with training patterns and adjusting the weights according to the desired output. That is, varying the weights in such a way that a predefined cost

function is minimized. This cost function can simply be a measure of the error between output and desired output. For each training pattern k, with $k = 1, \dots, K$, if $\boldsymbol{o}^k$ and $\boldsymbol{d}^k$ are, respectively, outputs and desired outputs, the error vector will be given by:

$$\boldsymbol{e}^k = \boldsymbol{o}^k - \boldsymbol{d}^k \tag{10}$$

For each training pattern a scalar measure of the error can be given by Equation (11) and, in the whole training set, the deviation of the network from its ideal behavior is given by Equation (12).

$$E^k = \|\boldsymbol{e}^k\|^2 \tag{11}$$

$$E = \sum_{k=1}^{K} E^k \tag{12}$$

The gradient descent method can then be used to update the weights:

$$\boldsymbol{w}^{n+1} = \boldsymbol{w}^n - \eta \nabla E \tag{13}$$

where η is the step size parameter, or learning rate. The main difficulty of this method is the computation of the gradient components. In practice this is achieved by using the backpropagation method. A new network, the error propagation network, is constructed from the initial network by linearizing nonlinear elements and reversing it. Each training pattern is input to the original network and the partial derivative of the error with respect to the output is then input to the error propagation network. The partial derivative relative to a weight is then simply given by the product of the inputs of the branches corresponding to that weight in the original network and in the backpropagation network. The training phase ends when a stopping criterion is reached (usually either when the error is below a predefined threshold or when the maximum number of epochs is reached). More details about the backpropagation algorithm, including examples, can be found in (Beale and Fiesler, 1997).

Training the network may become a very lengthy process. To deal with this limitation acceleration techniques are often adopted (e.g. adaptive step sizes or momentum). The weight update considering the momentum technique is given by the following equations:

$$\boldsymbol{w}^{n+1} = \boldsymbol{w}^n + \Delta \boldsymbol{w}^n \tag{14}$$

$$\Delta \boldsymbol{w}^n = -\eta \nabla E + \alpha \Delta \boldsymbol{w}^{n-1} \tag{15}$$

where α is the momentum term, $0 \leq \alpha < 1$. These equations can be interpreted as follows. At valleys where the gradient is relatively constant in terms of direction, the α term contributes to an increase of the contribution of this gradient at each iteration. This results in an increased speed of convergence. On the other hand, at points where the gradient oscillates a lot, this term cancels relatively well the gradient term depending on η, thus dampening oscillations.

3.4.3 Support Vector Machines

SVMs, like ANNs and kNN, are a type of supervised learning classifiers. Considering the example illustrated in Figure 21, the goal of the training process is to define the parameters that describe the boundary between the two different classes (boundary represented by a continuous line). This boundary should be the one that lies as far as possible from the closest training patterns. Once a new sample is presented it will be classified according to the side of the boundary it falls upon. Dashed lines represent the margins and the samples highlighted in green are referred to as support vectors. As can be seen these are the samples that lie the closest to the boundary. Although a two-dimensional problem is pictured here (only two features for each pattern), the idea is exactly the same for N-dimensional linearly separable data. In such case the boundary and margins will be hyperplanes.

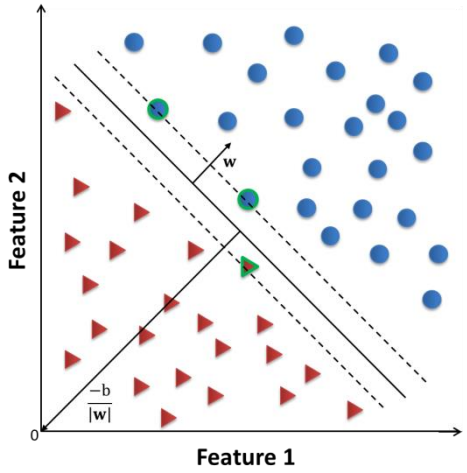

Figure 21: Example of a SVM binary classification problem. Highlighted in green are the three support vectors. Continuous and dashed lines represent respectively decision boundary and margins.

To describe the problem from a mathematical point of view let us consider that M training patterns of dimension N are available: $\boldsymbol{x}_i \; where \; i = 1 \dots M, \; \boldsymbol{x} \in \mathcal{R}^N$. We shall denote the class of the training pattern i by y_i. Each pattern belongs to one of the following two classes: $y_i = +1$ or $y_i = -1$. If $\boldsymbol{w}$ is normal to the hyperplane and $\frac{b}{\|\boldsymbol{w}\|}$ is the distance from the hyperplane to the origin, the hyperplane is described by $\boldsymbol{x} \cdot \boldsymbol{w} + b = 0$. The training patterns will then satisfy equations (16) and (17) which can be combined to (17).

$$\boldsymbol{x}_i \cdot \boldsymbol{w} + b \geq +1 \quad \text{for } y_i = +1 \tag{16}$$

$$\boldsymbol{x}_i \cdot \boldsymbol{w} + b \leq -1 \quad \text{for } y_i = -1 \tag{17}$$

$$y_i(\boldsymbol{x}_i \cdot \boldsymbol{w} + b) - 1 \geq 0 \quad \forall i \tag{18}$$

In order to maximize the margins, which are simply the distance between support vectors and the boundary, we must find the parameters $\boldsymbol{w}$ and b that respect:

$$\min \|\boldsymbol{w}\| \quad \text{such that} \quad y_i(\boldsymbol{x}_i \cdot \boldsymbol{w} + b) - 1 \geq 0 \quad \forall i \tag{19}$$

Since minimizing $\|\boldsymbol{w}\|$ is equivalent to minimizing $\frac{1}{2}\|\boldsymbol{w}\|^2$, this term can be substituted in the equation above. The problem is then reduced to a convex quadratic optimization problem and Lagrange multipliers are used to take into account the constraint (Fletcher, 2009).

The example considered here is a very simple one where the classes are fully linearly separable. In practice this is not the case and it becomes necessary to adjust equations (16) and (17) to allow misclassifications. This is done considering a new slack variable ξ_i for each training pattern i with $\xi_i \geq 0$ for all patterns. For each pattern the associated variable measures its degree of misclassification. Equations (20) and (21) are obtained and can be combined into equation (22). This formulation is commonly referred to as soft margin SVM.

$$\boldsymbol{x}_i \cdot \boldsymbol{w} + b \geq +1 - \xi_i \quad \text{for } y_i = +1 \tag{20}$$

$$\boldsymbol{x}_i \cdot \boldsymbol{w} + b \leq -1 + \xi_i \quad \text{for } y_i = -1 \tag{21}$$

$$y_i(\boldsymbol{x}_i \cdot \boldsymbol{w} + b) - 1 + \xi_i \geq 0 \quad \forall i \tag{22}$$

The new function to minimize is given by equation (23). A balance between maximizing the margins and reducing the number of misclassifications is sought. To control the trade-off between these two goals a penalty parameter C is introduced. By increasing C we ensure that more training patterns will be correctly classified, at the expense of a more complex, unsmooth, boundary surface. If a very high value is chosen for C then the classifier may lose its generalization capability.

$$\min \frac{1}{2}\|\boldsymbol{w}\|^2 + C\sum_{i=1}^{L}\xi_i \qquad \text{s.t.} \qquad y_i(\boldsymbol{x}_i \cdot \boldsymbol{w} + b) - 1 + \xi_i \geq 0 \quad \forall i \tag{23}$$

Until now it was assumed that the classes are linearly separable. However this is seldom the case and it becomes necessary to recur to a more complex procedure. The idea is to map the original features into a different feature space (commonly with a higher dimensionality) where they become linearly separable. In practice this mapping is done implicitly by using the well-known kernel trick (Fletcher, 2009).

SVMs were originally developed to solve binary classification problems. However, it is much more common to deal with multiclass problems. Multiple approaches have been proposed to adapt the SVM formulation for these types of problems. The one-against-one and the one against-all SVMs are the two most popular formulations. Here, the one-against-one approach was used, which has been shown to be a suitable choice (Hsu and Lin, 2002). For each pair of classes, a binary classifier is constructed, amounting to a total of $k(k-1)/2$ classifiers, where k is the total number of classes. Each classifier is trained using data from the two corresponding classes. Once a new pattern is presented all classifiers are 'activated' to assign it a label. The selected class label is the one that occurs the most.

4. Methodology

The methodology proposed in this thesis is schematized in Figure 22, encompassing the following steps: signal acquisition and processing (including filtering and segmentation steps) and finally rhythm classification.

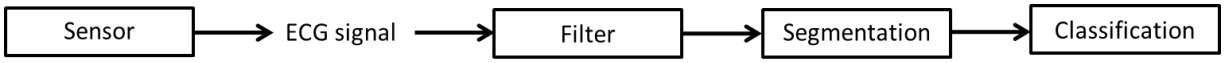

Figure 22: Automatic signal analysis methodology.

The classification phase is further detailed in Figure 23 where the main steps are feature extraction, feature normalization, classifier training and testing.

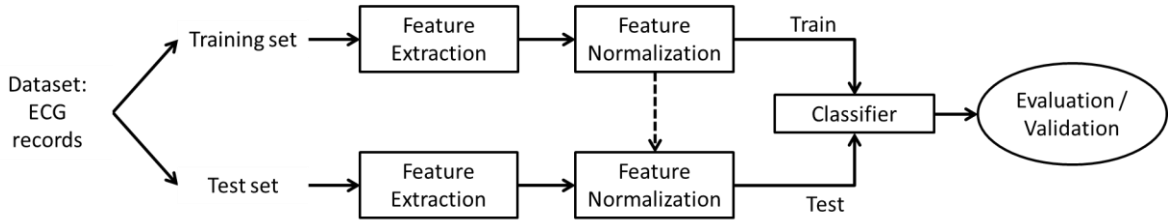

Figure 23: Steps of the classification task.

In the following subsections all the steps mentioned above will be detailed.

4.1 Signal Acquisition and Processing

4.1.1 BITalino system

The BITalino is a low-cost biosignal acquisition system (Guerreiro *et al*., 2013). It includes sensors for multiple physiological signals: electromyography, electrodermal activity and ECG. It further provides an accelerometer, a light sensor and a light-emitting diode. Software for real time acquisition and visualization is also available (Alves *et al*., 2013).

Figure 24: BITalino system used for ECG acquisitions.

Since a pervasive acquisition setup is sought, this system was used to acquire ECG records at the fingers. A sampling rate of 1000 Hz was used. It has been shown that the ECG acquired with the BITalino system at the fingers is highly correlated with lead I from traditional 12 leads systems (Carreiras *et al.*, 2013). It is therefore reasonable to expect that cardiac conditions that can be diagnosed by analyzing the lead I of the ECG can also be detected with this pervasive acquisition system.

4.1.2 Filtering

The filter process adopted here has been previously used with ECG data acquired with the BITalino system, mainly for biometric applications. First, two median filters are applied to remove the baseline, with window sizes of 0.2 and 0.3 seconds. A finite impulse response low-pass filter with cutoff frequency of 40 Hz is then used to deal with high frequency noise. Due to the characteristics of the acquisition system, muscular activity is frequently picked up, thus a final moving average filter, with a window of 28 milliseconds, is applied.

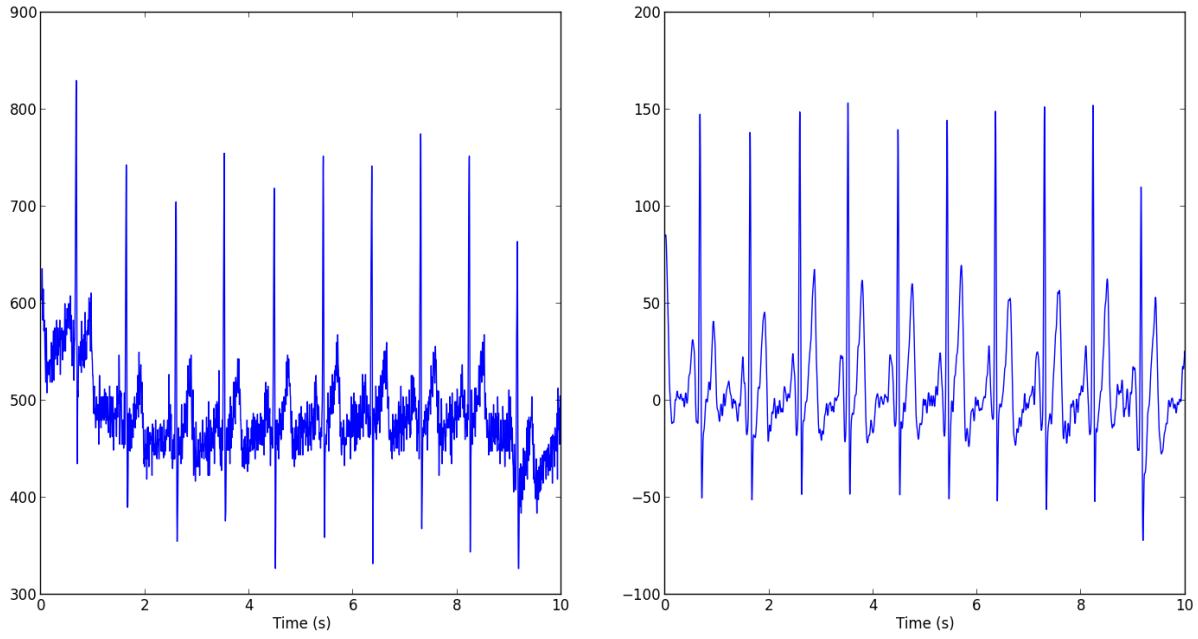

Figure 25: 10 seconds extract of an ECG acquired with the BITalino. Raw (left) and filtered (right) records are shown.

4.1.3 R peak detection

An algorithm based on the work of (Hamilton, 2002) was used to detect R peaks. As shown in Figure 26, the detection method starts with a filter step. First, low-pass and high-pass filters are applied to the signal, with cutoff frequencies respectively of 16 and 8 Hz. The derivative is then calculated and its absolute value is computed. Finally, a moving average with a window of 80 milliseconds is computed.

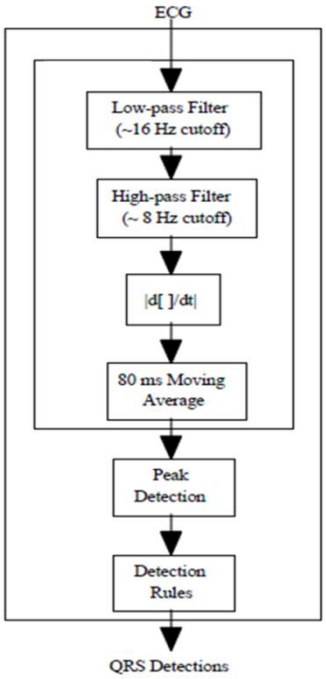

Figure 26: Schematic representation of the R peak detection algorithm. Adapted from (Hamilton, 2002).

Once the peaks are detected, they ought to be classified either as a QRS complex or noise. This decision relies upon a set of detection rules that take into consideration peak height, peak location (relative to the last QRS peak) and maximum derivative. The accuracy of the algorithm depends on the computation of a detection threshold, defined using QRS peaks and noise peaks heights, as shown in Equation 24.

$$\text{Detection Threshold} = \text{Average Noise Peak} + \text{TH} \times (\text{Average QRS Peak} - \text{Average Noise Peak}) \quad (24)$$

where TH is the threshold coefficient, which represents a compromise between correct and false detections. Decreasing the TH will lead to a higher number of correct detections, at the expense of false detections.

The following detection rules are applied:

1. All peaks that precede or follow larger peaks by less than 200 milliseconds are ignored.
2. If a peak occurs, the presence of both positive and negative slopes in the raw signal is checked. If these are not present, the peak represents a baseline shift.
3. If the peak occurred within 360 milliseconds of a previous detection, the value of the maximum derivative in the raw signal is checked. If it is smaller than half the maximum derivative of the previous detection, the peak is assumed to be a T-wave.
4. If the peak is larger than the detection threshold, it is considered a QRS complex, otherwise it should be considered noise.

5. If no QRS has been detected within 1.5 RR intervals, there was a peak that was larger than half the detection threshold, and the peak followed the preceding detection by at least 360 milliseconds, that peak should be considered a QRS complex

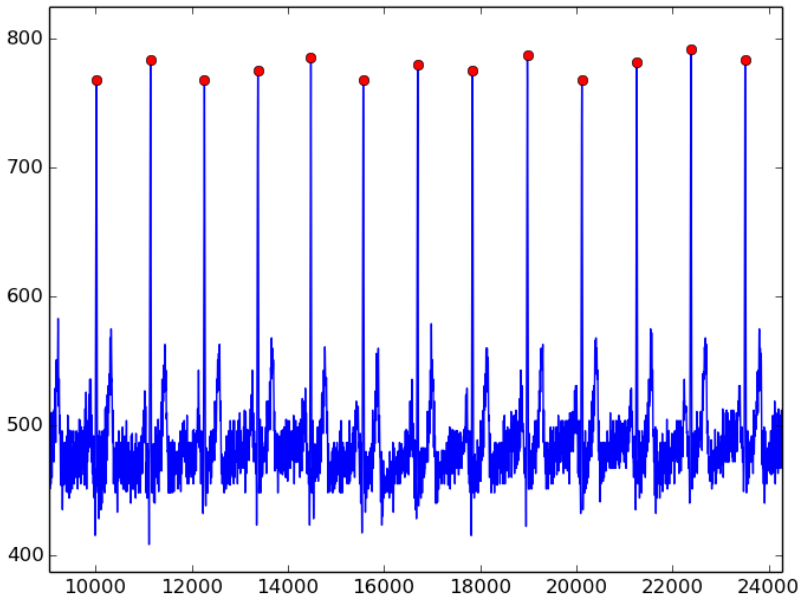

Figure 27: Result of the R peak detection algorithm on a normal sinus rhythm ECG.

Once the signal is processed, the classification task can be addressed, starting with the feature extraction process.

4.2 Feature Extraction

Two types of features were considered for rhythm classification: spectral features and time domain features. Spectral features were extracted using the wavelet transform and time domain parameters were used to provide information about heart rate characteristics.

4.2.1 Spectral Parameters

Spectral parameters were extracted following the scheme shown in Figure 28. The power spectral density (PSD) of the wavelet decomposition of the signals was computed and two different feature sets were constructed.

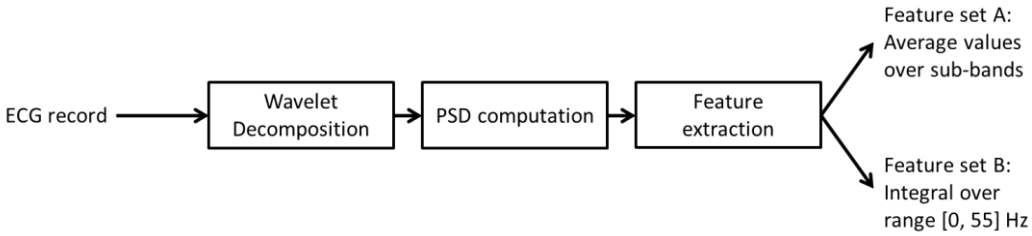

Figure 28: Feature extraction process of the spectral parameters.

Wavelet Decomposition

Signals were decomposed until the sixth level using the quadratic spline wavelet. The mother wavelet and the scaling function of the quadratic spline wavelet are represented in Figure 29. Details of this wavelet function and the coefficients of the corresponding finite impulse response filters are given in (Mallat and Zhong, 1992).

The quadratic spline wavelet has been mainly used for ECG delineation purposes because of the relation between ECG wave peaks and zero-crossings in the wavelet transform (Martínez *et al.*, 2004; Ranjith, Baby and Joseph, 2003). Inan, Giovangrandi and Kovacs (2006) used quadratic spline wavelets to extract features for a beat classification task. Here, quadratic spline wavelet decomposition is used to extract features for rhythm classification.

The decomposition was performed using the redundant discrete wavelet transform (RDWT), or *algorithme à trous* (Fowler, 2005).

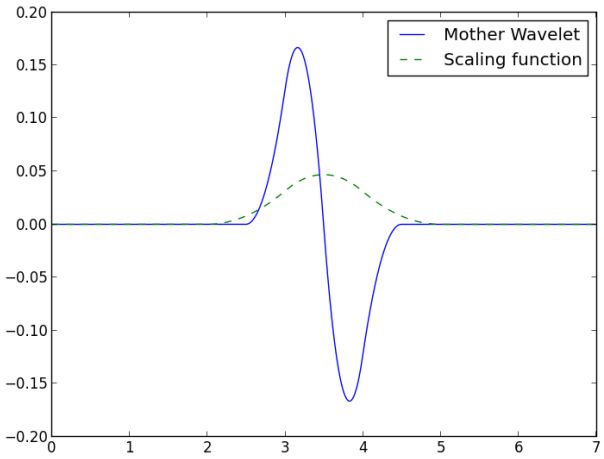

Figure 29: Mother wavelet and scaling function of the quadratic spline wavelet.

A 10 s extract of a sinus rhythm ECG is shown in Figure 30. In Figure 31 are represented the six detail and one approximation set of coefficients obtained from the wavelet decomposition.

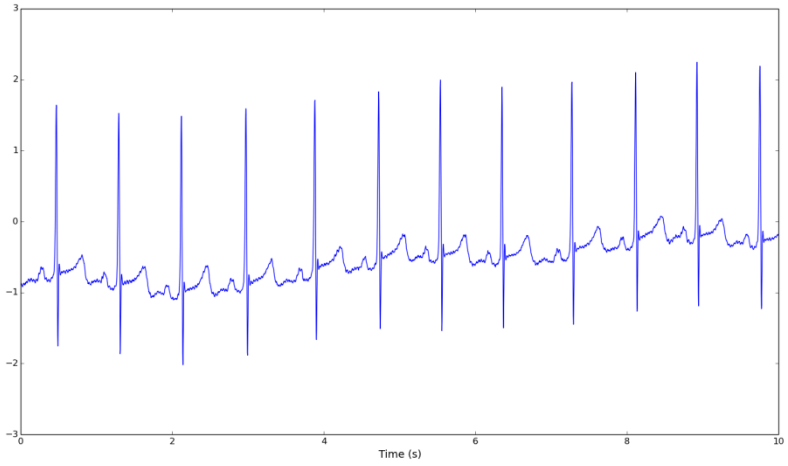

Figure 30: 10 seconds extract of a normal sinus rhythm ECG.

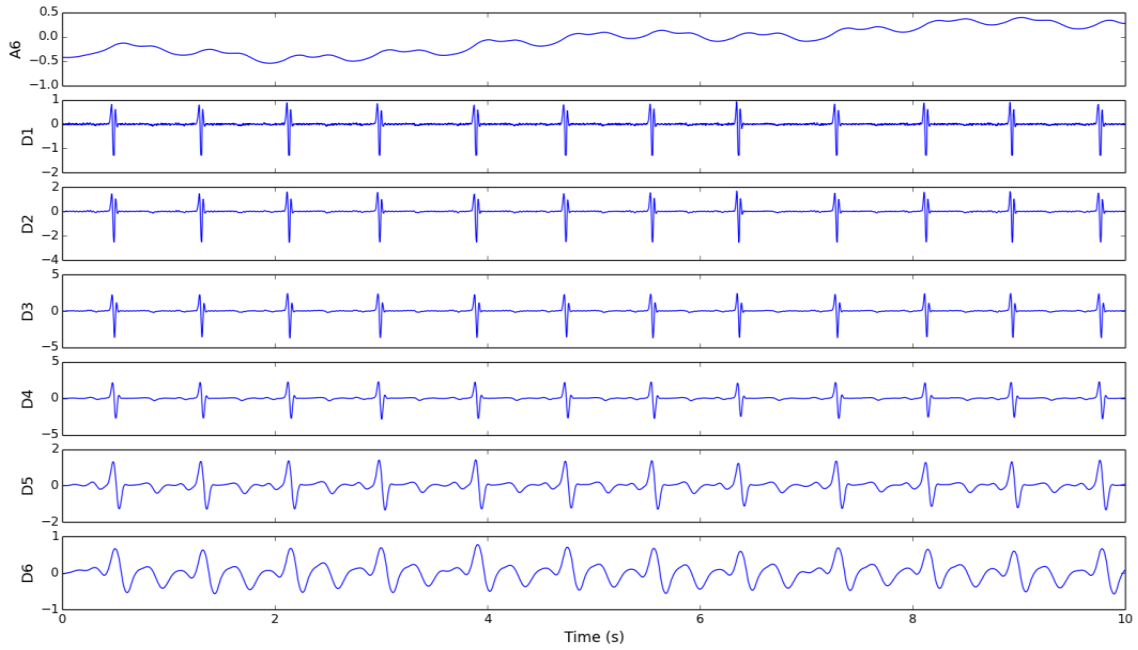

Figure 31: Approximation (A6) and detail (D1 to D6) coefficients of the wavelet decomposition of a 10 seconds normal sinus rhythm ECG.

Power Spectral Density Estimation

The PSD of each set of wavelet coefficients was estimated using Welch's method (Welch, 1967). Modified periodograms were computed over segments of 256 samples with 50% overlap and a Hanning window was employed. Figure 32 depicts the results of such estimation for the signal used above.

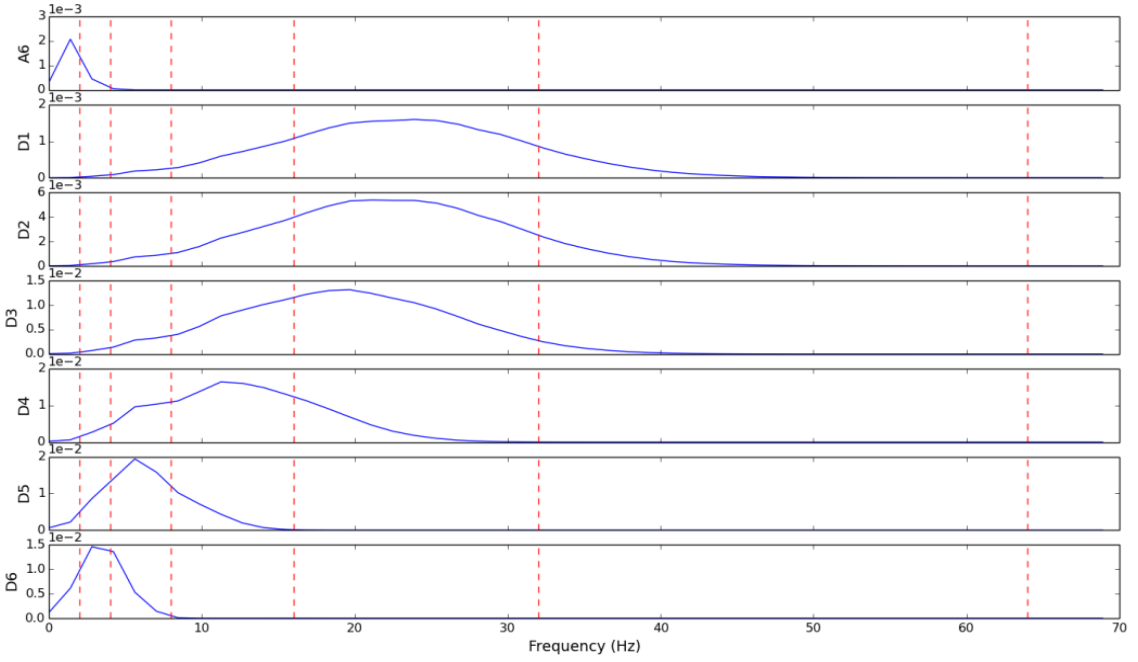

Figure 32: PSD of each one of the approximation (A6) and detail (D1 to D6) wavelet coefficients. Dotted red lines delimitate the sub-bands of feature set A.

Since the data was not filtered prior to wavelet decomposition, noise due to power line frequency is present in some records. This is clearly visible in the PSD of the detail signals of scale 1 and 2 where the power of 60 Hz and sometimes 30 Hz is considerable.

Two feature sets of wavelet-based features were extracted:

- For each one of the 7 PSD signals, the average value of the PSD over predefined sub-bands was computed. The 6 sub-bands considered were: [0, 2]; [2, 4]; [4, 8]; [8, 16]; [16, 32]; and [32, 64] Hz. These sub-bands are depicted in Figure 32. This feature set, henceforth referred to as feature set A, contains therefore 42 features (6 values for each one of the 7 signals). The same features are referred by Kara and Okandan (2007).
- For each one of the 7 PSD signals, the integral over the range [0, 55] Hz was calculated. This computation was performed using the trapezoidal rule. A total of 7 features are in this way selected to represent each pattern. This feature set shall be referred to as feature set B.

4.2.2 Time Domain Parameters

To complement the information given by spectral features, two time domain parameters were selected: average RR interval and standard deviation of RR intervals. These ought to be particularly interesting in the distinction of rhythms such as atrial fibrillation and normal rhythm due to the inherent irregularity of atrial fibrillation (refer to Figure 33). Feature set C contains these two parameters.

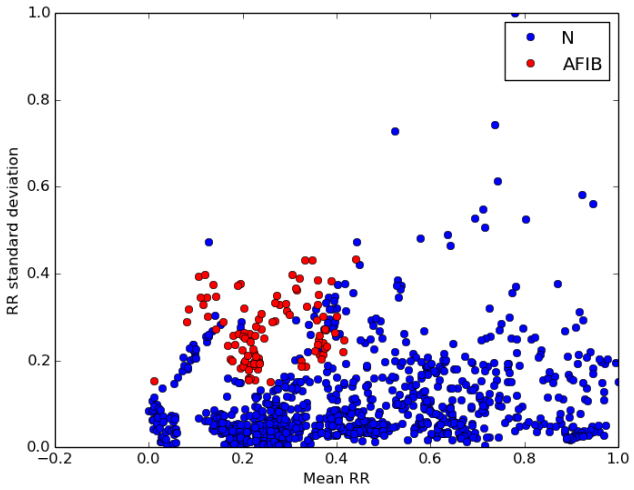

Figure 33: Distinction between normal sinus rhythm (N) and atrial fibrillation (AFIB) segments according to normalized average and standard deviation of RR intervals.

4.3 Feature Normalization

An important step in classification tasks is feature normalization. This can highly influence the classifier's performance. Once the dataset was divided into training and test sets, features from the training set were normalized and the same transformation was then applied to the test set. Two normalization schemes were considered: feature scaling to the range [0, 1] and feature standardization. These operations are detailed in Equations (25) and (26).

$$x_{scaled} = \frac{x - min\, x}{max\, x - min\, x} \tag{25}$$

$$x_{standardized} = \frac{x - \mu(x)}{\sigma(x)} \tag{26}$$

4.4 Classifiers

The three classifiers used for this analysis were the ones mentioned in the previous chapter: k-nearest neighbor, artificial neural network (more specifically multilayer perceptron) and support vector machine.

For the kNN classifier, the Euclidean metric was used to measure the distance between patterns. All neighbors were weighted equally. The most suitable number of neighbors used for each classification task was assessed by performing multiple tests.

Regarding the ANN classifier, the network was constructed with just one hidden layer. Input and output layers were linear and the activation function used for the hidden layer was the logistic sigmoid (Equation 27). Bias terms were included in the hidden and output layers. Figure 34 exemplifies the topology of the network for two input features, 3 neurons in the hidden layer and 2 outputs. For each classification task multiple tests were performed to choose the most suitable number of neurons in the hidden layer. The gradient descent method, combined with the momentum technique, was used to minimize the error and update the weights. Learning rate and momentum term were respectively set to 0.01 and 0.1. Backpropagation was used to compute the gradient terms. Each time the validation error hit a minimum, 10 more epochs were performed to check for a better result; the maximum number of epochs allowed was 1000. Additionally, 25% of the training set was used as validation set. This is meant to avoid overfitting of the network, thus assuring a better generalization capability.

$$S(s) = \frac{1}{1 + e^{-s}} \tag{27}$$

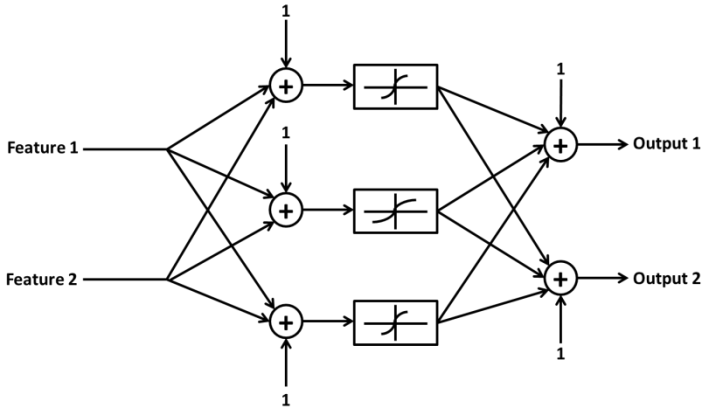

Figure 34: Example of the topology of a network with 2 input features, 3 hidden neurons and 2 outputs.

The kernel function used for classification with the SVM classifier was the radial basis function:

$$k(\boldsymbol{x}_i, \boldsymbol{x}_j) = e^{-\left(\frac{\|\boldsymbol{x}_i - \boldsymbol{x}_j\|^2}{2\sigma^2}\right)} = e^{-\left(\gamma \|\boldsymbol{x}_i - \boldsymbol{x}_j\|^2\right)} \quad with \quad \gamma = \frac{1}{2\sigma^2} \tag{28}$$

The kernel parameter γ (or σ) controls the kernel width and takes a user-defined value. The penalty parameter of the error term, C, must also be adapted to the task at hand. C and γ were varied in a logarithmic scale, respectively between [10^{-2}, 10^{8}] and [10^{-5}, 10^{3}].

The algorithm was implemented in the Python programming language and open source toolkits were used to test the classifiers. The scikit-learn Python module (Pedregosa *et al.*, 2011), a machine learning kit, was used to implement both the kNN and the SVM classifiers. ANNs were implemented using PyBrain, a modular machine learning library (Schaul *et al*., 2010).

4.5 Validation Setup

The validation setup adopted in this analysis is represented in Figure 35. Cross-validation was implemented to test the algorithm. A stratified 4-fold cross-validation was used: for each one of the 4 possible combinations, 3 folds were used as training data and the fourth served as test. This process was repeated for 50 runs, and for each run a balanced dataset was generated by randomly sampling on the existing data.

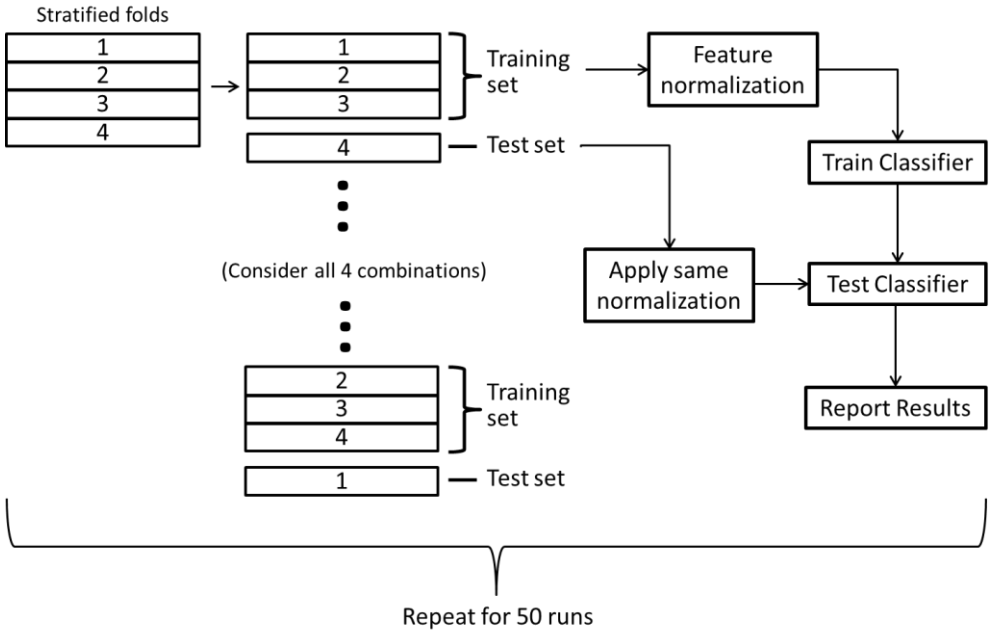

Figure 35: Scheme for training and testing the classifier.

The test error, Equation (29), or the accuracy, Equation (30), are the simplest measures of a classifier's performance.

$$Test\ Error\ = \frac{Number\ of\ Misclassifications}{Number\ of\ Test\ Samples} \tag{29}$$

$$Accuracy = \frac{Number\ of\ Correct\ Classifications}{Number\ of\ Test\ Samples} \tag{30}$$

To evaluate the classifier's performance a couple of accuracy measures, besides the error rate, were computed. Using the usual notation for true positives, true negatives, false positives and false negatives (that is TP, TN, FP and FN) we can define the precision (or positive predictive value) and the recall (or sensitivity) as shown in equations (31) and (32). The F_1 score also known as F-score or F-measure is the harmonic mean of precision and sensitivity and can be obtained by equation (33).

$$Precision = \frac{TP}{TP + FP} \tag{31}$$

$$Recall = \frac{TP}{TP + FN} \tag{32}$$

$$F_1 = \frac{2TP}{2TP + FP + FN} \tag{33}$$

5. Experimental Setup and Results

5.1 Experimental Setup

The validation of the proposed methodology was performed on benchmark data and ECG acquisitions performed in collaboration with Santa Marta Hospital, as described next.

5.1.1 BITalino Acquisitions

Acquisitions

ECG recordings were acquired with the BITalino at Santa Marta Hospital, in Lisbon, during the months of June and July. Subjects were either inpatients or came to the hospital for diagnosis (stress test or tilt table test) or rehabilitation purposes. All subjects gave written informed consent before the acquisition (see Annex A). They were asked to hold one electrode in each hand, between thumb and index finger. Simultaneous recordings were obtained with traditional 12-lead ECG and the BITalino system to allow an accurate ECG interpretation. Since automatic rhythm classification was to be performed, an attempt was made to acquire at least 60 seconds of data with the BITalino system. The OpenSignals software, available at (Plux Wireless Biosignals, 2014) and allowing real time visualization, was used to acquire the data.

During the acquisition process, it was clear that some rooms gave rise to a noisier ECG and the BITalino system was far more affected by this noise than the standard 12-lead system. Another difficulty encountered was the involuntary movement of some subjects, which resulted in ECGs with artefacts. It was particularly difficult to acquire data when the subject suffered with tremors due to the incapacity to keep the extremities still. Some subjects, although instructed otherwise, tended to hold the electrodes too tight, which also resulted in muscular noise. The technicians operating the 12-lead system complained about this situation since it also affected the standard ECG.

A total of 294 records were acquired, corresponding to 180 men with an age of approximately 46.78 ± 30.21 years and 114 women with an age of approximately 46.09 ± 30.65 years.

Annotations

Resorting to the standard 12-lead ECG, an experienced cardiologist interpreted the records in terms of type of rhythm and other meaningful information. These annotations are presented in the Annex B (Table 31). Naturally, the majority of the records had an underlying sinus rhythm. It was also common to capture premature ventricular contractions and a few atrial premature beats were recorded. Both these events can be recognized using lead I and thus are also visible in the BITalino ECG record. A couple of sinus bradycardia and sinus tachycardia ECG segments were recorded. Unsurprisingly, the more recurrent abnormal rhythm was the most common arrhythmia, atrial fibrillation. One can expect to be able to recognize such arrhythmia simply with lead I. The same can be said about atrial flutter although ECGs with this rhythm were much more rarely captured. Atrioventricular blocks and right or

left bundle-branch blocks were occasionally encountered. Finally, it should be mentioned that a considerable amount of paced rhythms, both ventricular and atrial, were collected.

5.1.2 Benchmark Data

For benchmarking purposes, the MIT-BIH (Massachusetts Institute of Technology – Beth Israel Hospital) arrhythmia database was used (Moody and Mark, 2001). A total of 48 two-channel Holter records are available, each approximately 30 minutes long. The upper signal is usually a modified limb lead II (MLII) but occasionally a modified lead V5. The lower signal is most often a modified lead V1 (occasionally V2 or V5, and in one instance V4). All signals were digitized at a sample rate of 360 Hz. The database includes different sets of annotations verified by more than one cardiologist. All beats are identified and labeled according to their type (i.e. normal beat, premature ventricular contraction…). Annotations that mark the beginning of a rhythm type are also available. Additional annotations, including peaks of P, T or U-waves and signal quality comments, are sometimes present.

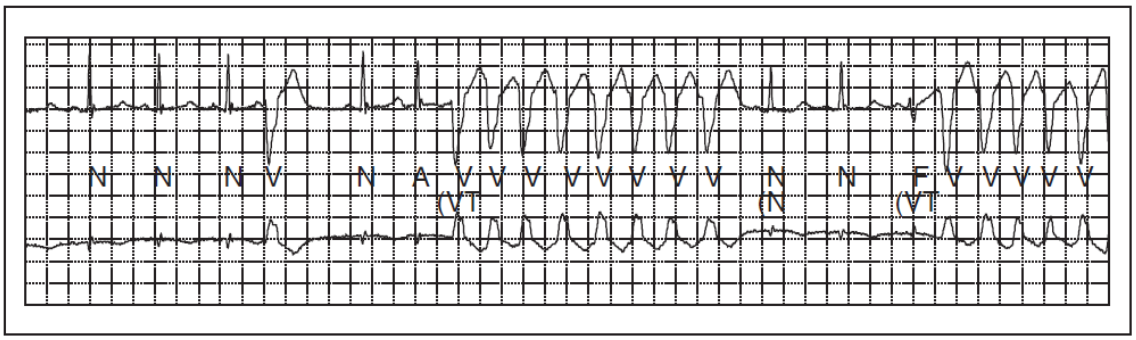

Figure 36: Ten seconds from a record of the MIT-BIH arrhythmia database. Each beat is individually labeled and rhythm changes appear below beat annotations (preceded by '(') (Moody and Mark, 2001).

The types of beats and rhythms present in this database are summarized in the table below.

Table 2: Types of beats and rhythms present in the MIT-BIH arrhythmia database.

Beat types	Rhythm type	Rhythm Annotation
Atrial premature beat	Atrial bigeminy	AB
Aberrated atrial premature beat	Atrial fibrillation	AFIB
Ventricular escape beat	Atrial flutter	AFL
Fusion of ventricular and normal beat	Ventricular bigeminy	B
Fusion of paced and normal beat	2° heart block	BII
Left bundle branch block beat	Idioventricular rhythm	IVR
Paced beat	Normal sinus rhythm	N
Normal beat	Nodal (A-V junctional) rhythm	NOD
Unclassifiable beat	Paced rhythm	P
Right bundle branch block beat	Pre-excitation (WPW)	PREX
Premature ventricular contraction	Sinus bradycardia	SBR
Isolated QRS-like artifact	Supraventricular tachyarrhythmia	SVTA
Nodal (junctional) escape beat	Ventricular trigeminy	T
Nodal (junctional) premature beat	Ventricular flutter	VFL
Atrial escape beat	Ventricular tachycardia	VT
Supraventricular premature or ectopic beat (atrial or nodal)		

For this analysis only MLII records were used (records number 102 and 104 were therefore excluded).

5.2 Results R Peak Detection

In order to evaluate the performance of the algorithm used for R-peak detection, the MIT-BIH arrhythmia database was used, taking advantage of the beat annotations present.

The Waveform Database (WFDB) Software Package, available in (Moody, 2014), was used for validation. For each ECG record, R peaks were detected and an annotation file containing their positions was generated. These positions were then compared to the reference annotations from the database. Standard comparison options were used: the comparison started 5 minutes after the beginning of the record and the match window, maximum absolute difference in annotation times allowable for matching annotations, was set to 0.15 second.

The results obtained, in terms of sensitivity and positive predictive value, are illustrated in Figure 37 for different threshold coefficients TH (see equation 24). As stated in section 4.1.3, larger TH values lead to a higher number of correct detections whereas smaller values are characterized by a small rate of false detections. A performance curve as a function of this threshold was therefore constructed.

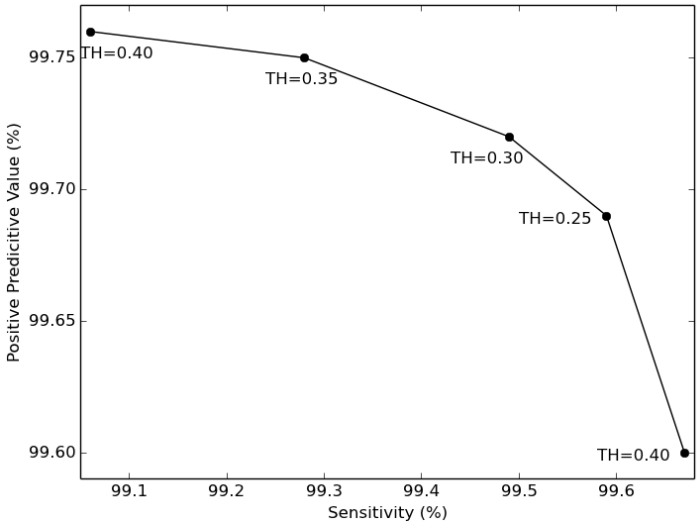

Figure 37: Sensitivity-positive predictive value curve for different threshold (TH) values.

A threshold coefficient of 0.25, corresponding to sensitivity and positive predictive values of 99.59 and 99.69%, respectively, was used for the remaining tests.

In order to understand which types of rhythms were more prone to detection errors, the following experiment was implemented. Records were first split according to their rhythm so that rhythm type did not vary within the segment (although beat types did vary). Then, for each segment, peaks were detected. Using again a match window of 0.15 second, annotations were compared to the reference annotations. Sensitivity and positive predictive values obtained for each rhythm type are summarized in Table 3.

Table 3: Sensitivity and positive predictive value of R peak detection according to the type of rhythm.

Rhythm type	Sensitivity (%)	Positive Predictive Value (%)
Atrial bigeminy	100	100
Atrial fibrillation	99.02	99.71
Atrial flutter	98.50	99.42
Ventricular bigeminy	99.61	99.85
2° heart block	100	100
Idioventricular rhythm	100	100
Normal sinus rhythm	99.57	99.71
Nodal (A-V junctional) rhythm	100	100
Paced rhythm	99.82	99.87
Pre-excitation (WPW)	100	100
Sinus bradycardia	100	99.55
Supraventricular tachyarrhythmia	100	100
Ventricular trigeminy	99.04	99.70
Ventricular flutter	96.25	98.47
Total	**99.50**	**99.71**

Analyzing the table above it seems that detection rates vary among rhythm type. The smallest values of sensitivity and positive predictive values were obtained for ventricular tachycardia. Trigeminy and bigeminy, which are characterized by an alternation of normal and ventricular beats, also present lower sensitivity values. Finally, the sensitivity for segments of atrial flutter and atrial fibrillation is also below average.

Additional information, concerning the amount of correct and missed detections per beat type, was gathered and is presented in Table 4. It should also be mentioned that a total of 632 false positives were obtained.

Table 4: Results of the R peak detection algorithm per beat type.

Beat type	Correct detections	Missed detections	Error rate (%)
Atrial premature beat	2540	1	0.04
Aberrated atrial premature beat	100	50	33.33
Ventricular escape beat	106	0	0
Fusion of ventricular and normal beat	798	5	0.62
Fusion of paced and normal beat	259	1	0.38
Left bundle branch block beat	8055	20	0.25
Paced beat	3619	1	0.03
Normal beat	74178	136	0.18
Unclassifiable beat	7	8	53.33
Right bundle branch block beat	7259	0	0
Premature ventricular contraction	6914	210	2.95
Isolated QRS-like artifact	41	91	68.94
Nodal (junctional) escape beat	229	0	0
Nodal (junctional) premature beat	83	0	0
Supraventricular premature or ectopic beat (atrial or nodal)	2	0	0
Atrial escape beat	16	0	0
Total	**104206**	**523**	**0.50**

Interesting conclusions can be draw from the information shown above. It is clear that some beat types are much more easily detected than others. Whilst the error rate is below 1% for the majority of beats, there are some noteworthy exceptions. The detection of premature ventricular contractions has an error rate close to 3%, which explains the results obtained previously for ventricular tachycardia, bigeminy and trigeminy. The worst results correspond however to aberrated atrial premature beats and unclassifiable beats, with error rates of, respectively, 33.33 and 53.33%. Referring to Figure 38 and Figure 39 it is understandable why such high error rates were obtained. Concerning false positive errors, two examples are shown in Figure 40. In the first case, where the R peak is inverted, the algorithm detected a P wave. In the second, premature ventricular contractions occurred, and the algorithm considered a T wave as an R peak. Other situations where false positive occurred consisted of records with artefacts.

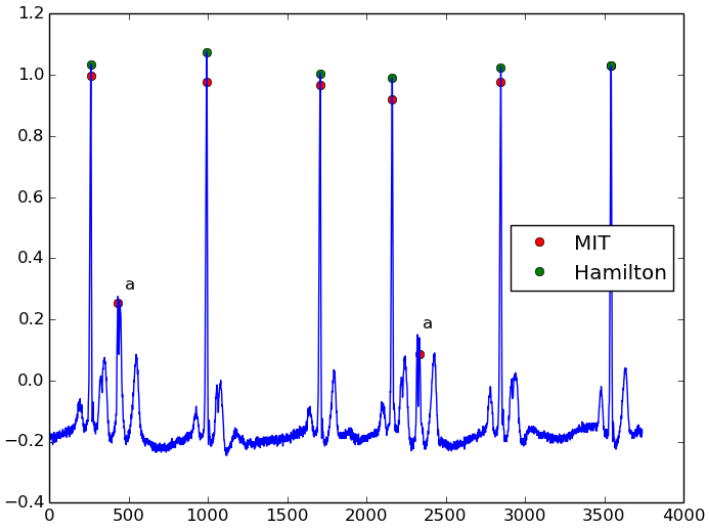

Figure 38: Example of two aberrated atrial premature beats (a) that were not detected by the segmentation algorithm.

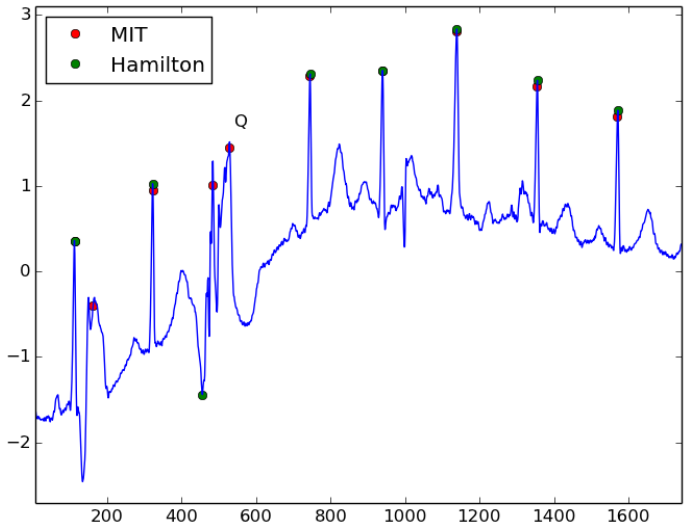

Figure 39: Example of one unclassifiable beat (Q) that was not detected by the segmentation algorithm.

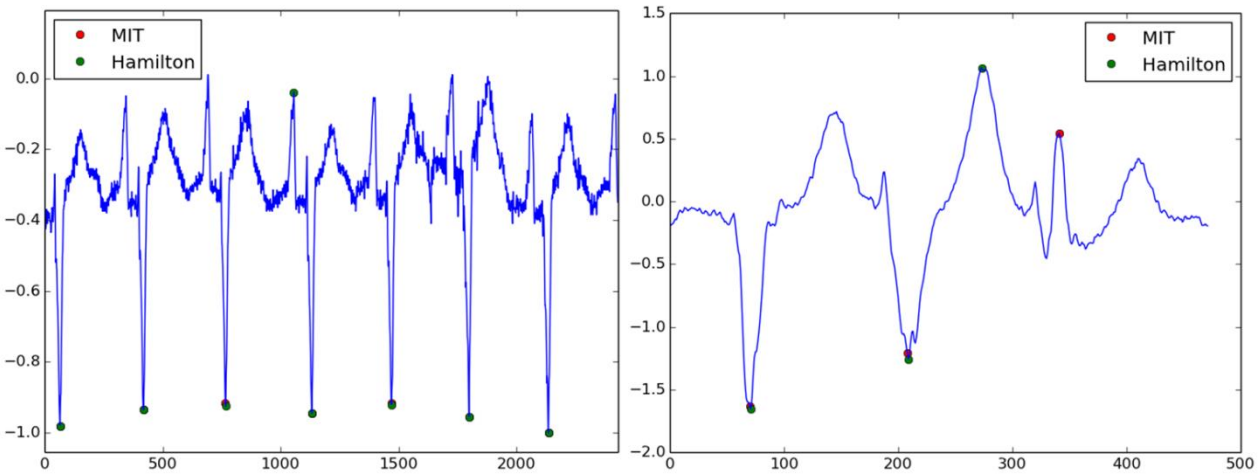

Figure 40: Example of two false positive errors. In the left, where R peaks are inverted, a P wave is detected. In the right, where PVCs occur, a T wave is detected.

5.3 Rhythm Classification on Benchmark Database

5.3.1 Database Assembly

The same database used to validate the R peak detection algorithm was used in this analysis. In order to perform rhythm classification, each record was split into multiple segments according to rhythm annotations. Additional cuts were made in a non-overlapping manner to obtain segments of predefined length. The total number of segments obtained for each type of rhythm and segment length is presented in Table 5. For the features based on the location of the R peaks, the position annotations present on the database were used. This assures that the performance of the algorithm is not affected by possible mistakes on the detection of the peaks.

Table 5: Number of segments per rhythm type for different segment's lengths.

Rhythm type	10 s segments	30 s segments	60 s segments
AB	7	2	1
AFIB	752	226	98
AFL	60	14	6
B	144	31	7
BII	68	21	9
IVR	12	3	1
N	6046	1920	911
NOD	7	0	0
P	316	99	45
PREX	36	6	1
SBR	180	60	30
SVTA	12	1	0
T	72	12	3
VFL	12	3	1
VT	8	2	0
Total	**7732**	**2400**	**1113**

5.3.2 Normal Sinus Rhythm vs. Atrial Fibrillation

The first set of experiments focused on the distinction of normal sinus rhythm and the most common arrhythmia, atrial fibrillation (AF). The three feature sets described in the previous chapter were considered, first individually and then in combination. The parameters of the classifiers were varied in order to find the most suitable values for each case. Segments with a length of 60 seconds were used. As shown in Table 5, 98 atrial fibrillation segments and 911 normal sinus rhythm segments are available. Thus, for each run, 98 segments of each class are selected and the validation process is carried out.

Time parameters (feature set C)

A first attempt was made to distinguish between normal sinus rhythm and AF ECG segments relying only on heart rate related features (feature set C). As stated in section 4.4, the classifiers' parameters were varied to find the most suitable values. For the SVM, the penalty parameter of the error term, C, and the kernel parameter, γ, were varied in a logarithmic scale, respectively between [10^{-2}, 10^{8}] and [10^{-5}, 10^{3}]. For the kNN, the number of neighbors considered for classification, k, was varied between 1 and 15. Regarding the ANN, the number of hidden neurons was varied, in this case, between 3 and 12. The classifiers' parameters that led to the best performance are summarized in Table 6. For the ANN the best result corresponded to standardized features with 10 neurons in the hidden layer. For the kNN classifier, the best performance was achieved when features were standardized and three neighbors were considered. Figure 41 and Figure 42 show, respectively, the variation of test error with the number of hidden neurons (for the ANN), and the number of neighbors (for the kNN). Concerning the SVM classifier, values of 1 and 10 respectively for the penalty, C, and kernel, γ, parameters led to a more successful classification. Figure 43 shows the heat map of the accuracy of the SVM classifier for different values of the penalty and kernel parameters.

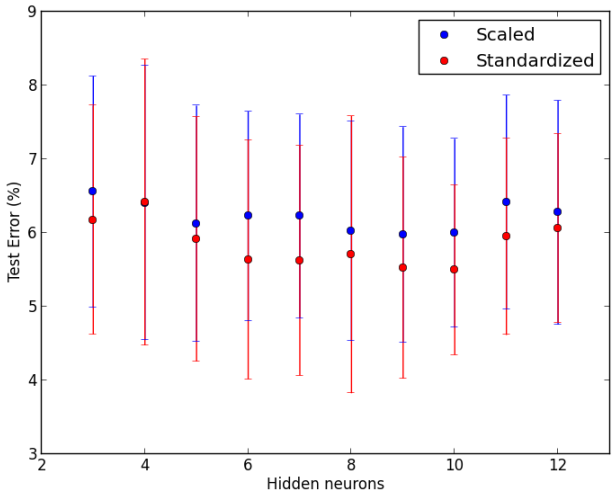

Figure 41: Mean and standard deviation of the test error as a function of the number of neurons in the hidden layer for the two normalization schemes, for feature set C.

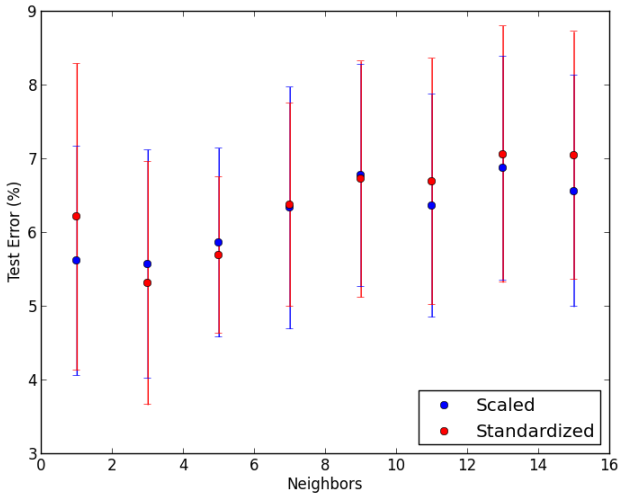

Figure 42: Mean and standard deviation of the test error as a function of the number of neighbors used for classification for the two normalization schemes, for feature set C.

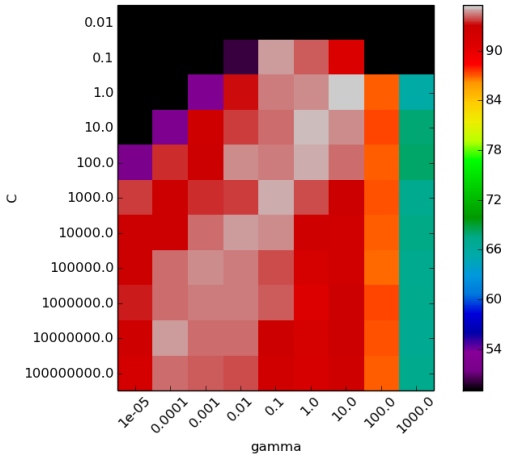

Figure 43: Heat map showing the accuracy of the SVM classifier for multiple values of C and gamma, for feature set C.

We can see that, for the ANN, standardizing features resulted better than scaling them. In terms of hidden neurons, the range 6 to 10 offered very similar results, with a poorer performance when selecting fewer or more neurons. For the kNN classifier, the two types of normalization schemes offered similar results. The test error was smaller when using three neighbors than a single one and then increased when more neighbors were considered. Regarding the SVM, the majority of C and γ combinations resulted in accuracy above 85%. The exception was for small values of C and large values of γ, which achieved far worse accuracies.

Table 6: Best classifiers' parameters for each classification task.

Feature set	Classifier	Normalization	Parameters
A	ANN	Scaling	55 Hidden Neurons
	kNN	Standardization	$k = 1$
	SVM	Standardization	$C = 10^3$; $\gamma = 10^{-2}$
B	ANN	Standardization	15 Hidden Neurons
	kNN		$k = 1$
	SVM		$C = 10^2$; $\gamma = 1$
C	ANN	Standardization	10 Hidden Neurons
	kNN		$k = 3$
	SVM		$C = 1$; $\gamma = 10$
A + C	ANN	Scaling	35 Hidden Neurons
	kNN	Scaling	$k = 1$
	SVM	Standardization	$C = 10^8$; $\gamma = 10^{-2}$
B + C	ANN	Standardization	14 Hidden Neurons
	kNN		$k = 1$
	SVM		$C = 10$; $\gamma = 1$

The results obtained for the three classifiers are summarized in Table 7, showing mean values and standard deviations computed over 50 runs (see section 4.5). Highlighted in bold are the highest values of precision, recall and F-score for each class, and the minimum test error achieved.

Table 7: Results obtained with feature set C.

Classifier	Rhythm	Precision (%)	Recall (%)	F-score (%)	Test error (%)
ANN	Normal	**98.66 ± 1.00**	90.31 ± 1.86	94.21 ± 1.22	5.49 ± 1.15
	Atrial Fibrillation	91.27 ± 1.62	**98.72 ± 0.98**	94.78 ± 1.08	
kNN	Normal	97.93 ± 1.34	91.4 ± 2.61	94.44 ± 1.77	5.31 ± 1.65
	Atrial Fibrillation	92.19 ± 2.22	97.98 ± 1.34	94.90 ± 1.55	
SVM	Normal	96.79 ± 1.41	**94.23 ± 2.20**	**95.39 ± 1.55**	**4.53 ± 1.50**
	Atrial Fibrillation	**94.56 ± 2.01**	96.71 ± 1.50	**95.53 ± 1.47**	

Overall, the SVM classifier was the one that performed better, achieving a test error of 4.53 ± 1.50%. ANN and kNN classifiers have a similar performance in terms of test error. For the ANN it is interesting to note that precision and recall values, respectively for normal and AF rhythms, are considerably high (approximately 99%).

The experimental results based on spectral features are presented next.

Average PSD Values (feature set A)

Feature set A, containing the 42 values obtained by averaging the PSD of the wavelet decomposition, was considered first. Figure 44, Figure 45 and Figure 46 illustrate the tests performed to assess the most suitable classifiers' parameters. The best results, presented in Table 8, were obtained with the parameters specified in Table 6. It should be mentioned that in this case, due to the large number of features, the number of hidden neurons was varied between 10 and 70, in steps of 5.

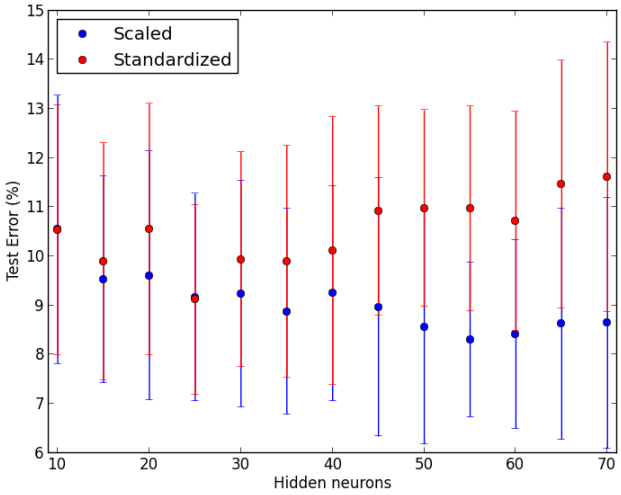

Figure 44: Mean and standard deviation of the test error as a function of the number of neurons in the hidden layer for the two normalization schemes, for feature set A.

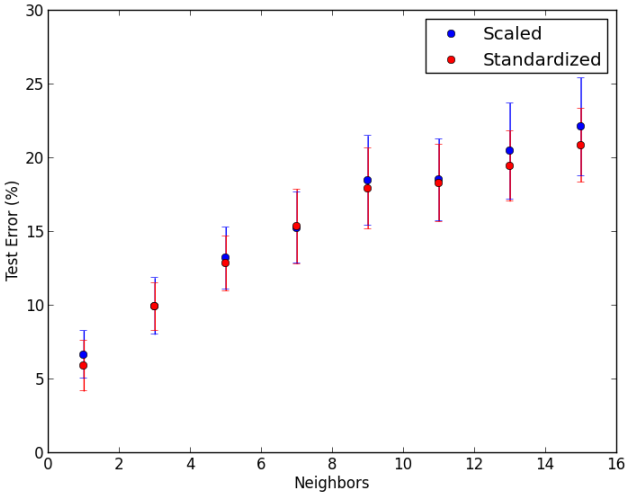

Figure 45: Mean and standard deviation of the test error as a function of the number of neighbors used for classification for the two normalization schemes, for feature set A.

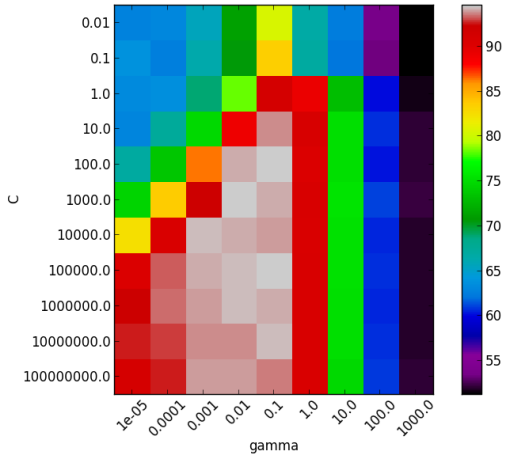

Figure 46: Heat map showing the accuracy of the SVM classifier for multiple values of C and gamma, for feature set A.

Analyzing Figure 44 it is clear that scaling the features results better than standardizing them when using a larger number of neurons in the hidden layer. It is also noteworthy that, in comparison with the previous feature set, a much larger number of neurons are needed to achieve the best performance. Obviously, this largely influences the time needed for training the network. Regarding the kNN, the two normalization schemes offer again similar results. In this case, the error rate increased when considering more neighbors for classification. For the SVM classifier, the higher accuracies corresponded to values of C and γ respectively between [10^2, 10^8] and [10^{-2}, 10^{-1}].

Table 8: Results obtained with feature set A.

Classifier	Rhythm	Precision (%)	Recall (%)	F-score (%)	Test error (%)
ANN	Normal	96.90 ± 1.83	86.36 ± 3.08	91.06 ± 1.83	8.29 ± 1.57
	Atrial Fibrillation	88.18 ± 2.28	97.07 ± 1.84	92.24 ± 1.41	
kNN	Normal	**96.92 ± 1.11**	91.27 ± 3.08	93.87 ± 1.88	5.87 ± 1.72
	Atrial Fibrillation	92.04 ± 2.62	**96.99 ± 1.15**	94.35 ± 1.60	
SVM	Normal	95.56 ± 1.62	**93.77 ± 2.00**	**94.54 ± 1.46**	**5.39 ± 1.44**
	Atrial Fibrillation	**94.10 ± 1.85**	95.45 ± 1.70	**94.66 ± 1.44**	

The smallest test error was obtained with the SVM classifier: 5.39 ± 1.44%. For the kNN, a test error below 6% was also achieved. The ANN proved to be the less capable classifier for distinguishing between the two rhythms. Additionally, it should be mentioned that the training process associated with this classifier was lengthier, due, in part, to the high number of hidden neurons required. Interestingly, precision and recall values, respectively for normal and AF, are very similar for kNN and ANN. However, the latter presents considerably smaller values of recall, for normal rhythm, and precision, for AF.

Large Range Power Features (feature set B)

The 7 large range power features (feature set B) were then tested in this binary classification problem. Table 6 indicates the best classifiers' parameters. Figure 47, Figure 48, and Figure 49 illustrate the multiple tests performed to obtain these values.

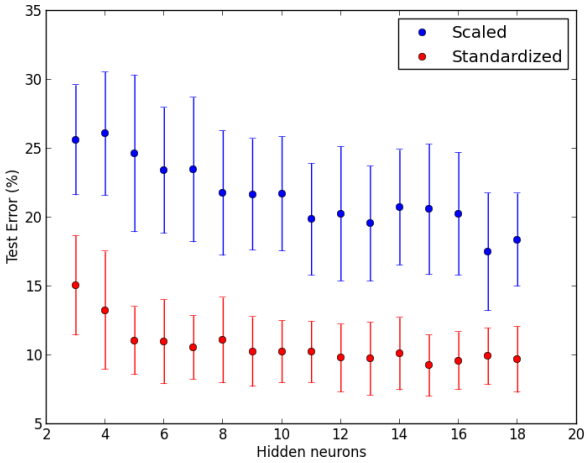

Figure 47: Mean and standard deviation of the test error as a function of the number of neurons in the hidden layer for the two normalization schemes, for feature set B.

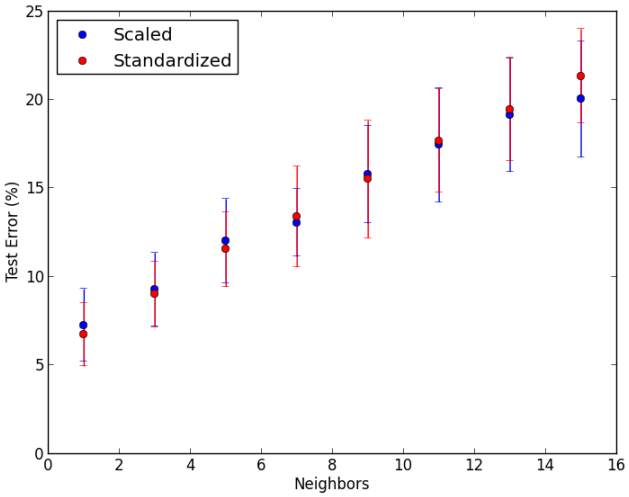

Figure 48: Mean and standard deviation of the test error as a function of the number of neighbors used for classification for the two normalization schemes, for feature set B.

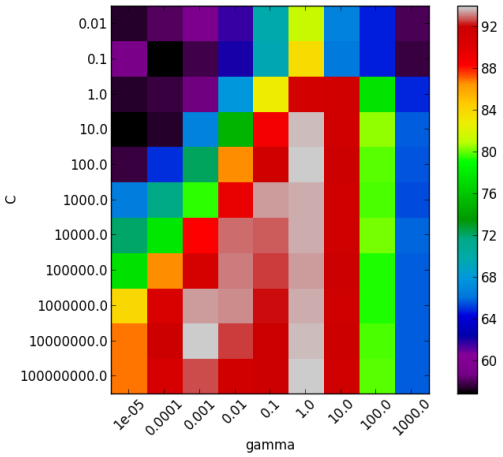

Figure 49: Heat map showing the accuracy of the SVM classifier for multiple values of C and gamma, for feature set B.

By varying the number of hidden neurons within the range [3, 18], it was possible to see that the error rate was higher when using very few neurons (3 and 4) but did not vary significantly from then onwards. Feature standardization proved to be the most suitable normalization scheme. For the kNN, as with feature set A, the two normalization schemes offered similar performances and using fewer neighbors resulted in smaller test errors. Regarding the SVM, higher accuracies were found with a γ value of 1 and penalty parameters above 10.

The best results obtained are summarized in Table 9.

Table 9: Results obtained with feature set B.

Classifier	Rhythm	Precision (%)	Recall (%)	F-score (%)	Test error (%)
ANN	Normal	95.24 ± 2.30	86.16 ± 3.60	90.18 ± 2.49	9.21 ± 2.23
	Atrial Fibrillation	87.83 ± 2.84	95.41 ± 2.33	91.26 ± 2.06	
kNN	Normal	96.73 ± 1.31	89.70 ± 3.38	92.91 ± 2.01	6.73 ± 1.80
	Atrial Fibrillation	90.75 ± 2.80	**96.84 ± 1.31**	93.56 ± 1.63	
SVM	Normal	**96.74 ± 1.46**	**91.13 ± 2.67**	**93.70 ± 1.76**	**6.04 ± 1.64**
	Atrial Fibrillation	**91.93 ± 2.31**	96.78 ± 1.49	**94.17 ± 1.55**	

Once again, the best results, in terms of test error, were obtained with the SVM classifier. The ANN classifier offered the worst performance. For all classifiers, recall values were considerably higher, and not very different, for AF segments. The differences in test error are therefore due to the values of recall obtained for normal segments (or, equivalently, to the values of precision for AF segments).

Figure 50 shows the performance, in terms of test error, of the three classifiers, for the three feature sets used. It is clear that time domain features performed better than spectral features. Feature set A, containing average values over sub-bands, achieved better results than feature set B, containing the large range power features. In terms of classifiers, SVM proved to be the most promising choice whilst ANN achieved the worst results for all sets of features.

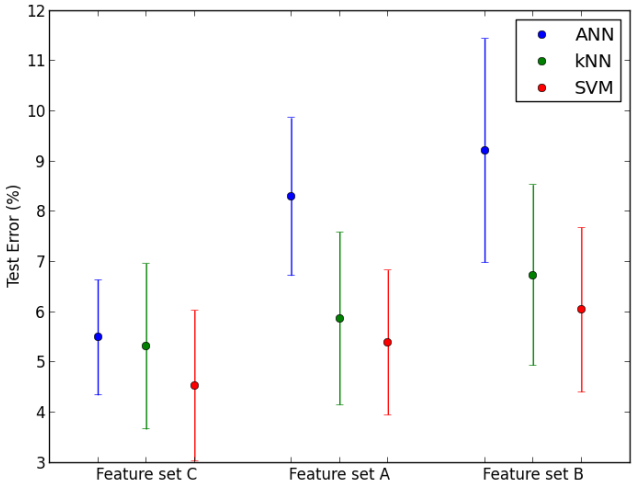

Figure 50: Means and standard deviations of test errors for feature sets C (time parameters), A (average PSD values) and B (large range power values).

The next step was to assess whether combining spectral and time domain features could improve the classifiers' performance.

Average PSD Values + Time Parameters (feature sets A + C)

The results obtained when combining feature sets A and C are presented in Table 10. Figure 51, Figure 52 and Figure 53 illustrate the tests performed to determine the best classifiers' parameters (summarized in Table 6).

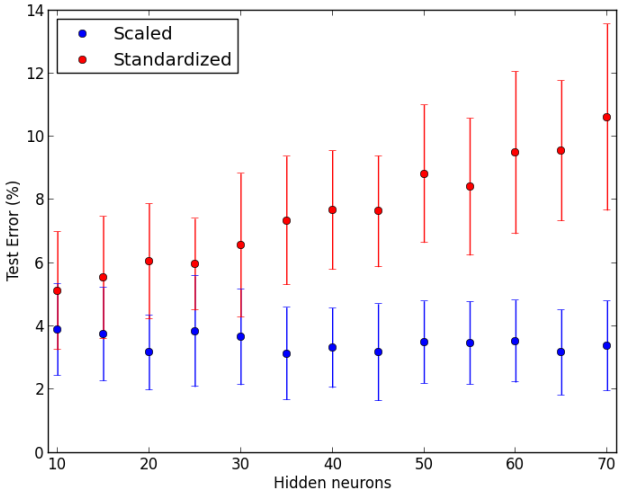

Figure 51: Mean and standard deviation of the test error as a function of the number of neurons in the hidden layer for the two normalization schemes, for feature set A + C.

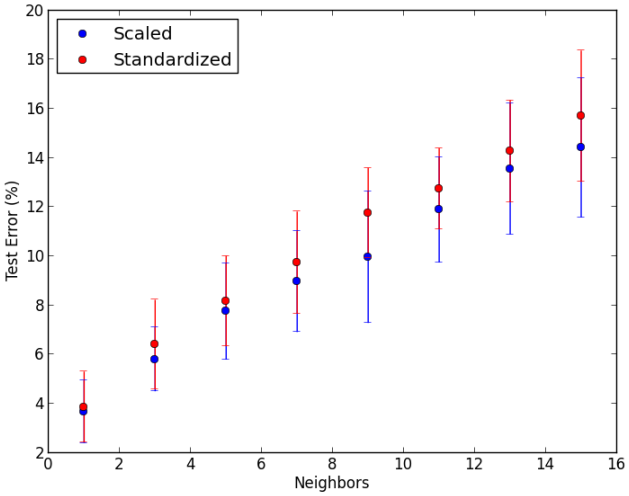

Figure 52: Mean and standard deviation of the test error as a function of the number of neighbors used for classification for the two normalization schemes, for feature set A + C.

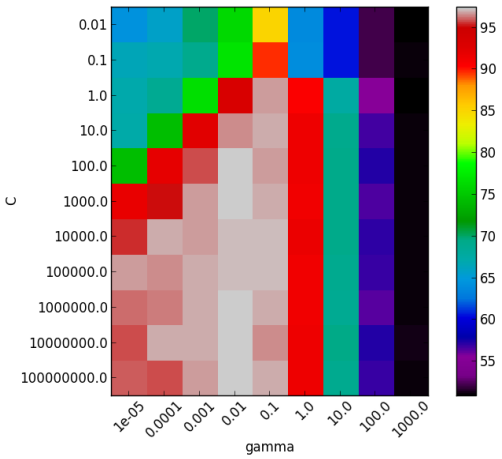

Figure 53: Heat map showing the accuracy of the SVM classifier for multiple values of C and gamma, for feature set A + C.

Regarding the ANN, scaling the features was the most suitable approach. Interestingly, the results obtained when standardizing the features seem to show that this normalization scheme works worst for a larger number of hidden neurons. Scaling the features also resulted in a smaller test error for the kNN classifier. Regarding the SVM, very high values of γ and small values of C achieved the smallest accuracies. A large number of combinations offered accuracy values above 95%.

Table 10: Results obtained with feature set A + C.

Classifier	Rhythm	Precision (%)	Recall (%)	F-score (%)	Test error (%)
ANN	Normal	**99.17 ± 0.95**	94.55 ± 2.57	96.73 ± 1.58	3.13 ± 1.46
	Atrial Fibrillation	94.98 ± 2.22	**99.19 ± 0.93**	96.98 ± 1.37	
kNN	Normal	98.29 ± 0.72	94.35 ± 2.48	96.19 ± 1.38	3.67 ± 1.27
	Atrial Fibrillation	94.77 ± 2.17	98.31 ± 0.72	96.44 ± 1.19	
SVM	Normal	98.23 ± 1.23	**96.69 ± 2.05**	**97.39 ± 1.40**	**2.55 ± 1.33**
	Atrial Fibrillation	**96.89 ± 1.80**	98.20 ± 1.25	**97.49 ± 1.28**	

This combination of spectral and time domain features achieved, for all classifiers, accuracies above 94%. The SVM classifier stood out, with a mean test error of 2.55%. Very high values of precision and recall, respectively for normal sinus rhythm and AF, were obtained with the ANN (above 99%). It should be mentioned that the mean training error obtained with this classifier was 0.97 ± 0.59%. Therefore it may be the case that the network has specialized its behavior for the training patterns, losing some of its generalization ability.

Large Range Power Features + Time Parameters (feature sets B + C)

The tests performed to select the best classifiers' parameters when using feature sets B and C are illustrated in Figure 54, Figure 55, and Figure 56, respectively for ANN, kNN and SVM. Again, the most suitable parameters are summarized in Table 6.

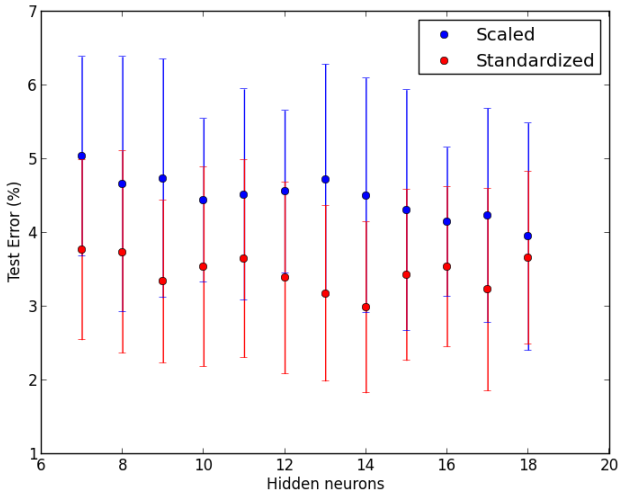

Figure 54: Mean and standard deviation of the test error as a function of the number of neurons in the hidden layer for the two normalization schemes, for feature set B + C.

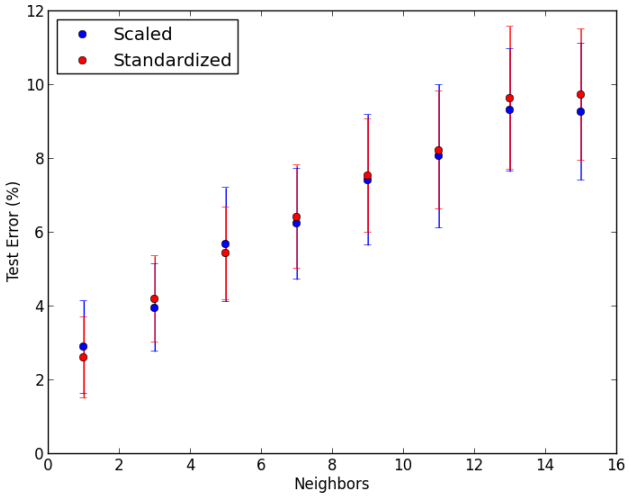

Figure 55: Mean and standard deviation of the test error as a function of the number of neighbors used for classification for the two normalization schemes, for feature set B + C.

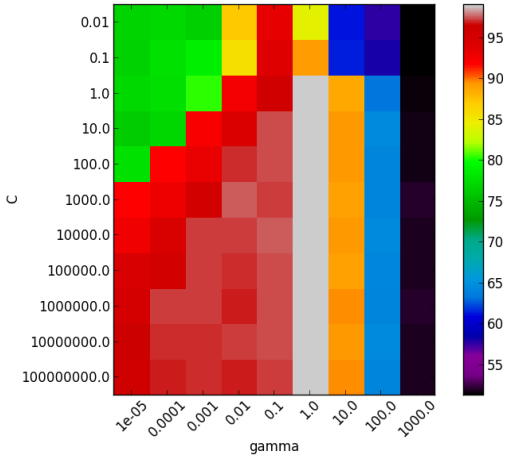

Figure 56: Heat map showing the accuracy of the SVM classifier for multiple values of C and gamma, for feature set B + C.

Regarding the ANN, standardizing the features offered better results when compared to scaling them. The test error oscillated with the number of hidden neurons and the smaller value was obtained with 14 neurons. For the kNN, similar results were obtained for the two normalization schemes and using a single neighbor was the most suitable choice. Referring to Figure 56 it is clear that the SVM classifier achieved the best performance when γ was set to 1 and C was above this value.

The results obtained are presented in Table 11.

Table 11: Results obtained with feature set B + C.

Classifier	Rhythm	Precision (%)	Recall (%)	F-score (%)	Test error (%)
ANN	Normal	**99.36 ± 0.58**	94.67 ± 2.30	96.89 ± 1.26	2.98 ± 1.16
	Atrial Fibrillation	95.11 ± 1.98	**99.37± 0.57**	97.14 ± 1.08	
kNN	Normal	99.06 ± 0.60	95.75 ± 2.10	97.31 ± 1.17	2.60 ± 1.10
	Atrial Fibrillation	96.07 ± 1.85	99.04 ± 0.67	97.48 ± 1.04	
SVM	Normal	98.64 ± 0.83	**99.59 ± 0.64**	**99.10 ± 0.64**	**0.92 ± 0.66**
	Atrial Fibrillation	**99.61 ± 0.62**	98.57 ± 0.92	**99.06 ± 0.68**	

With this feature set, all three classifiers achieved test errors below 3%. The best results were obtained with the SVM with an accuracy of 99.08% and F-scores above 99% for both classes. Although the worst results, in terms of test error, were obtained with the ANN, a very high recall rate was achieved for AF: 99.37%. This can be a valuable characteristic since it may be important to detect all AF events, even if this encompasses a larger number of false positive errors. It should again be mentioned that the training error for the ANN was considerably smaller than the test error: 0.91 ± 0.47%.

From the results presented above it became clear that combining time domain and spectral features considerably improves the classifiers' performance. This was true for the two combinations and for all three classifiers. The best results were obtained when combining feature sets B and C and using the SVM classifier, as shown in Figure 57.

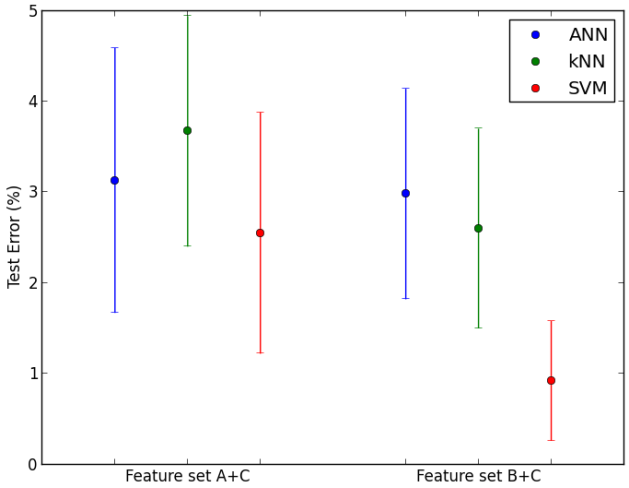

Figure 57: Means and standard deviations of test errors for feature sets A + C and B + C.

Influence of segments' length

The study of features presented above was carried out with ECG segments of 60 seconds. The influence of the segments' length on the performance of the classifiers is explored here. Features used for classification were the ones that held better results: large range power features in combination with time parameters (feature sets B + C). The classifiers' parameters were set to the values obtained previously with this set of features (see Table 6).

As shown in Table 5 the number of segments of different lengths varies greatly. This fact must be taken into account when performing this analysis; therefore the two following experiments were considered. First, for each classifier, segments' length of 60, 30 and 10 seconds were used while using as many samples per rhythm as available (i.e. 98, 226 and 752 respectively for 60, 30 and 10 seconds). Secondly, the number of samples was kept unchanged, 98, varying only the segments'

length. The results obtained are presented in Table 12, Table 13 and Table 14, respectively for ANN, kNN and SVM classifiers. A graphical representation of the test error for both experiments and all classifiers is shown in Figure 58.

Table 12: Results obtained when varying the segments' length for the ANN classifier.

Length (s)	Samples per rhythm	Rhythm	Precision (%)	Recall (%)	F-score (%)	Test error (%)
60	98	Normal	99.36 ± 0.58	94.67 ± 2.30	96.89 ± 1.26	2.98 ± 1.16
		Atrial Fibrillation	95.11 ± 1.98	99.37± 0.57	97.14 ± 1.08	
30	98	Normal	97.84 ± 1.48	92.65 ± 2.18	95.06 ± 1.49	4.76 ± 1.42
		Atrial Fibrillation	93.24 ± 1.92	97.86 ± 1.49	95.40 ± 1.36	
	226	Normal	98.36 ± 0.76	96.28 ± 1.36	97.27 ± 0.79	2.68 ± 0.76
		Atrial Fibrillation	96.43 ± 1.26	98.36 ± 0.77	97.36 ± 0.74	
10	98	Normal	94.94 ± 2.27	89.75 ± 2.21	92.09 ± 1.75	7.64 ± 1.70
		Atrial Fibrillation	90.58 ± 1.94	94.97 ± 2.31	92.58 ± 1.67	
	752	Normal	98.54 ± 0.41	96.19 ± 0.56	97.34 ± 0.34	2.62 ± 0.34
		Atrial Fibrillation	96.30 ± 0.52	98.56 ± 0.41	97.41 ± 0.33	

Table 13: Results obtained when varying the segments' length for the kNN classifier.

Length (s)	Samples per rhythm	Rhythm	Precision (%)	Recall (%)	F-score (%)	Test error (%)
60	98	Normal	99.06 ± 0.60	95.75 ± 2.10	97.31 ± 1.17	2.60 ± 1.10
		Atrial Fibrillation	96.07 ± 1.85	99.04 ± 0.67	97.48 ± 1.04	
30	98	Normal	98.51 ± 1.37	94.15 ± 2.10	96.21 ± 1.45	3.67 ± 1.41
		Atrial Fibrillation	94.56 ± 1.89	98.51 ± 1.42	96.43 ± 1.38	
	226	Normal	98.99 ± 0.57	96.68 ± 1.10	97.80 ± 0.71	2.16 ± 0.69
		Atrial Fibrillation	96.81 ± 1.04	99.00 ± 0.56	97.87 ± 0.68	
10	98	Normal	96.23 ± 1.97	91.05 ± 2.52	93.42 ± 1.79	6.36 ± 1.73
		Atrial Fibrillation	91.75 ± 2.24	96.24 ± 2.04	93.82 ± 1.69	
	752	Normal	98.53 ± 0.30	96.13 ± 0.55	97.31 ± 0.36	2.65 ± 0.35
		Atrial Fibrillation	96.24 ± 0.52	98.56 ± 0.30	97.38 ± 0.34	

Table 14: Results obtained when varying the segments' length for the SVM classifier.

Length (s)	Samples per rhythm	Rhythm	Precision (%)	Recall (%)	F-score (%)	Test error (%)
60	98	Normal	98.64 ± 0.83	99.59 ± 0.64	99.10 ± 0.64	0.92 ± 0.66
		Atrial Fibrillation	99.61 ± 0.62	98.57 ± 0.92	99.06 ± 0.68	
30	98	Normal	96.56 ± 1.46	98.18 ± 1.26	97.30 ± 1.02	2.73 ± 1.04
		Atrial Fibrillation	98.23 ± 1.21	96.35 ± 1.62	97.22 ± 1.07	
	226	Normal	97.93 ± 0.74	98.91 ± 0.57	98.41 ± 0.46	1.61 ± 0.47
		Atrial Fibrillation	98.92 ± 0.57	97.88 ± 0.77	98.38 ± 0.48	
10	98	Normal	91.65 ± 2.31	95.43 ± 2.34	93.35 ± 2.07	6.83 ± 2.11
		Atrial Fibrillation	95.41 ± 2.24	90.92 ± 2.59	92.95 ± 2.19	
	752	Normal	97.51 ± 0.42	97.72 ± 0.48	97.61 ± 0.34	2.40 ± 0.34
		Atrial Fibrillation	97.73 ± 0.47	97.49 ± 0.43	97.60 ± 0.34	

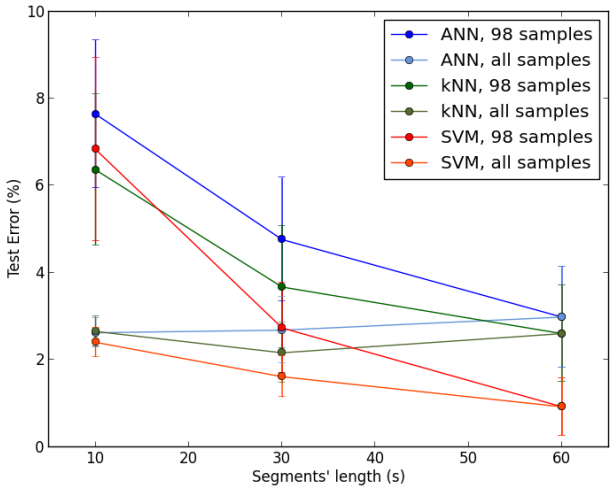

Figure 58: Mean and standard deviation of the test error as a function of the segments' length.

A few observations can be made from the results presented above. First, the results obtained for segments of 30 and 10 seconds are better when using all samples available as opposed to using only 98 samples. This is not surprising: for a fixed segment length, the performance of the classifiers is improved when more samples are provided for training.

For 10 seconds segments, when using all samples, the performance of the three classifiers is very similar. Mean test errors below 2.65% with small standard deviations are obtained in this case.

Analyzing each classifier individually, interesting differences can be noted. Regarding the SVM classifier, its performance worsens by reducing the segments' length. This is true when using always the same amount of samples, but also, to a lesser extent, when using all available samples. For the kNN classifier, when using all samples, the test error decreases for segments of 30 seconds but increases again when 10 seconds segments are used. The ANN classifier registers slight improvements for segments of 30 and 10 seconds if more samples are used for train and test.

From these observations it is clear that reducing the segments' length results in a loss of information, which affects the classifiers' performance. Depending on the classifier and the length of the segments, this loss of information is, in part, compensated by a larger number of samples available for training. It therefore seems as if there may be an 'ideal' segment length which will represent a compromise between the information that can be extracted and the total number of segments available. This 'ideal' length will be different for each classifier.

Influence of R peak detection

All the experiments carried out until this point used reference R peak annotations, included in the database. This allowed us to evaluate the performances of the classification algorithm in such a way that it was not affected by segmentation errors. It is now important to check the real influence of these R peak detection errors. In order to do so, the classification algorithm was reapplied, using this time R

peak annotations given by the segmentation algorithm described in the methodology section. The results obtained are summarized in Table 15 and the difference between these results and the ones obtained previously are illustrated in Figure 59.

Table 15: Results obtained with feature set B + C using non-reference R peak annotations.

Classifier	Rhythm	Precision (%)	Recall (%)	F-score (%)	Test error (%)
ANN	Normal	99.01 ± 0.76	93.67 ± 2.44	96.18 ± 1.34	3.65 ± 1.23
	Atrial Fibrillation	94.22 ± 2.10	99.02 ± 0.76	96.49 ± 1.14	
kNN	Normal	98.91 ± 0.68	95.32 ± 2.05	97.03 ± 1.16	2.88 ± 1.08
	Atrial Fibrillation	95.64 ± 1.81	98.93 ± 0.69	97.21 ± 1.02	
SVM	Normal	98.65 ± 0.72	98.98 ± 0.89	98.79 ± 0.61	1.22 ± 0.61
	Atrial Fibrillation	99.02 ± 0.85	98.57 ± 0.81	98.76 ± 0.62	

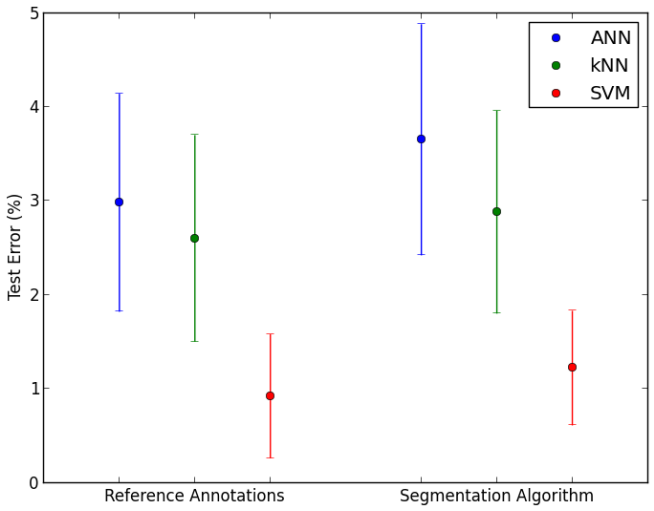

Figure 59: Comparison of rhythm classification error rate when using reference annotations and the segmentation algorithm.

Analyzing the figure above, it is clear that the results of the segmentation algorithm influence the performance of the classification. For all classifiers, the test error increased when including the R peak detection algorithm in the analysis. However, the results are still considerably good and the difference is not large. We can conclude that, although improvements can be achieved, the segmentation algorithm is reliable enough. It should nonetheless be expected that, with noisier data (e.g. acquisitions with the BITalino at the fingers), the segmentation will affect the results in a larger extent.

5.3.3 Multiple Rhythms

The first set of tests focused only on distinguishing normal sinus rhythm from the most common arrhythmia, atrial fibrillation. To test the performance of the algorithm in a more realistic situation, it is necessary to include other types of rhythms in the classification task. The results obtained with multiple rhythms are presented in this section. A few tests were performed maintaining a length of 60 seconds but, in order to have enough samples to include more rhythms, the segments' length was then shortened. The results presented here were obtained using the features that held best results:

large range power features in combination with time parameters (feature sets B and C). The classifiers' parameters were set to the corresponding values.

60 seconds segments

For segments of 60 seconds, and referring to Table 5, it is clear that there are not many samples of different rhythms. However, by including paced rhythms, besides normal and AF segments, 45 samples per rhythm can still be used. The results obtained for this ternary classification problem are presented in Table 16.

Table 16: Results obtained with feature sets B + C in the distinction of three rhythms.

Classifier	Rhythm	Precision (%)	Recall (%)	F-score (%)	Test error (%)
ANN	Normal	98.57 ± 1.44	88.70 ± 4.82	93.05 ± 2.89	4.25 ± 1.65
	Atrial Fibrillation	91.45 ± 3.46	98.54 ± 1.49	94.67 ± 2.02	
	Paced	98.76 ± 1.52	**100.0 ± 0.0**	99.35 ± 0.81	
kNN	Normal	**98.98 ± 1.35**	91.74 ± 4.10	95.00 ± 2.64	3.10 ± 1.60
	Atrial Fibrillation	93.87 ± 2.84	**98.97 ± 1.36**	96.22 ± 1.93	
	Paced	98.77 ± 1.48	**100.0 ± 0.0**	99.35 ± 0.78	
SVM	Normal	97.99 ± 1.88	**97.78 ± 1.90**	**97.79 ± 1.59**	**1.46 ± 1.05**
	Atrial Fibrillation	**97.98 ± 1.68**	98.5 ± 1.51	**98.16 ± 1.36**	
	Paced	**100.0 ± 0.0**	99.34 ± 1.19	**99.65 ± 0.62**	

The number of samples used for training and testing the classifier was significantly reduced by including paced rhythms (98 samples per rhythm for sinus rhythm versus atrial fibrillation, 45 samples when the three rhythms are considered). The performance of the classifiers declined when compared to the binary classification problem, but the results are still interesting. Again, SVM achieved the best performance, followed by kNN, whilst the results for the ANN were worse. It is interesting to note that very high rates of recognition of paced rhythm were obtained. For all three classifiers precision and recall values were above 98.7%, including a recall of 100% for kNN and ANN, and a precision of 100% for the SVM. The main difference between SVM and the two other classifiers was that the first managed to achieve high values of precision and recall respectively for atrial fibrillation and normal sinus rhythm.

An additional classification problem was addressed considering the following four rhythms: normal sinus rhythm, AF, paced rhythm and sinus bradycardia. A total of 30 samples per rhythm was selected in each run. The results obtained are presented in Table 17.

Table 17: Results obtained with feature sets B + C in the distinction of four rhythms.

Classifier	Rhythm	Precision (%)	Recall (%)	F-score (%)	Test error (%)
ANN	Normal	97.16 ± 3.46	82.54 ± 7.65	88.32 ± 5.54	5.71 ± 2.23
	Atrial Fibrillation	86.64 ± 4.95	96.99 ± 3.30	91.09 ± 3.45	
	Paced	98.44 ± 2.10	99.86 ± 1.0	**99.08 ± 1.33**	
	Sinus bradycardia	98.66 ± 2.07	97.79 ± 1.59	98.09 ± 1.51	
kNN	Normal	**97.91 ± 2.83**	82.72 ± 7.28	88.77 ± 5.14	5.18 ± 2.23
	Atrial Fibrillation	87.32 ± 4.92	**98.14 ± 2.92**	91.98 ± 3.48	
	Paced	98.14 ± 2.15	**100.0 ± 0.0**	99.00 ± 1.15	
	Sinus bradycardia	99.48 ± 1.24	**98.46 ± 1.67**	**98.90 ± 1.21**	
SVM	Normal	95.05 ± 2.92	**94.41 ± 3.33**	**94.39 ± 2.50**	**3.24 ± 1.25**
	Atrial Fibrillation	**94.39 ± 3.37**	97.47 ± 2.62	**95.64 ± 2.56**	
	Paced	**99.58 ± 1.05**	98.52 ± 2.15	98.97 ± 1.29	
	Sinus bradycardia	**99.63 ± 1.00**	96.65 ± 0.22	98.02 ± 0.51	

By including a fourth rhythm, and consequently decreasing the number of samples used for training and testing the classifier, the performance of the classifiers was again affected. Still, the overall accuracy for the SVM classifier was around 97%. It is interesting to note that precision and recall values for paced rhythm and sinus bradycardia are quite high, but the recognition of normal and atrial fibrillation segments becomes less obvious. This is true for the three classifiers.

30 seconds segments

The same four rhythms stated above were considered again, this time with 30 seconds segments. The total number of samples per rhythm could be raised to 60. The results obtained are presented in Table 18.

Table 18: Results obtained with feature sets B + C in the distinction of four rhythms.

Classifier	Rhythm	Precision (%)	Recall (%)	F-score (%)	Test error (%)
ANN	Normal	97.31 ± 2.12	88.3 ± 4.58	92.29 ± 3.06	4.06 ± 1.34
	Atrial Fibrillation	90.41 ± 3.48	96.93 ± 2.29	93.38 ± 2.37	
	Paced	98.81 ± 1.30	**100.0 ± 0.0**	99.38 ± 0.69	
	Sinus bradycardia	98.67 ± 1.31	98.53 ± 0.86	98.55 ± 0.82	
kNN	Normal	**98.00 ± 1.79**	88.83 ± 3.83	92.92 ± 2.58	3.48 ± 1.19
	Atrial Fibrillation	91.68 ± 3.13	**97.6 ± 1.74**	94.38 ± 2.11	
	Paced	98.87 ± 1.11	**100.0 ± 0.0**	99.41 ± 0.59	
	Sinus bradycardia	98.80 ± 1.25	99.63 ± 0.69	99.19 ± 0.76	
SVM	Normal	96.51 ± 2.08	**93.87 ± 2.78**	**95.00 ± 2.41**	**2.58 ± 1.06**
	Atrial Fibrillation	**95.01 ± 2.41**	97.07 ± 2.12	**95.89 ± 1.91**	
	Paced	**99.66 ± 0.72**	99.37 ± 0.94	**99.49 ± 0.58**	
	Sinus bradycardia	**99.20 ± 1.19**	99.4 ± 0.87	**99.27 ± 0.83**	

Comparing these results with the ones obtained previously, it is clear that the performance of the classifiers benefited from the reduction of the segments' length, and consequent rise of the number of samples (which doubled). Again, recognition of paced rhythm and sinus bradycardia is more precise than the two other rhythms.

A second test was performed with 30 seconds segments. This was meant to deal with bigeminal and trigeminal rhythms. Because of the similarities between these two arrhythmias, and considering the small number of segments available, the following experiments were carried out. First, using respectively 31 and 12 samples per rhythm, bigeminy and trigeminy were considered, individually, along the four rhythms considered previously. The results of these two experiments are presented in Table 19 and Table 20. Secondly, using 12 samples per rhythm, an attempt was made to distinguish between the six rhythms. These results are summarized in Table 21. Finally, a class that contains segments of trigeminy and bigeminy was constructed, and the distinction between this class and the four others was attempted. A total of 43 samples per rhythm was used in this case and the results are presented in Table 22.

Table 19: Results obtained with feature sets B + C in the distinction of five rhythms (31 samples per rhythm).

Classifier	Rhythm	Precision (%)	Recall (%)	F-score (%)	Test error (%)
ANN	Normal	95.33 ± 4.21	79.10 ± 7.67	85.61 ± 5.93	11.38 ± 2.51
	Atrial Fibrillation	80.04 ± 6.14	81.14 ± 5.95	79.24 ± 5.37	
	Paced	98.92 ± 1.67	99.88 ± 0.88	99.35 ± 0.99	
	Sinus bradycardia	95.10 ± 2.56	98.38 ± 1.63	96.51 ± 1.85	
	Bigeminy	80.60 ± 4.56	84.61 ± 6.40	81.51 ± 4.79	
kNN	Normal	**96.75 ± 4.05**	78.71 ± 7.67	85.89 ± 5.57	9.14 ± 2.35
	Atrial Fibrillation	82.71 ± 5.55	**89.87 ± 5.67**	85.38 ± 4.77	
	Paced	98.98 ± 1.47	**100.0 ± 0.0**	**99.46 ± 0.79**	
	Sinus bradycardia	95.05 ± 1.87	**99.02 ± 1.50**	96.84 ± 1.22	
	Bigeminy	86.84 ± 5.28	86.73 ± 2.72	86.07 ± 3.48	
SVM	Normal	90.91 ± 4.64	**88.71 ± 5.37**	**89.00 ± 4.60**	**7.80 ± 1.80**
	Atrial Fibrillation	**88.60 ± 3.92**	88.83 ± 5.68	**87.96 ± 3.97**	
	Paced	**99.94 ± 0.44**	97.02 ± 2.88	98.36 ± 1.65	
	Sinus bradycardia	**96.96 ± 2.17**	97.54 ± 2.84	**97.07 ± 2.31**	
	Bigeminy	**88.96 ± 3.90**	**88.88 ± 3.19**	**88.16 ± 2.70**	

Table 20: Results obtained with feature sets B + C in the distinction of five rhythms (12 samples per rhythm).

Classifier	Rhythm	Precision (%)	Recall (%)	F-score (%)	Test error (%)
ANN	Normal	72.01 ± 20.84	55.17 ± 18.55	59.20 ± 17.92	17.5 ± 5.69
	Atrial Fibrillation	76.32 ± 12.79	82.0 ± 11.10	76.45 ± 11.27	
	Paced	92.08 ± 6.17	98.67 ± 4.20	94.67 ± 4.71	
	Sinus bradycardia	95.31 ± 5.44	98.0 ± 3.93	96.00 ± 4.07	
	Trigeminy	82.86 ± 11.24	78.67 ± 8.84	77.72 ± 8.11	
kNN	Normal	**86.81 ± 14.97**	61.17 ± 13.70	68.83 ± 13.38	**13.43 ± 4.01**
	Atrial Fibrillation	83.1 ± 8.23	**86.67 ± 10.14**	82.68 ± 8.67	
	Paced	92.58 ± 2.60	**99.67 ± 1.63**	**95.51 ± 1.74**	
	Sinus bradycardia	**99.38 ± 1.88**	**99.0 ± 2.71**	**99.04 ± 2.19**	
	Trigeminy	80.21 ± 8.89	**86.33 ± 7.22**	81.20 ± 6.86	
SVM	Normal	70.10 ± 9.35	**73.33 ± 12.69**	**69.25 ± 10.13**	13.83 ± 3.76
	Atrial Fibrillation	**87.84 ± 7.93**	86.5 ± 9.98	**85.51 ± 8.44**	
	Paced	**99.75 ± 1.22**	92.67 ± 7.20	95.11 ± 4.84	
	Sinus bradycardia	99.25 ± 2.03	92.83 ± 6.24	95.83 ± 6.24	
	Trigeminy	**87.36 ± 7.67**	85.5 ± 5.48	**84.7 ± 6.13**	

A first comment can be made about the two tables above. By including a fifth rhythm, bigeminy or trigeminy, the performance of the classifiers worsened. This is understandable since not only is there one additional class to consider, but also the number of training patterns was reduced. As expected, the results are poorer with trigeminy segments than with bigeminy. Certainly, this can again be explained by the smaller number of training patterns (31 versus 12).

Table 21: Results obtained with feature sets B + C in the distinction of six rhythms (12 samples per rhythm).

Classifier	Rhythm	Precision (%)	Recall (%)	F-score (%)	Test error (%)
ANN	Normal	76.21 ± 18.17	56.17 ± 14.42	61.09 ± 13.66	21.53 ± 4.44
	Atrial Fibrillation	68.03 ± 12.46	74.5 ± 15.13	68.55 ± 12.20	
	Paced	93.74 ± 5.40	98.67 ± 3.86	95.54 ± 4.09	
	Sinus bradycardia	91.38 ± 6.63	97.5 ± 4.17	93.59 ± 4.91	
	Bigeminy	68.59 ± 13.03	69.17 ± 15.12	66.37 ± 12.40	
	Trigeminy	81.42 ± 11.87	74.83 ± 8.08	74.95 ± 6.95	
kNN	Normal	**85.5 ± 16.07**	57.67 ± 18.77	65.89 ± 17.29	**16.83 ± 4.74**
	Atrial Fibrillation	75.31 ± 11.16	**80.0 ± 11.18**	75.30 ± 9.70	
	Paced	93.28 ± 4.14	**99.67 ± 2.33**	**95.88 ± 2.64**	
	Sinus bradycardia	**95.07 ± 4.40**	**98.33 ± 3.33**	**96.21 ± 2.17**	
	Bigeminy	79.84 ± 9.05	77.17 ± 11.64	75.39 ± 8.15	
	Trigeminy	83.78 ± 10.87	**86.17 ± 7.38**	82.74 ± 8.14	
SVM	Normal	71.88 ± 11.92	**75.0 ± 13.43**	**70.17 ± 11.21**	17.03 ± 3.99
	Atrial Fibrillation	**82.02 ± 10.61**	76.67 ± 12.91	**76.35 ± 10.83**	
	Paced	**98.88 ± 3.89**	90.5 ± 8.98	93.29 ± 6.73	
	Sinus bradycardia	94.26 ± 4.65	94.17 ± 6.07	93.15 ± 5.35	
	Bigeminy	**81.47 ± 9.79**	**78.33 ± 9.57**	**76.93 ± 8.59**	
	Trigeminy	**88.0 ± 7.67**	83.17 ± 7.73	**83.68 ± 6.91**	

Table 22: Results obtained with feature sets B + C in the distinction of six classes (43 samples per rhythm).

Classifier	Rhythm	Precision (%)	Recall (%)	F-score (%)	Test error (%)
ANN	Normal	89.99 ± 5.78	79.91 ± 7.40	83.40 ± 5.71	12.76 ± 2.82
	Atrial Fibrillation	79.47 ± 5.42	85.85 ± 4.44	81.73 ± 4.05	
	Paced	98.21 ± 1.81	**100.0 ± 0.0**	99.06 ± 0.96	
	Sinus bradycardia	95.62 ± 2.61	98.29 ± 1.20	96.81 ± 1.50	
	Bigeminy + Trigeminy	78.33 ± 7.91	72.13 ± 10.38	73.59 ± 9.27	
kNN	Normal	**95.47 ± 2.68**	80.35 ± 7.05	86.59 ± 5.02	8.30 ± 1.70
	Atrial Fibrillation	86.43 ± 3.75	**92.38 ± 3.59**	88.87 ± 2.94	
	Paced	97.60 ± 1.54	**100.0 ± 0.0**	98.74 ± 0.82	
	Sinus bradycardia	95.70 ± 1.76	**99.44 ± 1.00**	**97.44 ± 1.06**	
	Bigeminy + Trigeminy	86.89 ± 4.52	86.36 ± 2.00	86.05 ± 2.87	
SVM	Normal	91.03 ± 3.73	**88.66 ± 4.25**	**89.32 ± 3.57**	**7.26 ± 1.42**
	Atrial Fibrillation	**91.15 ± 2.89**	90.84 ± 4.10	**90.57 ± 2.62**	
	Paced	**99.96 ± 0.29**	98.78 ± 1.58	**99.33 ± 0.87**	
	Sinus bradycardia	**96.46 ± 1.68**	98.19 ± 1.97	97.21 ± 1.54	
	Bigeminy + Trigeminy	**87.81 ± 3.53**	**87.24 ± 3.20**	**87.04 ± 2.57**	

When trying to distinguishing between the six rhythms, the results are quite poor. The kNN classifier performs best but the overall accuracy is barely above 83%. Even though paced and sinus bradycardia rhythms present precision and recall values above 90% for all classifiers, the recognition of the remaining rhythms is considerably worst.

By constructing a new class that encompasses bigeminy and trigeminy segments, the results improved. An overall correct classification of almost 93% was achieved with the SVM classifier. The biggest advantage of combining these two rhythms is that the number of samples available for training increases substantially. It should be mentioned that the two rhythms share similar characteristics (alternation between PVCs and sinus beats) and this can justify considering them under the same class.

The remaining multiclass experiments were performed with segments of 10 seconds.

10 seconds segments

With segments of 10 seconds more samples per rhythm are available and it is therefore possible to include more classes in the experiment. Besides the rhythms considered above, second heart block and atrial flutter were included in the analysis. Due to the conclusions of the previous section, bigeminy and trigeminy were considered as a single class. Atrial flutter presents some similarities with atrial fibrillation, namely the fast electrical discharge pattern in the atria, so the following two experiments were carried out. First, atrial flutter was considered individually; secondly, atrial flutter and atrial fibrillation were considered as a single class. The corresponding results are presented in Table 23 and Table 24.

Table 23: Results obtained with feature sets B + C in the distinction of seven classes (60 samples per rhythm).

Classifier	Rhythm	Precision (%)	Recall (%)	F-score (%)	Test error (%)
ANN	Normal	83.40 ± 5.06	78.77 ± 5.51	80.02 ± 4.75	15.0 ± 2.19
	Atrial Fibrillation	71.11 ± 5.64	71.8 ± 6.88	70.47 ± 5.38	
	Paced	98.02 ± 1.75	**99.57 ± 0.80**	98.74 ± 0.99	
	Sinus bradycardia	93.91 ± 3.29	89.07 ± 3.67	91.12 ± 2.91	
	Bigeminy + Trigeminy	76.46 ± 6.06	72.77 ± 7.98	73.35 ± 6.47	
	2nd heart block	98.87 ± 1.09	99.37 ± 0.81	99.09 ± 0.80	
	Atrial Flutter	79.75 ± 4.78	83.67 ± 5.03	81.02 ± 4.22	
kNN	Normal	**88.21 ± 5.65**	79.1 ± 6.16	**82.85 ± 5.58**	**11.43 ± 1.48**
	Atrial Fibrillation	76.27 ± 4.44	**77.17 ± 5.27**	76.17 ± 4.17	
	Paced	98.16 ± 1.71	99.5 ± 0.76	**98.78 ± 1.00**	
	Sinus bradycardia	94.67 ± 2.90	**97.43 ± 1.98**	**95.89 ± 2.02**	
	Bigeminy + Trigeminy	82.86 ± 4.65	**82.86 ± 4.65**	82.24 ± 4.37	
	2nd heart block	99.41 ± 0.82	**99.83 ± 0.5**	**99.61 ± 0.47**	
	Atrial Flutter	84.12 ± 3.99	84.3 ± 4.24	83.77 ± 3.46	
SVM	Normal	78.40 ± 5.22	**82.87 ± 3.99**	79.99 ± 3.91	11.43 ± 1.86
	Atrial Fibrillation	**80.28 ± 4.99**	76.47 ± 4.96	**77.79 ± 4.44**	
	Paced	**98.92 ± 1.39**	98.57 ± 1.53	98.69 ± 1.08	
	Sinus bradycardia	**95.35 ± 2.30**	94.5 ± 3.04	94.69 ± 2.12	
	Bigeminy + Trigeminy	**85.20 ± 4.06**	82.07 ± 6.77	**82.91 ± 5.42**	
	2nd heart block	**100.0 ± 0.0**	98.47 ± 0.45	99.21 ± 0.23	
	Atrial Flutter	**86.70 ± 4.18**	**87.07 ± 4.65**	**86.51 ± 3.90**	

Table 24: Results obtained with feature sets B + C in the distinction of six classes (68 samples per rhythm).

Classifier	Rhythm	Precision (%)	Recall (%)	F-score (%)	Test error (%)
ANN	Normal	83.76 ± 4.58	78.94 ± 4.42	80.60 ± 3.72	12.60 ± 1.56
	Atrial Fibrillation / Flutter	77.73 ± 4.02	82.5 ± 4.52	79.40 ± 3.61	
	Paced	97.88 ± 1.71	99.59 ± 0.72	98.69 ± 1.08	
	Sinus bradycardia	92.91 ± 3.66	89.5 ± 2.50	90.85 ± 2.31	
	Bigeminy + Trigeminy	77.68 ± 4.40	74.65 ± 7.29	75.30 ± 5.13	
	2nd heart block	98.90 ± 1.03	99.21 ± 0.73	99.02 ± 0.66	
kNN	Normal	**89.78 ± 4.95**	80.0 ± 4.69	**84.13 ± 4.27**	**8.32 ± 1.83**
	Atrial Fibrillation / Flutter	85.63 ± 4.27	**85.71 ± 4.26**	**85.71 ± 4.26**	
	Paced	97.93 ± 1.46	**99.76 ± 0.54**	98.80 ± 0.85	
	Sinus bradycardia	**94.96 ± 2.02**	**97.59 ± 1.92**	**96.14 ± 1.50**	
	Bigeminy + Trigeminy	84.70 ± 4.60	**87.26 ± 5.45**	**85.62 ± 4.69**	
	2nd heart block	99.31 ± 0.75	**99.76 ± 0.54**	**99.52 ± 0.47**	
SVM	Normal	80.85 ± 4.52	**83.18 ± 3.95**	81.49 ± 3.94	9.16 ± 1.67
	Atrial Fibrillation / Flutter	87.97 ± 4.66	84.24 ± 4.72	85.66 ± 1.28	
	Paced	**98.80 ± 1.04**	98.88 ± 1.23	**98.81 ± 0.86**	
	Sinus bradycardia	94.95 ± 2.58	94.65 ± 2.66	94.63 ± 2.02	
	Bigeminy + Trigeminy	**85.87 ± 4.04**	85.56 ± 4.45	85.28 ± 3.81	
	2nd heart block	**99.97 ± 0.19**	98.53 ± 0.0	99.23 ± 0.1	

Before analyzing the tables above, it is important to remember some facts. First, a total of 8 rhythms are now being considered. Secondly, these experiments were carried out with segments of 10

seconds. And thirdly, for each run, the number of samples per rhythm is now reduced to 60 or 70 samples. In the initial experiments, a binary classification problem was being addressed, segments of 60 seconds were used, and approximately 100 samples per rhythm were available. That is, not only are we trying to recognize more classes based on the same features, but this is being attempted using segments with less information and the number of training samples is reduced.

Comparing the results of Table 23 and Table 24 it appears that it may be advantageous to consider atrial fibrillation and atrial flutter as a single class. In fact, the results in terms of test error improve for all classifiers. It is interesting to note that, for the kNN classifier, precision and recall values for the class that encompasses atrial flutter and atrial fibrillation are superior to the ones obtained for each one of these rhythms when they are considered individually. Overall, the best classification was obtained with kNN, that reached an accuracy close to 92%. The best recall values for the arrhythmias and the paced rhythm were also obtained with this classifier, whereas SVM tended to reach the best results in terms of precision.

A final experiment was carried out to try to find a better solution for bigeminy and trigeminy segments, which seemed to be affecting the classifiers' performance. First, the class containing these rhythms was simply discarded. These results are summarized in Table 25. Secondly, bigeminy and trigeminy segments were considered in combination with normal sinus rhythm records, forming a class with three rhythms. These results are presented in Table 26.

Table 25: Results obtained with feature sets B + C in the distinction of five classes (68 samples per rhythm).

Classifier	Rhythm	Precision (%)	Recall (%)	F-score (%)	Test error (%)
ANN	Normal	88.60 ± 3.37	82.94 ± 4.97	85.18 ± 3.36	7.1 ± 1.30
	Atrial Fibrillation / Flutter	86.01 ± 3.85	91.21 ± 3.17	88.16 ± 2.83	
	Paced	97.74 ± 1.42	99.65 ± 0.69	98.65 ± 0.87	
	Sinus bradycardia	**95.67 ± 2.44**	91.24 ± 2.93	93.15 ± 2.12	
	2nd heart block	98.79 ± 1.16	99.47 ± 0.71	99.10 ± 0.71	
kNN	Normal	**92.86 ± 3.08**	84.35 ± 4.43	**88.04 ± 3.35**	**5.32 ± 1.19**
	Atrial Fibrillation / Flutter	90.06 ± 3.36	**91.74 ± 2.82**	**90.65 ± 2.62**	
	Paced	97.38 ± 1.69	**99.82 ± 0.48**	98.54 ± 0.88	
	Sinus bradycardia	95.10 ± 2.07	**97.74 ± 1.48**	**96.28 ± 1.28**	
	2nd heart block	99.17 ± 0.83	**99.74 ± 0.56**	**99.44 ± 0.59**	
SVM	Normal	85.42 ± 3.91	**87.03 ± 4.29**	85.79 ± 3.37	6.24 ± 1.34
	Atrial Fibrillation / Flutter	**91.79 ± 2.79**	89.94 ± 4.12	90.52 ± 3.10	
	Paced	**98.42 ± 1.26**	99.0 ± 1.23	**98.67 ± 0.94**	
	Sinus bradycardia	95.20 ± 2.74	94.32 ± 2.77	94.59 ± 1.98	
	2nd heart block	**100.0 ± 0.0**	98.53 ± 0.0	99.24 ± 0.0	

Table 26: Results obtained with feature sets B + C in the distinction of five classes (68 samples per rhythm).

Classifier	Rhythm	Precision (%)	Recall (%)	F-score (%)	Test error (%)
ANN	Normal + Bigeminy + Trigeminy	87.54 ± 3.44	81.40 ± 3.98	83.96 ± 3.05	7.63 ± 1.33
	Atrial Fibrillation / Flutter	84.57 ± 3.49	**90.85 ± 3.69**	87.27 ± 3.07	
	Paced	97.42 ± 1.49	99.59 ± 0.66	98.45 ± 0.85	
	Sinus bradycardia	95.40 ± 2.25	90.88 ± 2.08	92.85 ± 1.68	
	2nd heart block	99.05 ± 1.02	99.38 ± 0.73	99.20 ± 0.62	
kNN	Normal + Bigeminy + Trigeminy	**91.75 ± 3.15**	82.10 ± 4.38	86.21 ± 3.36	**6.05 ± 1.26**
	Atrial Fibrillation / Flutter	88.16 ± 3.00	90.53 ± 3.71	89.04 ± 2.73	
	Paced	97.24 ± 1.59	**99.74 ± 0.56**	98.44 ± 0.95	
	Sinus bradycardia	94.75 ± 2.41	**97.76 ± 1.51**	**96.12 ± 1.50**	
	2nd heart block	99.17 ± 0.82	**99.85 ± 0.44**	**99.50 ± 0.48**	
SVM	Normal + Bigeminy + Trigeminy	86.10 ± 3.33	**87.39 ± 3.76**	**86.32 ± 2.63**	6.18 ± 1.00
	Atrial Fibrillation / Flutter	**91.18 ± 3.26**	89.35 ± 3.05	**89.90 ± 2.29**	
	Paced	**98.45 ± 1.47**	99.15 ± 0.89	**98.77 ± 0.84**	
	Sinus bradycardia	**95.45 ± 2.37**	94.82 ± 2.62	94.97 ± 1.88	
	2nd heart block	**100.0 ± 0.0**	98.53 ± 0.0	99.24 ± 0.0	

By not including records of bigeminy and trigeminy, the performance of the classifiers was significantly improved. The best results were obtained with the kNN classifier. An overall accuracy close to 95% was achieved. However, this approach is not very realistic: if a bigeminy or trigeminy segment ought to be classified, there will be no similar training pattern available. Interestingly, when forming a class with normal, bigeminy and trigeminy segments, the results are only slightly worse. Depending on the goal of the classification task, one may take advantage of this fact. For instance, if the occurrence of bigeminal or trigeminal rhythms is of no practical relevance, these rhythms may be included in the normal class instead of considered individually.

The multiclass experiments led to interesting results and conclusions. With segments of 60 seconds, by including more rhythms in the classification, a smaller number of samples per rhythm had to be used. In terms of test error, the classifiers performed worse in comparison to the binary classification task. This was true even though precision and recall values for the newly included rhythms (paced and sinus bradycardia) were very high. A better performance was achieved by reducing the segment's length and thus augmenting the number of samples.

The tests with bigeminy and trigeminy segments showed the advantage of gathering these similar rhythms under the same class. Additionally, depending on the classification goal, it may be useful to consider bigeminy and trigeminy under the 'normal' class. With 10 seconds segments, it was shown that atrial fibrillation and atrial flutter could also be considered as a unique class, which provided best results in comparison with considering them individually.

In terms of classifiers, SVM and kNN proved to be the most suitable choices. Overall, the kNN classifier reached better recall values for the arrhythmic classes, whereas the precision values for these rhythms were better with the SVM classifier. Depending on the application, it may be more useful to opt for one or the other.

5.4. Rhythm Classification with BITalino Acquisitions

A total of 13 normal sinus rhythm and 13 AF records acquired with the BITalino were selected to perform a few classification tests. These had a length of approximately 60 seconds and were not too seriously affected with artefacts.

Two approaches were studied. In Experiment A, segments from the MIT-BIH arrhythmia database were used to train the classifiers and the BITalino acquisitions formed the test set. In Experiment B, training and testing were done entirely with BITalino acquisitions.

Experiment A

In this experiment, for each run, 98 normal sinus rhythm and AF segments were randomly selected from the MIT-BIH arrhythmia database to train the classifier. The 26 BITalino acquisitions were then classified. A few adjustments had to be considered for this analysis. Since the sampling rates are different (360 and 1000 Hz respectively for MIT-BIH database and the BITalino acquisitions), this had to be taken into account for the computations of average and standard deviation of RR intervals. Additionally, the voltage of each signal was scaled to the range [0, 1] prior to wavelet decomposition.

It should be noted that this use of the MIT-BIH database was an attempt to profit from a larger number of samples for training. However, major differences exist between the two datasets. Namely, MIT-BIH records corresponded to a modified limb II lead, whereas the BITalino ECGs were acquired at the fingers (corresponding to lead I).

This experiment was carried out first with filtered BITalino records and then using raw signals. The results are summarized respectively in Table 27 and Table 28.

Table 27: Results of Experiment A with filtered BITtalino records.

Classifier	Rhythm	Precision (%)	Recall (%)	F-score (%)	Test error (%)
ANN	Normal	62.04 ± 6.44	98.92 ± 3.08	76.01 ± 4.50	31.69 ± 7.68
	Atrial Fibrillation	98.32 ± 4.65	37.69 ± 16.37	52.27 ± 16.58	
kNN	Normal	**70.57 ± 4.04**	99.85 ± 1.08	**82.62 ± 2.91**	**21.15 ± 4.50**
	Atrial Fibrillation	**99.78 ± 1.56**	**57.85 ± 9.00**	**72.76 ± 8.10**	
SVM	Normal	51.92 ± 0.39	**100.0 ± 0.0**	68.35 ± 0.34	46.31 ± 0.75
	Atrial Fibrillation	96.0 ± 19.60	7.38 ± 1.51	13.71 ± 2.80	

Table 28: Results of Experiment A with raw BITalino records.

Classifier	Rhythm	Precision (%)	Recall (%)	F-score (%)	Test error (%)
ANN	Normal	71.13 ± 7.32	99.08 ± 2.50	82.56 ± 4.59	21.31 ± 6.63
	Atrial Fibrillation	98.60 ± 4.33	58.31 ± 13.77	72.31 ± 10.73	
kNN	Normal	**72.04 ± 3.14**	**100.0 ± 0.0**	**83.71 ± 2.10**	**19.54 ± 2.96**
	Atrial Fibrillation	**100.0 ± 0.0**	**60.92 ± 5.93**	**75.55 ± 4.53**	
SVM	Normal	56.52 ± 0.0	**100.0 ± 0.0**	72.22 ± 0.0	38.46 ± 0.0
	Atrial Fibrillation	**100.0 ± 0.0**	23.08 ± 0.0	37.5 ± 0.0	

Referring to the tables above it is clear that, for all classifiers, the results are better with raw segments than when compared to filtered signals. This is an interesting observation since it could save some time in a real time classification problem. However, it is possible that the filter applied was not the most suitable for this purpose. Further tests should be conducted to clarify this situation.

For the three classifiers the results obtained in terms of test error were poor. The kNN classifier achieved the best performance whilst the worst results were obtained with the SVM classifier. Overall, there was a tendency to obtain very poor recall values for AF. The precision values were very high, reaching often 100%.

Experiment B

Due to the small number of samples used in this experiment, adjustments to the validation setup were made. Instead of a 4-fold cross validation, a leave-one-out approach was adopted. That is, each sample was used once as test sample while the remaining formed the training set.

Like for the Experiment A, filtered and raw segments were used. The results are presented in Table 29 and Table 30.

Table 29: Results of Experiment B with filtered BITalino records.

Classifier	Rhythm	Precision (%)	Recall (%)	F-score (%)	Test error (%)
ANN	Normal	90.80 ± 5.86	**91.23 ± 5.10**	**90.84 ± 3.86**	**9.23 ± 4.00**
	Atrial Fibrillation	**91.39 ± 4.69**	90.31 ± 6.85	**90.65 ± 4.25**	
kNN	Normal	**91.67**	84.62	88.0	11.54
	Atrial Fibrillation	85.71	**92.31**	88.89	
SVM	Normal	**91.67**	84.62	88.0	11.54
	Atrial Fibrillation	85.71	**92.31**	88.89	

Table 30: Results of Experiment B with raw BITalino records.

Classifier	Rhythm	Precision (%)	Recall (%)	F-score (%)	Test error (%)
ANN	Normal	87.32 ± 7.76	83.38 ± 5.83	**85.08 ± 5.18**	**14.69 ± 5.37**
	Atrial Fibrillation	**84.12 ± 5.10**	87.23 ± 8.51	85.46 ± 5.67	
kNN	Normal	78.57	**84.62**	81.48	19.23
	Atrial Fibrillation	83.33	76.92	80.0	
SVM	Normal	90.91	76.92	83.33	15.38
	Atrial Fibrillation	80.0	**92.31**	**85.71**	

On this occasion, all classifiers achieved a better performance with filtered signals. A test error of 9.23% was reached with the ANN classifier and filtered signals. In that situation, precision and recall values were above 90%. It is possible that a fine tuning of the classifiers' parameters could lead to better results.

The results obtained with Experiment A were quite poor: using different databases for training and testing proved not to be the best solution. Despite the small number of samples used, interesting results were obtained with Experiment B. Although the results were not as good as the ones obtained previously, these experiments prove that it is possible to distinguish AF from normal sinus rhythm ECG records acquired with the BITalino system. With a more thorough analysis, including a fine tuning of the classifiers' parameters, a larger amount of samples, and the inclusion of more rhythms, we should be able to successfully apply the automatic ECG analysis methodology described in this work.

6. Conclusions and Future Work

With the continuous development of tools for cardiac monitoring, an enormous amount of data can be collected and has to be analyzed. It is therefore critical to develop new algorithms that will aid in this analysis, automatizing, to a certain extent, the process. The recognition of arrhythmias is one important part of the problem and pattern recognition methods have been successfully applied. In this work, a methodology for automatic ECG analysis was proposed, encompassing data acquisition, processing and classification. Automatic arrhythmia classification was attempted using both spectral and time domain features. The performance of three supervised learning classifiers was compared. Validation of the proposed method was performed resorting to benchmarked data from a widely used arrhythmia database. Additionally, initial experiments were carried out to assess the feasibility of classifying ECG records acquired with the BITalino at the fingers.

The segmentation algorithm employed was compared against reference annotations on the MIT-BIH arrhythmia database. Precision and positive predictive values of, respectively, 99.59 and 99.69% were obtained, attesting to the reliability of the algorithm. The remaining work focused on the classification task.

At first, only normal sinus rhythm and AF records were considered. A number of tests were carried out to determine the best set of features and corresponding classifiers' parameters. It was shown that the combination of spectral and time domain features offered the best results. SVM reached an overall accuracy of 99.08% with F-scores above 99% for both classes. An additional test was conducted to try to understand the influence of the segments' length. It was shown that it is important to find a balance between the number of samples available for training and the information contained in each segment.

The inclusion of other rhythms on the classification task was then attempted. In order to do so, and due to the small number of samples per rhythm available, the segments' length was reduced. It was not possible to reach accuracies as high as before but interesting results were obtained and a few conclusions were drawn. In the last experiment, when 5 classes representing a total of 8 rhythms were considered, the kNN classifier reached an overall classification rate close to 94%.

As the number of classes increased (and the number of samples diminished), the classifiers were less able to distinguish between different rhythms. This is not to say that the recognition of all classes was equally difficult. In fact, rhythms such as paced rhythm or 2nd heart block were easily classified.

It also became clear that measures could be taken to improve the classifiers' performance. Depending on the ultimate goal, it was shown that it can be helpful to gather different but similar rhythms under the same class (e.g. bigeminy and trigeminy or AF and atrial flutter). As a future development, it may be interesting to develop a step-by-step classification process. That is, to perform the classification in different phases, determining which rhythms ought to be distinguished in each phase. Additionally, it may be worthwhile to adapt the features to the type of rhythms we sought to distinguish. For instance, due to the characteristics of the rhythms, it is possible that distinguishing between normal sinus rhythm and sinus bradycardia could rely solely on the heart rate. When selecting the features to use,

one should take into account the amount of time necessary to extract them (in this case, spectral features required a lengthier processing method).

In terms of classifier, SVM and kNN proved to be the most suitable choices. Interestingly, the latter provided higher values of recall for arrhythmias whereas precision values were higher for the first. Again, depending on the application, it may be more useful to opt for one or the other. When making this choice, one should also consider the time available for classification since the length of training and testing phases is different for each classifier.

Finally, the experiments performed with records acquired with the BITalino proved that it is possible to develop algorithms that will automatically analyze and classify ECG records acquired with this system. With further developments, more rhythms can be included in the analysis and real time applications can be considered. For instance, the BITalino can be embedded in day-to-day objects and alarms can be triggered when an arrhythmia is present.

References

Addison, P. (2005). Wavelet transforms and the ECG: a review. *Physiological measurement*, 26(5), p.155.

Al-Fahoum, A. and Howitt, I. (1999). Combined wavelet transformation and radial basis neural networks for classifying life-threatening cardiac arrhythmias. *Medical & biological engineering & computing*, 37(5), pp.566--573.

Alves, A., Silva, H., Lourenço, A. and Fred, A. (2013). BITalino: A Biosignal Acquisition System based on the Arduino. *Proc. of Intl. Conf. BIODEVICES, SCITEPRESS*, pp.261--264.

Anas, E., Lee, S. and Hasan, M. (2010). Sequential algorithm for life threatening cardiac pathologies detection based on mean signal strength and EMD functions. *Biomedical engineering online*, 9(1), p.43.

Artis, S., Mark, R. and Moody, G. (1991). Detection of atrial fibrillation using artificial neural networks. *Computers in Cardiology 1991, Proceedings*, pp.173--176.

Bakhshi, A., Maud, M., Aamir, K. and Loan, A. (2010). Cardiac arrhythmia detection using instantaneous frequency estimation of ECG signals. *Information and Emerging Technologies (ICIET), 2010 International Conference on.* IEEE. pp.1--5.

Barrett, P., Komatireddy, R., Haaser, S., Topol, S., Sheard, J., Encinas, J., Fought, A. and Topol, E. (2014). Comparison of 24-hour Holter Monitoring with 14-day Novel Adhesive Patch Electrocardiographic Monitoring. *The American journal of medicine*, 127(1), pp.95--11.

Batista, D. and Fred, A. (2014). Spectral and Time Domain Parameters for the Classification of Atrial Fibrillation. In *8th International Conference on Bio-inspired Systems and Signal Processing*. [Submitted]

Beale, R. and Fiesler, E. (1997). *Handbook of neural computation*. Bristol: Institute of Physics Pub.

Brignole, M., Vardas, P., Hoffman, E., Huikuri, H., Moya, A., Ricci, R., Sulke, N., Wieling, W., Auricchio, A., Lip, G. and others, (2009). Indications for the use of diagnostic implantable and external ECG loop recorders. *Europace*, 11(5), pp.671--687.

Burri, H. and Senouf, D. (2009). Remote monitoring and follow-up of pacemakers and implantable cardioverter defibrillators. *Europace*, 11(6), pp.701--709.

CardioNet, (2014). *CardioNet MCOT*. [image] Available at: https://www.cardionet.com/patients_03.htm [Accessed 10 Oct. 2014].

Carreiras, C., Lourenço, A., Silva, H., and Fred, A. (2013). Comparative study of medical-grade and off- the-person ecg systems. In *Int. Congress on Cardio- vascular Technologies*.

Ceylan, R. and Özbay, Y. (2007). Comparison of FCM, PCA and WT techniques for classification ECG arrhythmias using artificial neural network. *Expert Systems with Applications*, 33(2), pp.286--295.

Chiu, C., Lin, T. and Liau, B. (2005). Using correlation coefficient in ECG waveform for arrhythmia detection. *Biomedical Engineering: Applications, Basis and Communications*, 17(03), pp.147--152.

Clayton, R., Murray, A. and Campbell, R. (1994). Recognition of ventricular fibrillation using neural networks. *Medical and Biological Engineering and Computing*, 32(2), pp.217--220.

Crawford, M., Bernstein, S., Deedwania, P., DiMarco, J., Ferrick, K., Garson, A., Green, L., Greene, H., Silka, M., Stone, P. and others, (1999). ACC/AHA Guidelines for Ambulatory Electrocardiography: Executive Summary and Recommendations A Report of the American College of Cardiology/American Heart Association Task Force on Practice Guidelines (Committee to Revise the Guidelines for Ambulatory Electrocardiography) Developed in Collaboration With the North American Society for Pacing and Electrophysiology. *Circulation*, 100(8), pp.886--893.

De Chazal, P., O'Dwyer, M. and Reilly, R. (2004). Automatic classification of heartbeats using ECG morphology and heartbeat interval features. *Biomedical Engineering, IEEE Transactions on*, 51(7), pp.1196--1206.

Duda, R., Hart, P. and Stork, D. (2001). *Pattern classification*. New York: Wiley.

Fletcher, T. (2009). Support vector machines explained. Tutorial paper. [online] Available at: http://www.tristanfletcher.co.uk/. [Accessed 5 Nov. 2014]

Fowler, J. (2005). The redundant discrete wavelet transform and additive noise. *Signal Processing Letters, IEEE*, 12(9), pp.629--632.

Garcia, T. and Miller, G. (2004). *Arrhythmia recognition*. Sudbury, Mass.: Jones and Bartlett Publishers.

Ge, D., Srinivasan, N. and Krishnan, S. (2002). Cardiac arrhythmia classification using autoregressive modeling. *Biomedical engineering online*, 1(1), p.5.

Guerreiro, J., Martins, R., Silva, H., Lourenço, A. and Fred, A. (2013). BITalino-A Multimodal Platform for Physiological Computing. *ICINCO (1)* pp.500--506.

Güler, I. and Übeyli, E. (2005). ECG beat classifier designed by combined neural network model. *Pattern recognition*, 38(2), pp.199--208.

Hamilton, P. (2002). *Open Source ECG Analysis Software Documentation*. 1st ed. [ebook] E.P. Limited. Available at: http://www.eplimited.com/osea13.pdf [Accessed 26 Oct. 2014].

Hsu, C. and Lin, C. (2002). A comparison of methods for multiclass support vector machines. *Neural Networks, IEEE Transactions on*, 13(2), pp.415--425.

Hu, Y., Tompkins, W., Urrusti, J. and Afonso, V. (1993). Applications of artificial neural networks for ECG signal detection and classification. *Journal of electrocardiology*, 26, pp.66--73.

Huff, J. (2006). *ECG workout*. Ambler, PA: Lippincott Williams & Wilkins.

Iliev, I., Krasteva, V. and Tabakov, S. (2007). Real-time detection of pathological cardiac events in the electrocardiogram. *Physiological measurement*, 28(3), p.259.

Inan, O., Giovangrandi, L. and Kovacs, G. (2006). Robust neural-network-based classification of premature ventricular contractions using wavelet transform and timing interval features. *Biomedical Engineering, IEEE Transactions on*, 53(12), pp.2507--2515.

iRhythm, (2014). *iRhythm ZIO XT Patch Monitoring Process*. [image] Available at: http://www.irhythmtech.com/zio-solution/zio-system/index.html [Accessed 10 Oct. 2014].

Kaiser, S., Kirst, M. and Kunze, C. (2010). Automatic Detection of Atrial Fibrillation for Mobile Devices. *Biomedical Engineering Systems and Technologies*. Springer Berlin Heidelberg, pp.258--270.

Kara, S. and Okandan, M. (2007). Atrial fibrillation classification with artificial neural networks. *Pattern Recognition*, 40(11), pp.2967--2973.

Khadra, L., Al-Fahoum, A. and Al-Nashash, H. (1997). Detection of life-threatening cardiac arrhythmias using the wavelet transformation. *Medical and Biological Engineering and Computing*, 35(6), pp.626--632.

Lau, J., Lowres, N., Neubeck, L., Brieger, D., Sy, R., Galloway, C., Albert, D. and Freedman, S. (2013). iPhone ECG application for community screening to detect silent atrial fibrillation: A novel technology to prevent stroke. *International Journal of Cardiology*, 165(1), pp.193-194.

Lobodzinski, S. and Laks, M. (2012). New devices for very long-term ECG monitoring. *Cardiology journal*, 19(2), pp.210--214.

Lobodzinski, S. (2013). ECG Patch Monitors for Assessment of Cardiac Rhythm Abnormalities. *Progress in cardiovascular diseases*, 56(2), pp.224--229.

Mallat, S. and Zhong, S. (1992). Characterization of signals from multiscale edges. *IEEE Transactions on pattern analysis and machine intelligence*, 14(7), pp.710--732.

Mallat, S. (1989). A theory for multiresolution signal decomposition: the wavelet representation. *Pattern Analysis and Machine Intelligence, IEEE Transactions on*, 11(7), pp.674--693.

Martínez, J., Almeida, R., Olmos, S., Rocha, A. and Laguna, P. (2004). A wavelet-based ECG delineator: evaluation on standard databases. *Biomedical Engineering, IEEE Transactions on*, 51(4), pp.570--581.

Martis, R., Krishnan, M., Chakraborty, C., Pal, S., Sarkar, D., Mandana, K. and Ray, A. (2012). Automated screening of arrhythmia using wavelet based machine learning techniques. *Journal of medical systems*, 36(2), pp.677--688.

Medtronic, (2013). *Reveal LINQ LNQ11 Insertable Cardiac Monitor*. 1st ed. [ebook] Available at: http://manuals.medtronic.com/manuals/search?region=US&cfn=LNQ11&keyword=RevealLINQ ClinManMAR14&manualType=Clinician+Manual&manualLanguage=EN [Accessed 11 Apr. 2014].

Medtronic, (2014). *Reveal XT ICM*. [image] Available at: http://www.medtronicdiagnostics.com/us/cardiac-monitors/Reveal-XT-ICM-Device/index.htm [Accessed 10 Oct. 2014].

Melgani, F. and Bazi, Y. (2008). Classification of electrocardiogram signals with support vector machines and particle swarm optimization. *Information Technology in Biomedicine, IEEE Transactions on*, 12(5), pp.667--677.

Mittal, S., Movsowitz, C. and Steinberg, J. (2011). Ambulatory External Electrocardiographic Monitoring. *Journal of the American College of Cardiology*, 58(17), pp.1741-1749.

Moody, G. and Mark, R. (2001). The impact of the MIT-BIH arrhythmia database. *Engineering in Medicine and Biology Magazine, IEEE*, 20(3), pp.45--50.

Moody, G. and Mark, R. (1983). A new method for detecting atrial fibrillation using RR intervals. *Computers in Cardiology*, 10, pp.227-230.

Moody, G. (2014). *WFDB Applications Guide*. [online] Physionet.org. Available at: http://www.physionet.org/physiotools/wag/wag.htm [Accessed 29 Oct. 2014].

Owis, M., Abou-Zied, A., Youssef, A. and Kadah, Y. (2002). Study of features based on nonlinear dynamical modeling in ECG arrhythmia detection and classification. *Biomedical Engineering, IEEE Transactions on*, 49(7), pp.733--736.

Pedregosa, F., Varoquaux, G., Gramfort, A., Michel, V., Thirion, B., Grisel, O., Blondel, M., Prettenhofer, P., Weiss, R., Dubourg, V. and others, (2011). Scikit-learn: Machine learning in Python. *The Journal of Machine Learning Research*, 12, pp.2825--2830.

Philips, (2014). *Philips DigiTrak XT Holter Recorder*. [image] Available at: http://www.usa.philips.com/healthcare-products/HC860322/digitrak-xt-holter-monitor [Accessed 10 Oct. 2014].

Plux Wireless Biosignals, (2014). *Software*. [online] Bitalino.com. Available at: http://bitalino.com/index.php/software [Accessed 5 Nov. 2014].

Prasad, G. and Sahambi, J. (2003). Classification of ECG arrhythmias using multi-resolution analysis and neural networks. 1, pp.227--231.

Ranjith, P., Baby, P. and Joseph, P. (2003). ECG analysis using wavelet transform: application to myocardial ischemia detection. *ITBM-RBM*, 24(1), pp.44--47.

Reiffel, J., Schwarzberg, R. and Murry, M. (2005). Comparison of Autotriggered Memory Loop Recorders vs Standard Loop Recorders vs 24-hour Holter Monitors for Arrhythmia Detection. *The American Journal of Cardiology*, 95(9), pp.1055-1059.

Rothman, S., Laughlin, J., Seltzer, J., Walia, J., Baman, R., Siouffi, S., Sangrigoli, R. and Kowey, P. (2007). The Diagnosis of Cardiac Arrhythmias: A Prospective Multi-Center Randomized Study Comparing Mobile Cardiac Outpatient Telemetry Versus Standard Loop Event Monitoring. *J Cardiovasc Electrophysiol*, [online] 18(3), pp.241-247. Available at: http://dx.doi.org/10.1111/j.1540-8167.2006.00729.x [Accessed 18 Oct. 2014].

Sambhu, D. and Umesh, A. (2013). Automatic Classification of ECG Signals with Features Extracted Using Wavelet Transform and Support Vector Machines. *International Journal of Advanced Research in Electrical, Electronics and Instrumentation Engineering*, [online] 2(1). Available at: http://ijareeie.com.

Schaul, T., Bayer, J., Wierstra, D., Sun, Y., Felder, M., Sehnke, F., Rückstiess, T. and Schmidhuber, J. (2010). PyBrain. *The Journal of Machine Learning Research*, 11, pp.743--746.

Shen, C., Kao, W., Yang, Y., Hsu, M., Wu, Y. and Lai, F. (2012). Detection of cardiac arrhythmia in electrocardiograms using adaptive feature extraction and modified support vector machines. *Expert Systems with Applications*, 39(9), pp.7845--7852.

Silipo, R. and Marchesi, C. (1998). Artificial neural networks for automatic ECG analysis. *Signal Processing, IEEE Transactions on*, 46(5), pp.1417--1425.

Sivakumaran, S., Krahn, A., Klein, G., Finan, J., Yee, R., Renner, S. and Skanes, A. (2003). A prospective randomized comparison of loop recorders versus Holter monitors in patients with syncope or presyncope. *The American journal of medicine*, 115(1), pp.1--5.

Sufi, F., Khalil, I. and Mahmood, A. (2011). A clustering based system for instant detection of cardiac abnormalities from compressed ECG. *Expert Systems with Applications*, 38(5), pp.4705--4713.

Thakor, N. and Zhu, Y. (1991). Applications of adaptive filtering to ECG analysis: noise cancellation and arrhythmia detection. *Biomedical Engineering, IEEE Transactions on*, 38(8), pp.785--794.

Tsipouras, M. and Fotiadis, D. (2004). Automatic arrhythmia detection based on time and time--frequency analysis of heart rate variability. *Computer methods and programs in biomedicine*, 74(2), pp.95--108.

Tsipouras, M., Fotiadis, D. and Sideris, D. (2005). An arrhythmia classification system based on the RR-interval signal. *Artificial Intelligence in Medicine*, 33(3), pp.237--250.

Wang, Y., Zhu, Y., Thakor, N. and Xu, Y. (2001). A short-time multifractal approach for arrhythmia detection based on fuzzy neural network. *Biomedical Engineering, IEEE Transactions on*, 48(9), pp.989--995.

Welch, P. (1967). The use of fast Fourier transform for the estimation of power spectra: a method based on time averaging over short, modified periodograms. *IEEE Transactions on audio and electroacoustics*, 15(2), pp.70--73.

Williams, L. (2010). *ECG interpretation made incredibly easy!*. 5th ed. Philadelphia: Lippincott Williams & Wilkins.

Yan, G. and Kowey, P. (2011). *Management of cardiac arrhythmias*. New York: Humana Press.

Yang, T., Devine, B. and Macfarlane, P. (1994). Artificial neural networks for the diagnosis of atrial fibrillation. *Medical and Biological Engineering and Computing*, 32(6), pp.615--619.

Ye, C., Kumar, B. and Coimbra, M. (2012). Heartbeat classification using morphological and dynamic features of ECG signals. *Biomedical Engineering, IEEE Transactions on*, 59(10), pp.2930--2941.

Zimetbaum, P. and Goldman, A. (2010). Ambulatory Arrhythmia Monitoring Choosing the Right Device. *Circulation*, 122(16), pp.1629--1636.

Annex A

CONSENTIMENTO INFORMADO

Integrado no projecto "LearningS – Learning from Sequences" é pedida a sua permissão para utilizar a sua informação electrocardiográfica.

Os investigadores do projecto LearningS aprovado pela Faculdade de Ciências e Tecnologia, que está a ser desenvolvido em cooperação com o Hospital de Santa Marta, solicitam a sua colaboração para recolher o seu sinal eléctrico cardíaco e utilizar os seus dados para fins de investigação.

Esta investigação pretende adquirir bases de dados de sinais electrocardiográficos de populações com características distintas, utilizando um sensor dérmico denominado BITalino e o Software SignalBIT. Os principais objectivos do projecto são avaliar a variabilidade interpessoal do sinal de ECG em indivíduos saudáveis e com patologias e definir os padrões considerados normais e patológicos para cada população consoante os dados biométricos.

Da participação neste estudo não decorre qualquer risco para o participante, quer em termos de saúde quer de privacidade. Toda a informação / dados recolhidos serão mantidos em sigilo e anonimato, sendo para exclusiva utilização no âmbito do projecto LearningS. Os resultados resultantes da investigação / estudo poderão ser publicados.

O direito à total liberdade de recusar a participar neste estudo será respeitado. Seguindo estes mesmos critérios éticos, solicitamos que preencha o consentimento que lhe será facultado.

Agradecemos a sua participação.

Principal Investigadora do Projecto: Profª Ana Fred

Supervisor do Projecto: Prof. Dr. Eduardo Antunes

Declaro ter lido e compreendido este documento, bem como as informações verbais que me foram fornecidas. Desta forma, aceito participar neste estudo, de forma inteiramente voluntária, e permito a utilização dos dados nas garantias de confidencialidade e anonimato que me foram dadas pelos investigadores.

Data: …… /…… /……

Assinatura:

Annex B

Table 31: ECG interpretation for the acquisitions with the BITalino System.

Record	Rhythm and other meaningful information
001	Sinus rhythm with borderline PQ interval.
002	Sinus rhythm with PVC.
003	Sinus rhythm with PAC.
004	Sinus rhythm.
005	Sinus rhythm with borderline PQ interval and negative T wave in D1.
006	Sinus rhythm.
007	Sinus rhythm. Inferior myocardial infarction scar. Poor R wave progression from V1 to V3.
008	Sinus rhythm with complete RBBB and LAFB.
009	Sinus rhythm
010	Sinus rhythm. Left ventricular hypertrophy
011	Sinus rhythm with anteroseptal myocardial infarction scar. Negative T wave in D1.
012	Sinus rhythm with anterior myocardial infarction scar. Right atrial dilatation. First degree AV block. LAFB.
013	Atrial fibrillation.
014	Ventricular pacing rhythm (VDD mode).
015	Ventricular pacing rhythm.
016	Ventricular pacing rhythm.
017	Sinus rhythm with first degree AV block and complete LBBB.
018	Atrial fibrillation with slow heart rate. Diphasic T wave in D1.
019	Sinus rhythm.
020	Sinus rhythm.
021	Sinus rhythm with PVC.
022	Sinus rhythm.
023	Sinus rhythm with PAC.
024	Sinus rhythm with inferior myocardial infarction scar.
025	Sinus rhythm.
026	Sinus rhythm.
027	Sinus rhythm.
028	Pacing rhythm (VDD mode) with PVC.
029	Ventricular pacing rhythm (VDD mode).
030	Sinus rhythm with complete LBBB.
031	Sinus rhythm with PVC.
032	Sinus rhythm with first degree AV block.
033	Sinus rhythm. Poor R wave progression from V1 to V3.
034	Sinus rhythm with PAC.
035	Sinus rhythm.
036	Sinus rhythm with inferior myocardial infarction scar.
037	Atrial fibrillation.
038	Atrial fibrillation.
039	Sinus rhythm.
040	Sinus rhythm. Multiple artefacts.
041	Sinus rhythm.
042	Sinus rhythm.
043	Sinus rhythm with complete RBBB.
044	Sinus rhythm. Poor R wave progression from V1 to V3.
045	Sinus rhythm with RBBB and LAFB. Pathological Q waves from V1 to V4.
046	Atrial fibrillation with wide QRS complex and left axis deviation in the frontal plane.
047	Atrial fibrillation with PVC.
048	Sinus rhythm with short PQ (LGL pre-excitation).
049	Sinus rhythm with WPW pre-excitation.
050	Sinus rhythm with first degree AV block.

Record	Rhythm and other meaningful information
051	Sinus rhythm, sinus bradycardia.
052	Sinus rhythm.
053	Atrial fibrillation, alternating with ventricular paced rhythm.
054	Sinus rhythm with left axis deviation. LAFB.
055	Ventricular pacing rhythm.
056	Sinus rhythm.
057	Auricular pacing rhythm.
058	Sinus rhythm.
059	Sinus rhythm.
060	Sinus rhythm with short PQ (LGL).
061	Sinus rhythm.
062	Sinus rhythm.
063	Sinus rhythm with LAFB and PVC.
064	Sinus rhythm.
065	Sinus rhythm with PVC.
066	Sinus rhythm.
067	Sinus rhythm. Poor R wave progression from V1 to V4.
068	Sinus rhythm.
069	Sinus rhythm. Sinus rhythm, sinus bradycardia. Lateral myocardial infarction scar. Switched electrodes?
070	Sinus rhythm.
071	Sinus rhythm with left ventricular hypertrophy and PAC.
072	Sinus rhythm and left ventricular hytpertrophy criteria.
073	Sinus rhythm, sinus bradycardia and LAFB.
074	Sinus rhythm. LAFB.
075	Ventricular pacing rhythm.
076	Atrial fibrillation with fast heart rate.
077	Atrial fibrillation alternating with ventricular pacing rhythm.
078	Sinus rhythm. Poor R wave progression from V1 to V4.
079	Ventricular pacing rhythm with PVC.
080	Sinus rhythm with RBBB and LAFB.
081	Sinus rhythm with PAC.
082	Sinus rhythm.
083	Sinus rhythm.
084	Sinus rhythm.
085	Sinus bradycardia with RBBB, LAFB and PAC.
086	Sinus rhythm with RBBB and LAFB.
087	Sinus rhythm. Possible inferior myocardial infarction scar.
088	Sinus rhythm with first degree AV block.
089	Ventricular pacing rhythm.
090	Sinus rhythm.
091	Sinus rhythm.
092	Ventricular pacing rhythm and PVC.
093	Sinus rhythm.
094	Sinus rhythm. Possible inferior myocardial infarction scar.
095	Sinus rhythm with complete RBBB.
096	Sinus rhythm with first degree AV block.
097	Ventricular pacing rhythm with PVC.
098	Ventricular pacing rhythm (VDD mode).
099	Sinus rhythm.
100	Sinus rhythm with PVC and left ventricular hypertrophy.
101	Atrial flutter-fibrillation.
102	Sinus rhythm.
103	Sinus rhythm with complete LBBB.

Record	Rhythm and other meaningful information
104	Sinus bradycardia with complete RBBB and first degree AV block.
105	Sinus rhythm.
106	Sinus rhythm with first degree AV block. Anteroseptal myocardial infarction scar.
107	Ventricular pacing rhythm (VDD mode) and PVC.
108	Sinus rhythm. Pacemaker undersensing. Anteroseptal myocardial infarction scar.
109	Sinus tachycardia with incomplete LBBB.
110	Ventricular pacing rhythm (VDD mode).
111	Sinus rhythm with first degree AV block and complete LBBB.
112	Sinus rhythm.
113	Sinus rhythm with PVC.
114	Atrial fibrillation.
115	Sinus rhythm.
116	Sinus bradycardia with first degree AV block. Negative T wave in D1.
117	Sinus rhythm with Brugada pattern.
118	Sinus rhythm with left ventricular hypertrophy.
119	Sinus rhythm with first degree AV block, RBBB and left ventricular hypertrophy.
120	Sinus rhythm with short PQ in D1. Intraventricular conduction perturbations.
121	Atrial fibrillation. Anteroseptal myocardial infarction scar.
122	Sinus rhythm.
123	Sinus bradycardia and PAC.
124	Sinus rhythm.
125	Sinus rhythm.
126	Sinus rhythm. Possible right atrial dilatation.
127	Sinus rhythm with complete RBBB and left ventricular hypertrophy.
128	Ventricular pacing rhythm (VDD mode).
129	Atrial flutter with 2:1 conduction ratio.
130	Sinus rhythm with long PQ. Complete RBBB and left ventricular hypertrophy.
131	Sinus rhythm with first degree AV block and PAC.
132	Sinus tachycardia.
133	Atrial fibrillation.
134	Sinus rhythm.
135	Sinus rhythm with intraventricular conduction perturbations.
136	Sinus rhythm with left ventricular hypertrophy.
137	Sinus rhythm.
138	Atrial fibrillation. Periods of complete AV block?
139	Sinus rhythm.
140	Sinus rhythm with pattern of LBBB.
141	Junctional rhythm at 30 bpm.
142	Sinus rhythm.
143	Sinus rhythm.
144	Sinus rhythm with complete RBBB, left ventricular hypertrophy and first degree AV block.
145	Sinus rhythm.
146	Sinus rhythm with first degree AV block.
147	Sinus rhythm.
148	Sinus rhythm.
149	Atrial brady-fibrillation with complete RBBB and left ventricular hypertrophy.
150	Sinus rhythm with PVC.
151	Sinus rhythm.
152	Atrial fibrillation with PVC.
153	Ventricular pacing rhythm. Atrial fibrillation?
154	Sinus rhythm.
155	Sinus rhythm.
156	Sinus bradycardia.
157	Sinus bradycardia and left ventricular hypertrophy.

Record	Rhythm and other meaningful information
158	Sinus rhythm.
159	Sinus rhythm. LPFB
160	Sinus rhythm. LPFB.
161	Sinus rhythm.
162	Sinus bradycardia with LBBB.
163	Sinus rhytm with LAFB.
164	Sinus rhythm. Intraventricular conduction perturbations.
165	Sinus rhythm.
166	Sinus rhythm with PVC and short PQ (LGL).
167	Sinus rhythm with complete RBBB and left ventricular hypertrophy.
168	Sinus rhythm with left ventricular hypertrophy.
169	Sinus rhythm.
170	Sinus rhythm with PAC.
171	Sinus rhythm.
172	Sinus rhythm.
173	Sinus rhythm.
174	Sinus rhythm.
175	Sinus rhythm with lateral myocardial infarction scar.
176	Sinus rhythm.
177	Sinus rhythm with short PQ (LGL).
178	Sinus rhythm.
179	Sinus rhythm. Anteroseptal myocardial infarction scar.
180	Sinus rhythm with left ventricular hypertrophy.
181	Sinus rhythm.
182	Sinus rhythm with short PQ (LGL).
183	(1) Ventricular pacing rhythm; (2) Interrupted pacing – complete AV block.
184	Sinus rhythm with left ventricular hypertrophy.
185	Sinus rhythm.
186	Sinus rhythm.
187	Sinus rhythm.
188	Sinus rhythm.
189	Sinus rhythm.
190	Sinus rhythm.
191	Sinus rhythm with left ventricular hypertrophy.
192	Sinus rhythm with first degree AV block and anteroseptal myocardial infarction scar.
193	Sinus bradycardia with complete RBBB, left ventricular hypertrophy and PAC.
194	Sinus rhythm with left ventricular hypertrophy.
195	Sinus rhythm.
196	Sinus bradycardia with first degree AV block.
197	Sinus bradycardia.
198	Sinus rhythm with inferiorposterior myocardial infarction scar.
199	Ventricular pacing rhythm.
200	Sinus rhythm with complete RBBB.
201	Sinus rhythm.
202	Sinus rhythm.
203	Sinus rhythm with left ventricular hypertrophy.
204	Atrial flutter with variable AV conduction.
205	Sinus rhythm.
206	Ventricular pacing rhythm alternating with intrinsic rhythm. PVC.
207	Sinus rhythm with left ventricular hypertrophy and lateral myocardial infarction scar.
208	Atrial fibrillation.
209	Atrial fibrillation.
210	Ventricular pacing rhythm.
211	Sinus bradycardia.

Record	Rhythm and other meaningful information
212	Sinus rhythm.
213	Sinus rhythm with PVC and left ventricular hypertrophy.
214	Sinus tachycardia with PVC.
215	Ventricular pacing rhythm.
216	Atrial fibrillation.
217	Sinus rhythm with PAC.
218	Sinus rhythm.
219	Atrial fibrillation alternating with ventricular pacing rhythm.
220	Sinus rhythm with left ventricular hypertrophy.
221	Sinus rhythm. negative T wave in D1.
222	Sinus rhythm with complete RBBB and left ventricular hypertrophy. PVC:
223	Sinus rhythm.
224	Sinus rhythm.
225	Fast atrial fibrillation.
226	Sinus rhythm.
227	Sinus rhythm with LPFB.
228	Sinus rhythm with complete RBBB.
229	Sinus rhythm.
230	Sinus rhythm.
231	Sinus bradycardia.
232	Sinus rhythm with LAFB.
233	Sinus rhythm.
234	Sinus rhythm – ventricular bigeminy.
235	Sinus rhythm.
236	Sinus rhythm.
237	Sinus rhythm.
238	Sinus rhythm with PAC.
239	Sinus tachycardia.
240	Sinus rhythm.
241	Sinus rhythm.
242	Sinus rhythm.
243	Sinus rhythm. Anteroseptal myocardial infarction scar.
244	Sinus rhythm.
245	Sinus rhythm. Inferior myocardial infarction scar.
246	Sinus rhythm.
247	Sinus rhythm with left ventricular hypertrophy and left atrial dilatation.
248	Sinus rhythm with first degree AV block. Anteroseptal myocardial infarction scar.
249	Ventricular pacing rhythm alternating with intrinsic atrial fibrillation rhythm.
250	Sinus rhythm with PAC.
251	Sinus rhythm.
252	Sinus rhythm. Inferior myocardial infarction scar.
253	Sinus rhythm.
254	Sinus rhythm with complete LBBB.
255	Sinus rhythm with LAFB.
256	Sinus rhythm.
257	Sinus rhythm.
258	Sinus rhythm.
259	Sinus rhythm.
260	Sinus rhythm.
261	Sinus rhythm.
262	Sinus rhythm.
263	Sinus rhythm.
264	Sinus rhythm with LAFB. Anteroseptal myocardial infarction scar.
265	Sinus rhythm with first degree AV block.

Record	Rhythm and other meaningful information
266	Sinus rhythm.
267	Sinus rhythm. Switched electrodes.
268	Sinus rhythm.
269	Ventricular pacing rhythm. Atrial fibrillation.
270	Sinus rhythm with first degree AV block.
271	Sinus rhythm with LAFB. Anteroseptal myocardial infarction scar.
272	Sinus rhythm.
273	Sinus rhythm.
274	Sinus rhythm with complete RBBB.
275	Sinus rhythm.
276	Sinus rhythm.
277	Sinus rhythm.
278	Sinus rhythm.
279	Sinus bradycardia. Left ventricular hypertrophy criteria. Negative T wave in D1.
280	Sinus rhythm.
281	Sinus rhythm.
282	Sinus rhythm. PVC and PAC.
283	Sinus rhythm with complete RBBB. left ventricular hypertrophy.
284	Atrial fibrillation with PVC.
285	Atrial fibrillation.
286	Sinus rhythm.
287	Sinus rhythm with left ventricular hypertrophy.
288	Sinus rhythm.
289	Atrial fibrillation.
290	Sinus rhythm with intraventricular conduction aberrancy.
291	Sinus rhythm. Inferior myocardial infarction scar.
292	Sinus rhythm.
293	Sinus rhythm with anteroseptal myocardial infarction scar.
294	Sinus rhythm with complete RBBB.